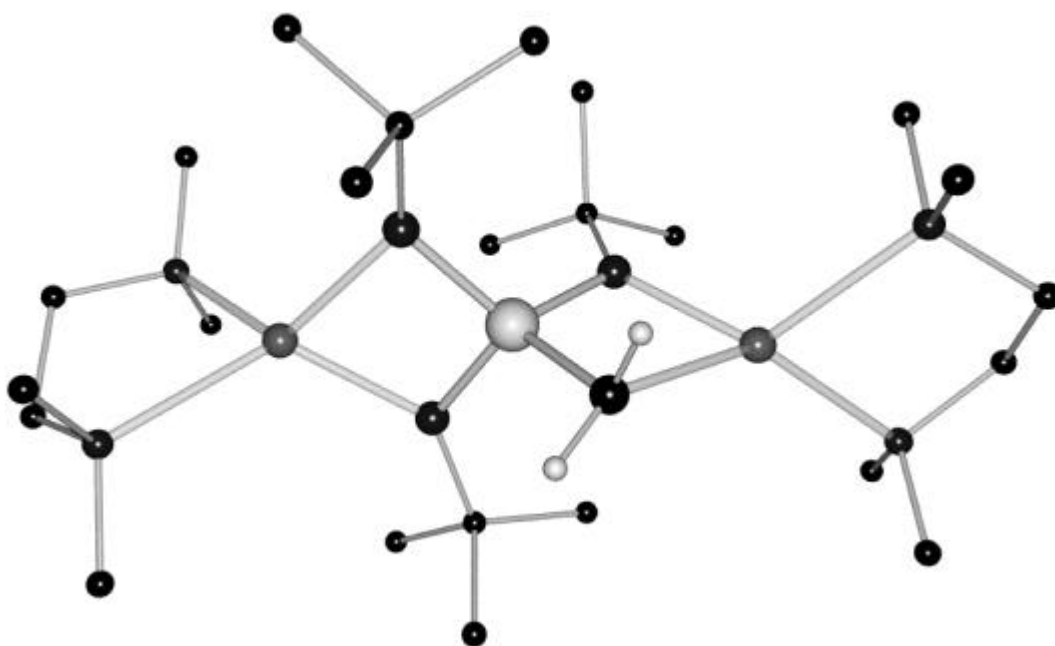

Novel Dianionic Sulfur Ylides and Related Compounds



Novel Dianionic Sulfur Ylides and Related Compounds

Dissertation zur Erlangung des
naturwissenschaftlichen Doktorgrades
der Bayerischen Julius-Maximilians-Universität Würzburg

vorgelegt von
Bernhard Walfort
aus Marbach am Neckar

Würzburg 2001

Eingereicht am:.....

1. Gutachter:.....

2. Gutachter:.....

der Dissertation

1. Prüfer:.....

2. Prüfer:.....

der mündlichen Prüfung

Tag der mündlichen Prüfung:.....

Doktorurkunde ausgehändigt am:.....

Wer nichts als Chemie versteht,
versteht auch die nicht recht.

Georg Christoph Lichtenberg (1742 - 1799)

Für die Möglichkeit zur völligen wissenschaftlichen Entfaltungsfreiheit und die ständige Rückendeckung gilt mein ganz besonderer Dank Herrn Prof. Dr. D. Stalke. Ich habe die letzten zwei Jahre wahrlich "genossen", nicht zuletzt wegen der ausgezeichneten Arbeitsbedingungen und der guten Atmosphäre.

An dieser Stelle sei auch allen Arbeitskreismitgliedern für ihre ständige Hilfsbereitschaft und Diskussionsfreudigkeit gedankt.

Unserem Dipl. Physiker Dirk Leusser danke ich für die kritischen Hinterfragungen aller wissenschaftlichen Arbeiten. Die kristallographischen Diskussionen haben mir sehr viel Spass bereitet und waren stets sehr informativ.

Meiner Leidensgenossin (auf chemischer Basis) Carola Selinka und Thomas Stey danke ich für die Aufnahme zahlreicher NMR Spektren.

Dipl. Chem. Alexander Murso und Dipl. Chem. Dagmar Ilge danke ich ganz herzlich für die Entlastung bei der Systemadministration der zahlreichen Rechner im Arbeitskreis.

Tanja Auth, Björn Degel und Holger Helten danke ich für die gute und auch erfolgreiche Zusammenarbeit während ihres F-Praktikums. Es hat mich sehr gefreut, daß sie trotz einiger misslungener Versuche immer mit Begeisterung dabei waren.

Dem Glasbläser Fertig danke ich für die prompte Anfertigung ausgefallener Glasgeräte. Herrn Dr. Buchner und Herrn Dr. Bertermann danke ich für die Anfertigung zahlreicher NMR Spektren und Herrn Dr. Kneiss danke ich für die Messung der CHN Analysen.

Ich danke allen die diese Arbeit so prompt korrektur gelesen haben: Dirk Leusser und Carola Selinka, aber vor allem Dr. Mahalakshmi L. für die Konvertierung der Arbeit von gemäßigttem "Genglish" in perfektes "Indian English".

Meiner Freundin Antje als auch meinen Eltern und Geschwistern danke ich für die Unterstützung die Sie mir während meines gesamten Studiums zukommen lassen.

Contents

1 Introduction	1
2 S(IV)-Compounds	7
2.1 Introduction.....	7
2.2 Triimidosulfites.....	7
2.2.1 Transmetalation Reactions	8
2.2.1.1 Transmetalation with Coinage Metal Halides.....	9
2.2.1.2 Transmetalation with Fe(AcAc) ₂	16
2.2.2 Anion-Solvation.....	18
2.2.2.1 Halide-Addition.....	19
2.2.2.2 Carbanion-Addition.....	20
2.2.2.3 Ethylenoxidadduct.....	23
2.2.2.4 Conclusion.....	28
2.3 Alkylendiimidosulfites.....	29
2.3.1 Synthesis of [(thf)Li ₂ {(H ₂ C)S(N ^t Bu) ₂ }] ₂ (9) and [(thf)Li ₂ {(Et)(Me)CS(N ^t Bu) ₂ }] ₂ (10)	30
2.3.2 Crystal Structures of [(thf)Li ₂ {H ₂ CS(N ^t Bu) ₂ }] ₂ (9) and [(thf)Li ₂ {(Et)(Me)CS(N ^t Bu) ₂ }] ₂ (10):	31
2.4 Alkylen-bis-diimidosulfites.....	35
2.4.1 Addition Reactions of [(thf)Li ₂ {H ₂ CS(N ^t Bu) ₂ }] ₂ (9) and [(thf)Li ₂ {(Et)(Me)CS(N ^t Bu) ₂ }] ₂ (10) to a Sulfurdiimide:.....	35
2.4.2 Crystal Structure of [(thf)Li ₃ {((N ^t Bu) ₂ S) ₂ CH}] ₂ (11).....	37
3 S(VI)-Compounds	39
3.1 Introduction.....	39
3.2 Alkyltriimidosulfonates	39
3.2.1 Synthesis and Structure of the S-methyl-tri(<i>tert</i> -butyl)triimidosulfonic Acid MeS(N ^t Bu) ₂ NH ^t Bu (12).....	40
3.2.2 Insertion of Sulfur Triimide into the Metal Carbon Bond of Trimethyl Aluminum and Dimethyl Zinc.....	41
3.2.3 Structures of [Me ₂ Al(N ^t Bu) ₃ SMe] (13), [Zn{(N ^t Bu) ₃ SMe} ₂] (14) and [(thf) ₂ Li{(N ^t Bu) ₃ SMe}•ZnMe ₂] (15)	42

3.2.4 Lithium-S-phenylalkynyl-N,N',N''-tri(<i>tert</i> butyl)triimidodisulfonate [(thf) ₂ Li{(N ^t Bu) ₃ SCCPh}] (16).....	45
3.2.5 Structural Comparison of the known Triimidodisulfonates	49
3.3 Alkylentriimidodisulfates	50
3.4 Triimidodisulfate.....	52
3.5 Methane-di-triimidodisulfonates	55
3.5.1 Syntheses and Structure of [(thf) ₂ Li ₂ {(N ^t Bu) ₃ S ₂ CH ₂ }] (19)	55
3.5.2 Syntheses and Structure of H ₂ C{S(N ^t Bu) ₂ (NH ^t Bu)} ₂ (20)	56
4 Conclusion	59
4.1 S(IV) and S(VI) Polyimido Compounds	59
4.1.1 Triimidodisulfites.....	59
4.1.2 Alkyltriimidodisulfonates.....	61
4.2 S(IV) and S(VI) carba/imido compounds.....	63
4.2.1 Alkylendiimidodisulfites.....	63
4.2.2 Methylentriimidodisulfate	64
5 Zusammenfassung	66
6 Experimental.....	73
7 Crystallographic Section.....	80
7.1 Crystal Application.....	80
7.2 Data collection.....	80
7.2.1 Procedure at the Enraf-Nonius CAD4 Diffractometer	80
7.2.2 Procedure at the STOE IPDS diffractometer.....	81
7.2.1 Procedure at the Bruker Smart Apex CCD D8 Diffractometer.....	81
7.3 Structure Solution and Refinement.....	82
7.3.1 Twin refinement.....	82
7.3.2 Twinning Types and its Effect on Reflections Overlap.....	83
7.3.3 Twin Solution Strategy.....	84
7.4 Structural Details	89
7.4.1 [(thf) ₂ Cu ₃ Li ₂ I{(N ^t Bu) ₃ S ₂ }] (1):.....	89
7.4.2 [(thf) ₂ Ag ₃ Li ₂ Br{(N ^t Bu) ₃ S ₂ }] (2), [(thf)Ag ₃ Li ₂ Br{(N ^t Bu) ₃ S ₂ }] ₂ (3), [(thf) ₂ Ag ₃ Li ₃ Br ₂ {(N ^t Bu) ₃ S ₂ }] ₂ (4):.....	89
7.4.3 [Fe(N ^t Bu){(N ^t Bu) ₂ S}] ₂ (5):.....	92
7.4.4 [(thf) ₂ Li ₃ Cl{(N ^t Bu) ₃ S}] ₂ (6):.....	93

7.4.5 [(thf) ₃ Li ₃ Me{(N ^t Bu) ₃ S}] (7):	93
7.4.6 [(thf) ₃ Li ₃ (OCHCH ₂){(N ^t Bu) ₃ S}] (8a,b):	94
7.4.7 [(thf)Li ₂ {(CH ₂)(N ^t Bu) ₂ S}] ₂ (9):	96
7.4.8 [(thf)Li ₂ {(Et)(Me)CS(N ^t Bu) ₂ }] ₂ (10):	97
7.4.9 [(thf)Li ₃ {((N ^t Bu) ₂ S) ₂ CH}] ₂ (11a-c):	97
7.4.10 H(N ^t Bu) ₃ SMe (12):	98
7.4.11 [Me ₂ Al{(N ^t Bu) ₃ SMe}] (13):	99
7.4.12 [Zn{(N ^t Bu) ₃ SMe}] ₂ (14):	100
7.4.13 [(thf) ₂ Li{(N ^t Bu) ₃ SMe}•ZnMe ₂] (15):	100
7.4.14 [(thf) ₂ Li{(N ^t Bu) ₃ SCCPh}] (16):	101
7.4.15 [(tmeda) ₂ Li ₂ {(CH ₂)S(N ^t Bu) ₃ }] (17):	102
7.4.16 [(tmeda)Li ₂ {(O)S(N ^t Bu) ₃ }] ₃ (18):	102
7.4.17 [(thf) ₂ Li ₂ {((N ^t Bu) ₃ S) ₂ CH ₂ }] (19):	103
7.4.18 H ₂ C{S(N ^t Bu) ₂ (NH ^t Bu)} ₂ (20):	104
7.5 Crystallographic Data	105
8 Literature	113

Abbreviations

2D	two dimensional
AcAc	acetylacetonate
adp	anisotropic displacement parameter
av.	average
cal.	calculated
CCD	charged coupled device
CP	cross polarisation
e.g.	exempli gratia
esd	estimated standard deviation
ESR	electron spin resonance
Et	ethyl
eq.	equation
ext.	extern
Fig.	Figure
FT	Fourier transformation
h	hour
Hal.	Halogen or halide
Hz	Hertz
iPr.	<i>iso</i> -propyl
IR	infrared
MAS	magic-angle spinning
Me	methyl
mid.	middle
mL	millilitre
Mp.	Melting point
MQ	magnetic quadrupol
nBu	neo-butyl
NMR	nuclear magnetic resonance
No.	number
Ph	phenyl
Py	pyridyl

Pyz	pyrazolyl
R	rest
refln.	reflection
rt	room temperature
sec.Bu	secondary butyl
^t Bu	tertiary butyl
tmeda	tetramethylethylenediamin
thf	tetrahydrofuran
sof	site occupancy factor
vs.	versus

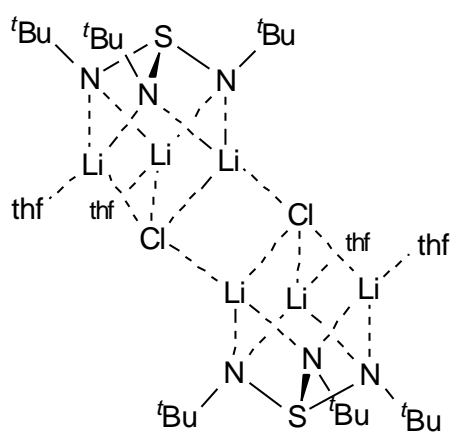
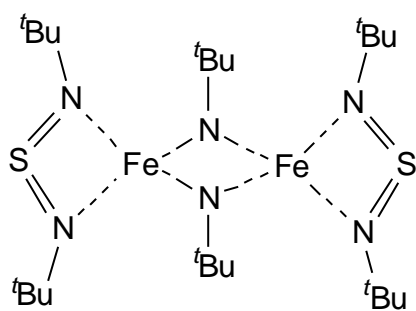
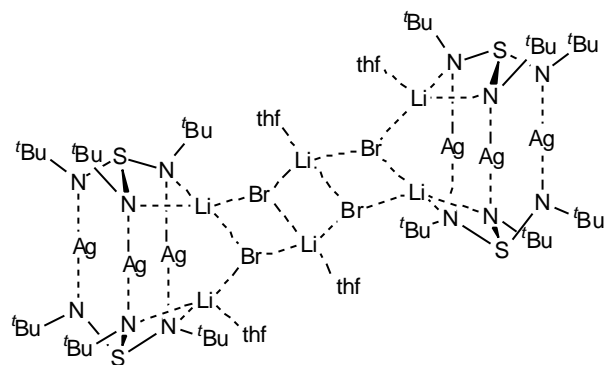
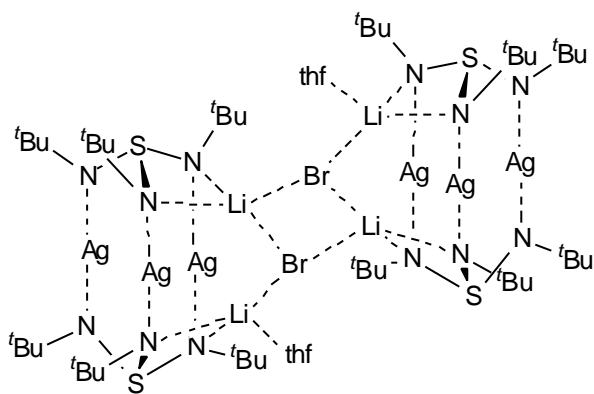
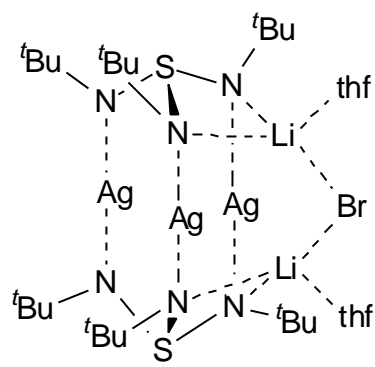
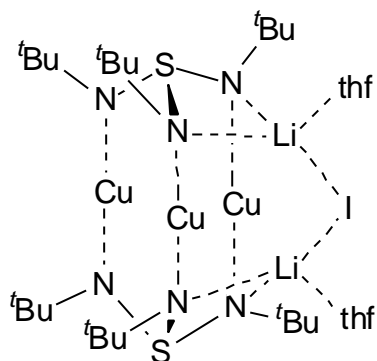
Many results presented in this thesis have already been published in various chemical journals:

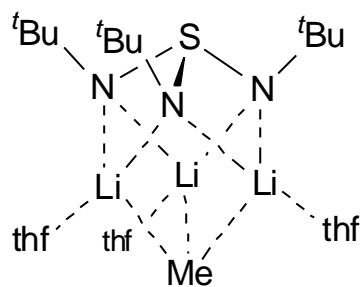
1. R. Fleischer, B. Walfort, A. Gbureck, P. Scholz, W. Kiefer, D. Stalke,
Raman spectroscopic investigation and coordination behavior of the polyimido
S(VI) anions $[\text{RS}(\text{NR})_3]^-$ and $[\text{S}(\text{NR})_4]^{2-}$
Chemistry, Eur. J. **1998**, 4, 2266.
2. B. Walfort, R. Bertermann, D. Stalke,
A new class of dianionic sulfur-ylides: alkylendiazasulfites
Chemistry, Eur. J. **2001**, 7, 1424.
3. B. Walfort, L. Lameyer, W. Weiss, R. Herbst-Irmer, R. Bertermann, J. Rocha, D.
Stalke,
 $[\{(\text{MeLi})_4(\text{dem})_{1.5}\}_\infty]$ and $[(\text{thf})_3\text{Li}_3\text{Me}\{(\text{N}^t\text{Bu})_3\text{S}\}]$ – how to reduce aggregation of
parent methyllithium
Chemistry, Eur. J. **2001**, 7, 1417.
4. B. Walfort, S. Panday, D. Stalke,
The inverse podant $[\text{Li}_3(\text{N}^t\text{Bu})_3\text{S}]^+$ stabilises a single lithium enolate $\text{LiOCH}=\text{CH}_2$
in a high and low temperature solid state phase of $[(\text{thf})_3\text{Li}_3(\text{OCH}=\text{CH}_2)\{(\text{N}^t\text{Bu})_3\text{S}\}]$
Chem. Comm. **2001**, 17, 1640.
5. B. Walfort, A. P. Leedham, C. A. Russel, D. Stalke,
Triimidosulfonic Acid and Organometallic Triimidosulfonates – S^+-N^- versus $\text{S}=\text{N}$
Bonding
Inorg. Chem. **2001**, 40, 5668.
6. B. Walfort, D. Stalke,
Methylene triimidosulfate $[\text{H}_2\text{CS}(\text{N}^t\text{Bu})_3]^{2-}$ – The First Dianionic Sulfur(VI)-Ylide
Angew. Chem. **2001**, 113, 3965.
7. D. Leusser, B. Walfort, D. Stalke,
Charge Density Study of Methane-di(triimido)sulfonic Acid $\text{CH}_2\{\text{S}(\text{N}^t\text{Bu})_2(\text{NH}^t\text{Bu})\}_2$
– the NR Analogue of $\text{H}_2\text{C}\{\text{S}(\text{O})_2(\text{OH})\}_2$
Angew. Chem. **2001**, im Druck.

List of Compounds

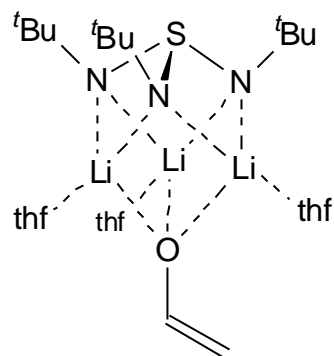
Compound	Number	Structure Code
$[(\text{thf})_2\text{Cu}_3\text{Li}_2\text{I}\{(\text{N}^t\text{Bu})_3\text{S}\}_2]$	1	Cuio
$[(\text{thf})_2\text{Ag}_3\text{Li}_2\text{Br}\{(\text{N}^t\text{Bu})_3\text{S}\}_2]$	2	Agba1
$[(\text{thf})\text{Ag}_3\text{Li}_2\text{Br}\{(\text{N}^t\text{Bu})_3\text{S}\}_2]_2$	3	Agba2
$[(\text{thf})_2\text{Ag}_3\text{Li}_3\text{Br}_2\{(\text{N}^t\text{Bu})_3\text{S}\}_2]_2$	4	Agba3
$[\text{Fe}(\text{N}^t\text{Bu})\{(\text{N}^t\text{Bu})_2\text{S}\}_2]$	5	Feim
$[(\text{thf})_2\text{Li}_3\text{Cl}\{(\text{N}^t\text{Bu})_3\text{S}\}_2]$	6	Cladd
$[(\text{thf})_3\text{Li}_3\text{Me}\{(\text{N}^t\text{Bu})_3\text{S}\}]$	7	Melia
$[(\text{thf})_3\text{Li}_3(\text{OCHCH}_2)\{(\text{N}^t\text{Bu})_3\text{S}\}]$	8a,b	Etox1 and Etox2
$[(\text{thf})\text{Li}_2\{(\text{CH}_2)(\text{N}^t\text{Bu})_2\text{S}\}_2]$	9	Ch2si
$[(\text{thf})\text{Li}_2\{(\text{Et})(\text{Me})\text{CS}(\text{N}^t\text{Bu})_2\}_2]$	10	Sbusi
$[(\text{thf})\text{Li}_3\{((\text{N}^t\text{Bu})_2\text{S})_2\text{CH}\}_2]$	11a-c	Didi1, Didi2 and Didi3
$\text{H}(\text{N}^t\text{Bu})_3\text{SMe}$	12	Soth
$[\text{Me}_2\text{Al}\{(\text{N}^t\text{Bu})_3\text{SMe}\}]$	13	Sotal
$[\text{Zn}\{(\text{N}^t\text{Bu})_3\text{SMe}\}_2]$	14	Sotzn
$[(\text{thf})_2\text{Li}\{(\text{N}^t\text{Bu})_3\text{SMe}\}\cdot\text{ZnMe}_2]$	15	Sotzl
$[(\text{thf})_2\text{Li}\{(\text{N}^t\text{Bu})_3\text{SCCPh}\}]$	16	Sotac
$[(\text{tmeda})_2\text{Li}_2\{(\text{CH}_2)\text{S}(\text{N}^t\text{Bu})_3\}]$	17	Ch2sa
$[(\text{tmeda})\text{Li}_2\{(\text{O})\text{S}(\text{N}^t\text{Bu})_3\}]_3$	18	Onnn
$[(\text{thf})_2\text{Li}_2\{((\text{N}^t\text{Bu})_3\text{S})_2\text{CH}_2\}]$	19	Tritr
$\text{H}_2\text{C}\{\text{S}(\text{N}^t\text{Bu})_2(\text{NH}^t\text{Bu})\}_2$	20	Trith

Lewis Diagrams of Compounds 1-20

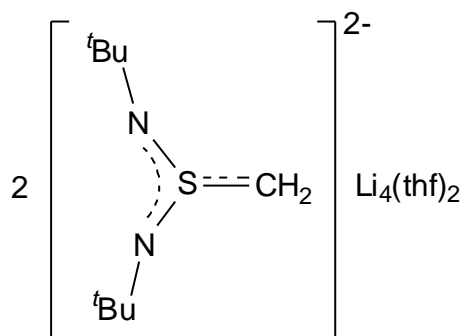




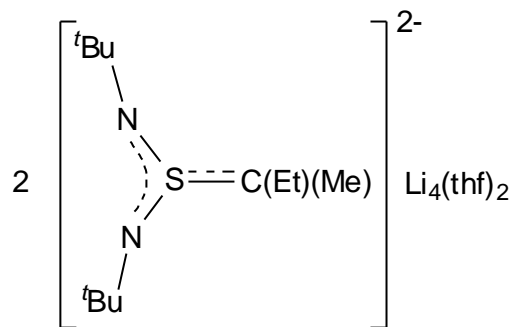
7



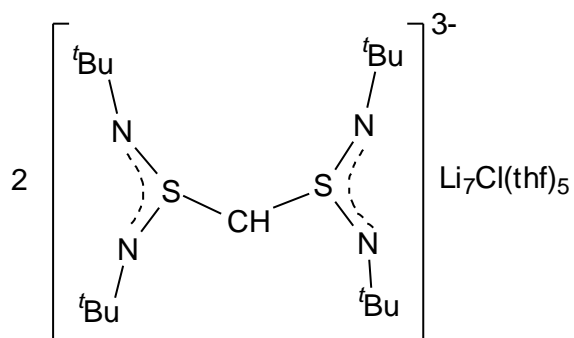
8 a,b



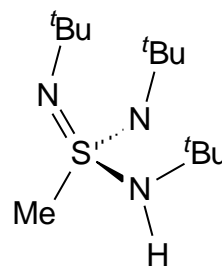
9



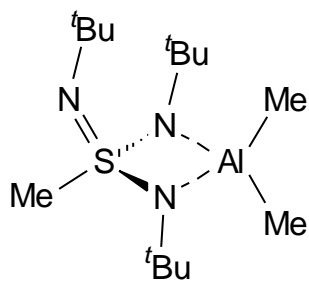
10



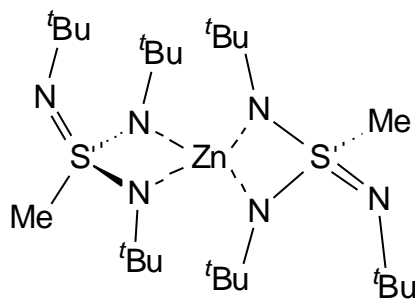
11 a-c



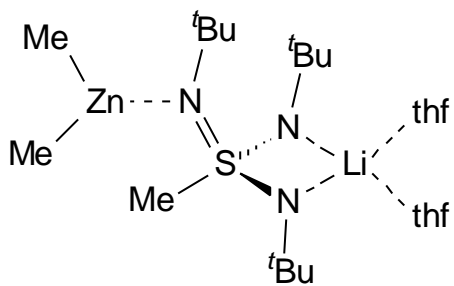
12



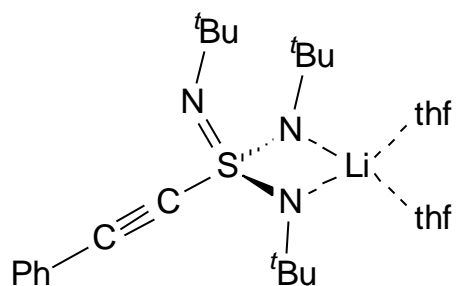
13



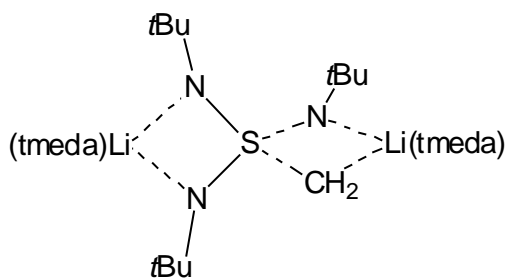
14



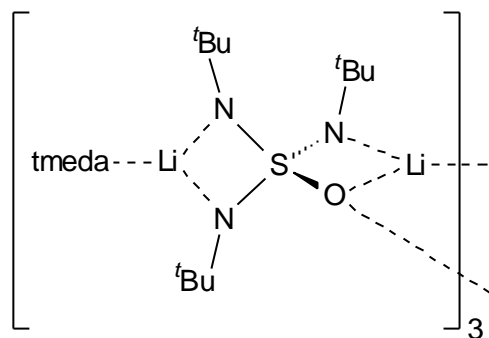
15



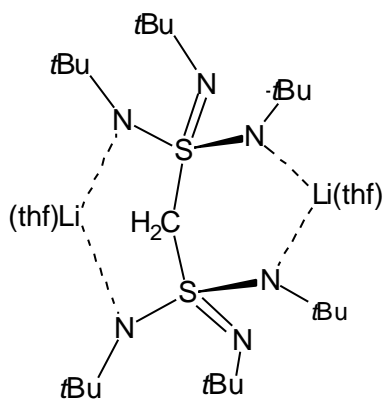
16



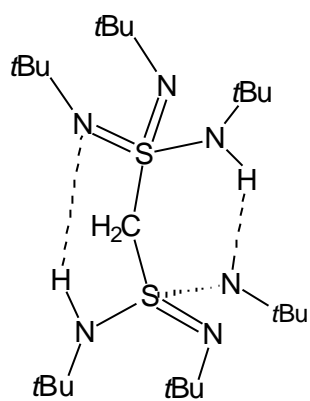
17



18



19



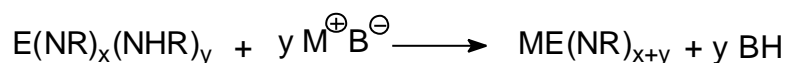
20

1 Introduction

The “isoelectronic principle”, first espoused by Langmuir,^[1] is a simple and useful concept, especially in inorganic chemistry. It is frequently invoked in the application of Valence Shell Electron Pair Repulsion Theory for the prediction of the shapes of molecules with a central p-block element. For the synthetic chemist the first preparation of an unknown compound has often been prompted by the existence of an isoelectronic analogue. The full or partial isoelectronic replacement of the oxygen atom of common p-block element oxoanions, SiO_4^{4-} , PO_3^- , AsO_3^{3-} , SbO_3^{3-} , PO_4^{3-} , SO_3^{2-} , SeO_3^{2-} , TeO_3^{2-} or SO_4^{2-} by NR generates a new class of polyimido polyanions like $\text{Si}(\text{NR})_4^{4-}$, $\text{P}(\text{NR})_3^-$, $\text{As}(\text{NR})_3^{3-}$, $\text{Sb}(\text{NR})_3^{3-}$, $\text{P}(\text{NR})_4^{3-}$, $\text{S}(\text{NR})_3^{2-}$, $\text{Se}(\text{NR})_3^{2-}$, $\text{Te}(\text{NR})_3^{2-}$ or $\text{S}(\text{NR})_4^{2-}$.^[2] The presence of an organic substituent in the latter gives rise to significant differences in the chemical and physical properties of the isoelectronic analogues. For example, CO_2 and $\text{C}(\text{NR})_2$ are both multiply bonded monomers, but carbon dioxide is at standard conditions a gas whereas $\text{C}(\text{NR})_2$ are liquids. The appropriate choice of NR groups may allow the synthesis of functional materials with specific applications. These anions are also attracting attention as multidentate ligands with unusual electronic and stereochemical characteristics that may furnish new metal-centred compounds.

A variety of methodologies have been employed for the synthesis of polyimido systems. However, three general strategies have emerged as the most versatile:

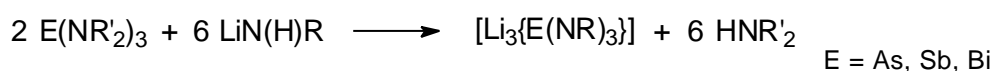
– *Metalation of Primary Amido Complexes:*



E = C, Si; M = Li; B = base; x,y = 1-4

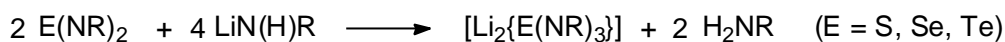
Examples are the metalation of $\text{PhN}=\text{C}(\text{NPh})_2$ or $(^t\text{BuNH})\text{Si}(\mu\text{-N}^t\text{Bu})_2\text{Si}(\text{NH}^t\text{Bu})_2$ with *n*butyllithium to $[(\text{thf})_3\text{Li}_2\{(\text{NPh})_3\text{C}\}]_2$ ^[3] and $[\text{Li}_2\{(\text{N}^t\text{Bu})_3\text{Si}\}]_n$.^[4]

– *Transamination Reactions:*



Wright *et al.* have established a versatile synthetic path to group 15 imido compounds via transamination of -NR_2 with $\text{-N}^\ominus\text{R}$.^[2f,g;5]

– *Nucleophilic Addition:*



Nucleophilic addition of primary lithiumamide reagents to heteroallenes (or their group 16 analogues) and simultaneous deprotonation of the remaining hydrogen, represent a versatile route to homoleptic polyimido anions of group 16 elements.^[2h-j;6]

Sulfur nitrogen compounds attracted much research interest in the 1970's and 1980's. The discovery of $(\text{SN})_x$,^[7a] a metallic compound with superconducting properties at low temperatures ($< 0.33\text{K}$),^[7b] gave a fresh impetus to the sulfur nitrogen chemistry and resulted in a great variety of binary sulfur nitrogen compounds.

Table 1: Sulfur oxygen compounds and their sulfur nitrogen analogues.

S–O	Mixed S–O / S–N			S–N
SO_2			OSNR	$\text{S}(\text{NR})_2$
SO_3^{2-}		O_2SNR	$\text{OS}(\text{NR})_2^{2-}$	$\text{S}(\text{NR})_3^{2-}$
RSO_2^-			$\text{RS}(\text{O})\text{NR}^-$	$\text{RS}(\text{NR})_2^-$
R_2SO				R_2SNR
SO_3		O_2SNR	$\text{OS}(\text{NR})_2$	$\text{S}(\text{NR})_3$
SO_4^{2-}	$\text{O}_3\text{S}(\text{NR})^{2-}$	$\text{O}_2\text{S}(\text{NR})_2^{2-}$	$\text{OS}(\text{NR})_3^{2-}$	$\text{S}(\text{NR})_4^{2-}$
RSO_3^-		$\text{RS}(\text{O})_2(\text{NR})$	$\text{RS}(\text{O})(\text{NR})_2^-$	$\text{RS}(\text{NR})_3^-$
R_2SO_2			$\text{R}_2\text{S}(\text{O})(\text{NR})$	$\text{R}_2\text{S}(\text{NR})_2$
SO_4	$\text{O}_3\text{S}(\text{NR})$	$\text{O}_2\text{S}(\text{NR})_2$	$\text{OS}(\text{NR})_3$	$\text{S}(\text{NR})_4$

Highlighted compounds have not been reported previously

In 1956 *Goehring* and *Weis* succeeded in the landmark synthesis of the first sulfur diimide $\text{S}(\text{NR})_2$.^[8] In the subsequent years several syntheses of sulfur diimides were developed. Due to their manifold reactivity, sulfur diimides have been employed

in different reactions in various fields of chemistry e.g. cycloaddition and en reactions,^[9] asymmetric amination,^[10] and dehydration.^[11]

Our research group began initially to work with $S(NR)_2$ to obtain alkyldiimidosulfinate as monoanionic ligands by nucleophilic addition of alkali metal alkyls or aryls to the $S=N$ formal double bond.^[12]

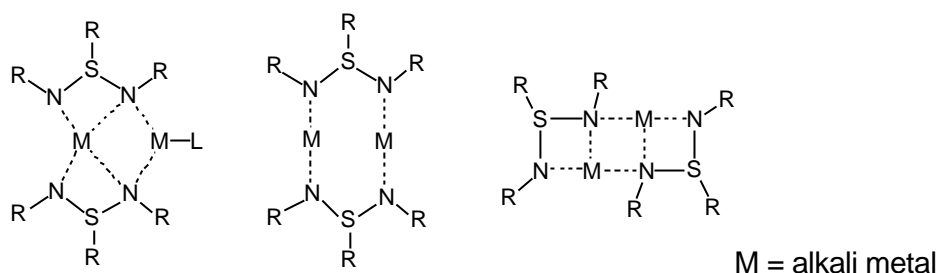


Figure 1: Coordination mode of alkyldiimidosulfinate.^[12]

To expand this initial work, a metal amide instead of a metal alkyl was used in the addition reaction, yielding, after deprotonation of the remaining hydrogen atom, a tripodal dianionic $S(NR)_3^{2-}$ ligand.^[2h] The ligand shows fascinating redox properties. Even traces of an oxidant, like oxygen, lead to a deep blue colour of the compound, indicating the presence of a radical species.

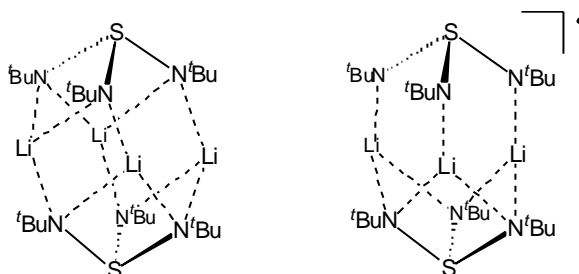


Figure 2: Structures of triimidosulfite and its blue radical.^[13]

The structure of the radical could be determined via ESR spectroscopy. The spectra show a decet of a septet indicating an interaction of the unpaired electron with three nitrogen and three lithium atoms. The radical monoanion $S(N^tBu)_3^{\bullet-}$ forms a dimeric structure with a $S(N^tBu)_3^{2-}$ dianion and three lithium atoms.^[13] Recent works of *Chivers et al.* show subsequently the same result for the heavier congeners.^[14] The formation of stable radicals in the S,N chemistry is quite common. As early as 1925 *Lecher et al.* succeeded in the oxidation of dibenzenesulfeneimine to $PhSNSPh^{\bullet}$, the existence was confirmed 50 years later by ESR spectroscopy.^[15] Many stable

radicals have been reported in the literature. Examples are the N-alkyl-N-(alkylthio)aminyl-radicals $R_1NSR_1^*$, synthesised by *Miura et al.*^[16], or the N-aminothiyl-N-alkylamino radicals $R_1NSN(R_1)MR^*$,^[17] synthesised by *Brunton et al.* Recently *Banister et al.*^[18] succeeded in the synthesis of a stable dithiadiazolyl radical with magnetic properties at low temperatures. Quite notable is the binary sulfurnitride radical $S_2N_3^{+}$,^[19] which is an electron rich inorganic aromatic ring system.

Complete oxidation of the triimidosulfite dianion with halogens leads to sulfurtriimide.^[2k] Until recently, only two reactions were known in which the sulfurtriimide backbone is formed. These syntheses starting from NSF_3 ^[20] or OSF_4 ^[21] are quite hazardous and give poor yields. The new syntheses via triimidosulfite is relatively simple and gives high yields. The reactivity of sulfurtriimide, similar to sulfurdiimide, is dominated by the electropositive character of the sulfur atom. Nucleophilic addition of a lithium alkyl gives alkyltriimidosulfonates.^[22] In 1968 several alkyltriimidosulfonic acids were prepared by the reaction of thioles with chloroamine and alkylamine.^[23]

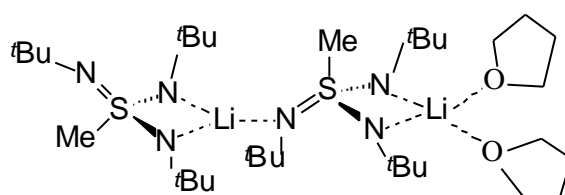


Figure 3: Structure of S-Methyltriimidosulfonate.^[2k]

Sulfate compounds with one or more oxygen atoms isoelectronically replaced by a NR group are known since 1968. *Appel* and *Ross* reported about the syntheses of $[K_2(HN)_4S \cdot KNH_2]$ ^[24] from S,S-dimethylsulfurdiimin with KNH_2 in liquid ammonia, the first binary tetraimidosulfate compound. The addition of a lithiumamide to sulfurtriimide and subsequent deprotonation leads to tetraimidosulfate, the imido analogues of SO_4^{2-} .^[2k]

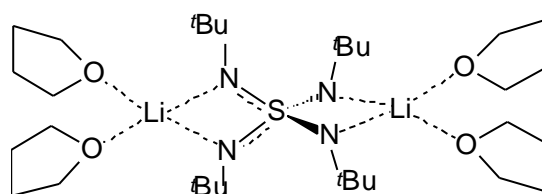
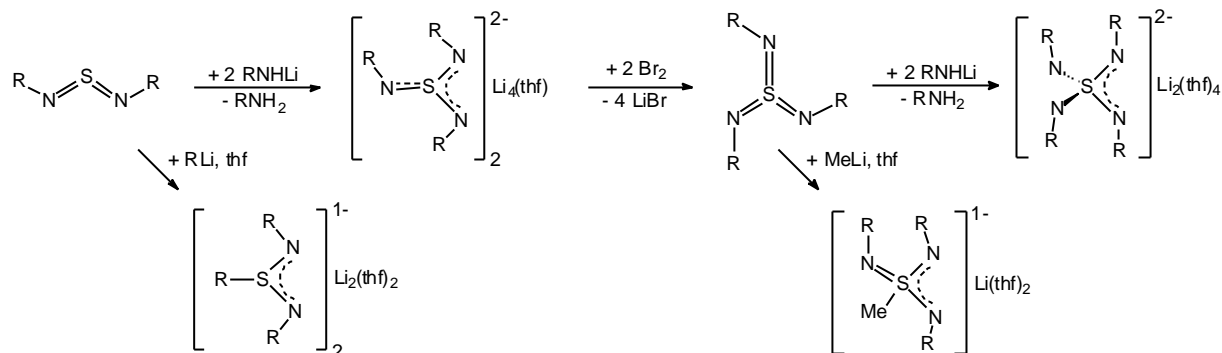


Figure 4: Structure of tetraimidosulfate.^[2k]

All these polyimido sulfur anions are soluble, even in nonpolar organic solvents. In contrast to the simple oxoanions they form molecular contact ion pairs in cage complexes surrounded by a lipophilic layer rather than infinite solid state lattices by multiple oxygen/cation contacts.



Scheme 1: Synthetic pathways to the imido sulfur compounds established by Pauer, Fleischer and Ilge in our group.

In analogy to the sulfur compounds, a series of compounds with the higher homologues of sulfur (selenium and tellurium) are known. In 1976 *Derkach, Barashenko* and coworkers reported the syntheses of seleniumdiimides ($\text{Se}(\text{NR})_2$, $\text{R} = \text{acyl, sulfonyl}$).^[25] *Herberhold and Jellen*, in 1986 succeeded in the isolation of the first aliphatically substituted seleniumdiimide $\text{Se}(\text{N}^t\text{Bu})_2$.^[26] *Chivers* and coworkers reported the syntheses and structure of the $\text{Se}(\text{N}^t\text{Bu})_3^{2-}$ dianion,^[21] as well as the tellurium compounds $\text{Te}(\text{N}^t\text{Bu})_2$ ^[27] and $[\text{Li}_2\{(\text{N}^t\text{Bu})_3\text{Te}\}]_2$.^[21] Although less stable, the selenium and tellurium compounds provide a similar reactivity.

Many of the group 6 metal complexes (Cr, Mo, W) resemble the chemical and structural features of the sulfur compounds presented here. This close relationship is exemplified by the metal oxygen compounds which behave very similar to the sulfur oxygen compounds. In 1980 *Nugent* and coworkers reported the syntheses of $\text{W}(\text{N}^t\text{Bu})_4\text{H}_2$.^[28] In the following decades a great variety of complexes containing the $\text{M}(\text{NR})_4^{2-}$ units have been synthesised by *Wilkinson* and some structures have been reported.^[29]

Scope of the thesis:

Priority task of the thesis was to replace oxygen atoms in sulfur oxoanions SO_n^{m-} or imido groups in sulfur polyimido anions $\text{S}(\text{NR})_n^{m-}$ isoelectronically by R_2C -methylene groups. This would open a wide avenue to new target molecules containing a formally double bonded carbon next to formally double bonded nitrogen atoms in highly charged sulfur-centred anions like $\text{S}(\text{CR}_2)_x(\text{NR})_y^{m-}$. They clearly are reminiscent to sulfur ylides, but at the beginning of this thesis dianionic mixed sulfur imide ylides have been completely unknown. This is even more regrettable as like *Wittig's* phosphonium ylides they should be powerful synthetic tools in $\text{C}=\text{C}$ and $\text{C}=\text{N}$ bond formation reactions. They resemble potential NR and CR_2 transfer to functional groups in organic chemistry in the same molecule. It would be a particularly advantageous aim to fine-tune the NR / CR_2 reactivity to various functional organic groups possibly simultaneously present in the starting material.

To tackle that challenge more information about the already established systems was required. Although *Fleischer* and *Ilge* in our group already investigated several aspects of sulfurtriiimides, triimidosulfites, tetraimidosulfates and S-methyl-triimidosulfonates many questions remained open:

- What is the nature and reactivity of the $\text{S}-\text{NR}$ bond ($\text{S}=\text{N}$ vs. S^+-N^-)?
- Is that nature and reactivity affected by the coordinated metal?
- What would be the synthetic route to mixed sulfur imide ylides?
- How would they react?
- What is the nature and reactivity of the $\text{S}-\text{CR}_2$ bond (ylidic vs. ylenic character)?

Thus, first of all the metal coordination of the triimidosulfite followed by anion solvation was elucidated. Since the S-methyl-triimidosulfonates seemed appropriate starting materials for the sulfur ylides their metal coordination has been studied first to get some insights on the $\text{S}-\text{NR}$ bonding and to evaluate the opportunity of additional deprotonation of the methyl group. The synthesis and structural characterisation of the first dianionic sulfur(IV) and sulfur(VI) ylides are presented and their reactivity has been investigated briefly.

2 S(IV)-Compounds

2.1 Introduction

To date the only established sulfur(IV) polyimido species are the sulfurdiimides $S(NR)_2$, triimidosulfites $S(NR)_3^{2-}$ and alkyl- or aryldiimidosulfates $RS(NR)_2$. Because of the variable metal coordination and the rich redox chemistry involving single electron oxidation we were predominately interested in reactions of the triimidosulfites. In transmetalation reactions starting from $[Li_4\{(N^tBu)_3S\}_2]$ many metal complexes were obtained, mainly containing Group 2 or Group 14 metals. However, an orbital controlled transition metal coordination should have a considerable impact on the S–N bond properties compared to mainly electrostatic interactions in the known examples.

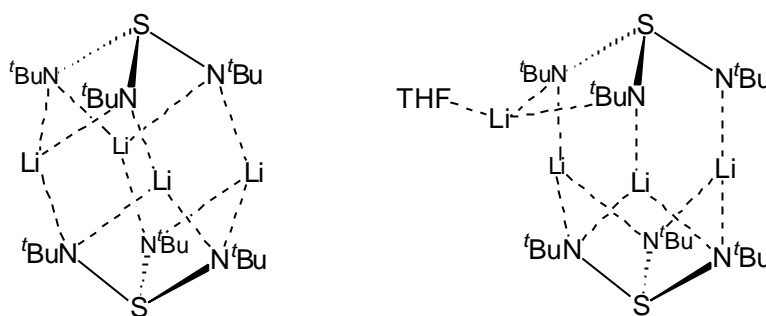
The results presented in the second part took advantage of the fact that the two lithium atoms in the $[Li_2\{(N^tBu)_3S\}]$ monomer provide a vacant coordination site for a metal. Once the missing metal is coordinated the preorganised Li_2M triangle templates a η^3 bonding site capable of anion solvation.

Finally, the synthesis and structure of the first sulfur(IV) ylide starting from alkyl-diimidosulfate $RS(NR)_2$ is presented. The new class of alkylendiimidosulfates and its unprecedented coordination and reactivity is revealed.

2.2 Triimidosulfites

Only three different triimidosulfites $S(NR)_3^{2-}$ are known. First *Gieren* and *Narayanan*^[30] reported about a sulfoxyl substituted compound with $R = SO_2(C_6H_4)Me$. *Roesky* and coworkers^[31] reported a similar compound with $R = SO_2Ph$. In 1992, *Pauer*,^[2h] a member of our research group, succeeded in the synthesis of the alkyl substituted triimidosulfite with $R = ^tBu$. The lithium salt $[Li_2\{(N^tBu)_3S\}]_2$ exhibits a dimeric structure, comprising two cap shaped dianions, facing each other with their concave sites in a staggered conformation (Scheme 2, left). In the presence of a donor molecule like thf one lithium atom leaves the

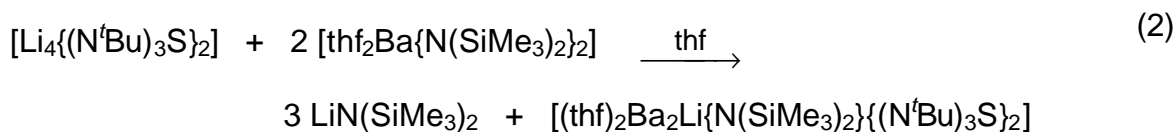
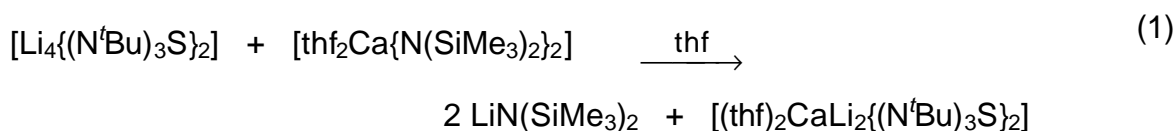
hexameric cage to the periphery and is coordinated only by two nitrogen atoms (Scheme 2, right).



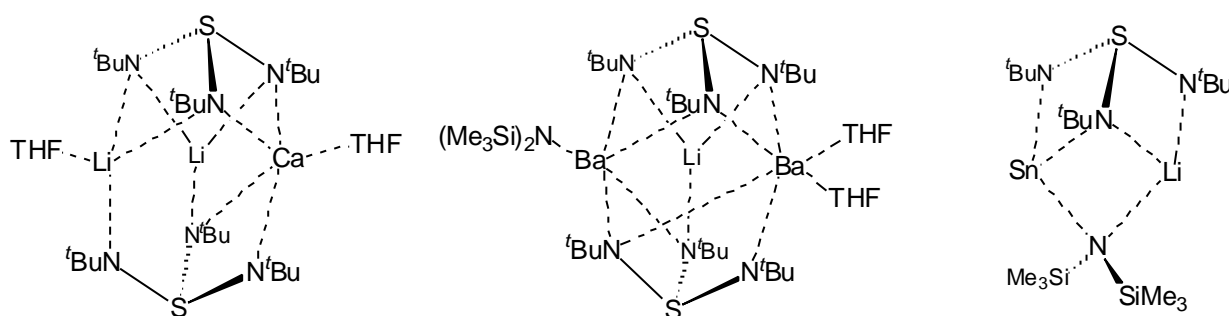
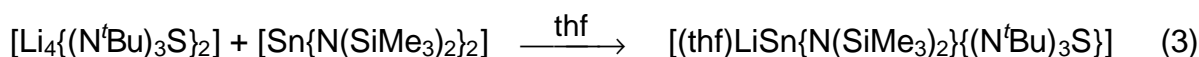
Scheme 2: Structure of $[Li_2\{(N^tBu)_3S\}]_2$ (left) and its thf adduct (right).

2.2.1 Transmetalation Reactions

It is an obvious course to employ the tripodal triimidosulfite in metal coordination. While various monoanionic (e.g. tripyrazolylborate)^[32] and trianionic (e.g. triamidomethane and –silane)^[33] tripodal ligand systems are known, the triimidosulfite anion is the first dianionic system. Their coordination chemistry is unique among the chelating nitrogen ligands due to the two negative charges and its cap shaped geometry. In contrast to the $S(NR)_3^{2-}$ dianion the analogous carbon compounds (guanidates $C(NR)_3^{2-}$) are planar.^[6a] The cap shaped geometry together with the steric demand of the nitrogen bonded substituents should enable homoleptic metal(II) complexes. Several transmetalation reactions with main group metals have been reported in the last few years from *Fleischer et al.* in our group. Metal amides of alkaline earth metals (Mg, Ca, Ba) and Sn,^[34] predominantly used in deprotonation reactions, are used. Different types of complexes are obtained in the reactions with $[thf_2M\{N(SiMe_3)_2\}_2]$ (M = Ca, Ba). While two lithium atoms are still present in the calcium derivative (eq 1) only one remains in the barium complex (eq. 2). Hence, they exhibit different levels of transmetalation. In the calcium complex only half the equivalent of the present lithium cations is replaced by calcium dications, whereas in the barium complex three out of four lithium cations are exchanged by two barium dications. The bis(trimethylsilyl)amide group found in the barium complex provides charge balance. In both compounds the dimeric structure of two cap shaped ligands facing each other with their concave sides is retained (Scheme 3).



The monomeric tin derivative is obtained in the analogue reaction of triimidosulfite with $[\text{Sn}\{\text{N}(\text{SiMe}_3)_2\}_2]$ (eq. 3).^[34]



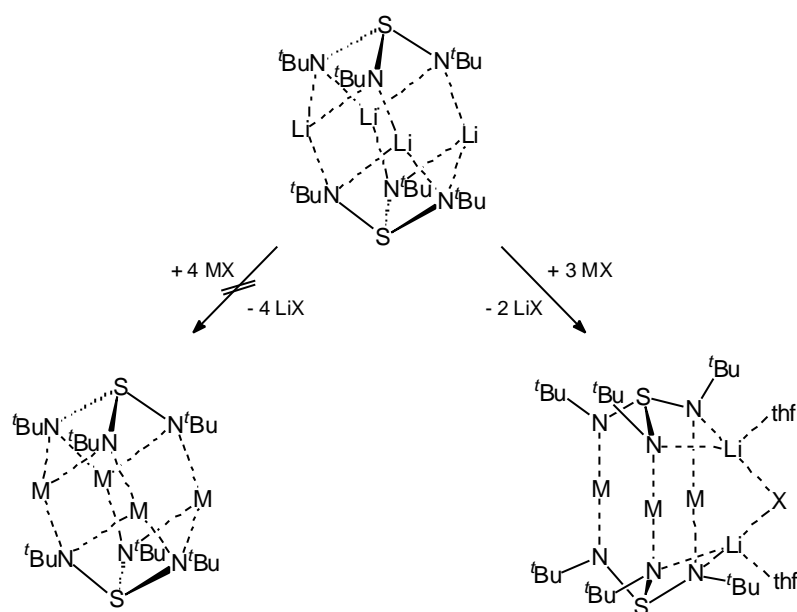
Scheme 3: Structures of the transmetalation products with $M\{\text{N}(\text{SiMe}_3)_2\}_2$ ($M = \text{Ca}, \text{Ba}, \text{Sn}$).

Depending on the electronic requirements, different resonance forms of the ligand are utilized, by which the charges of the coordinated cations are stabilised. The electronic requirements of different cations can also be satisfied simultaneously. Therefore, mixed metal complexes are quite common in the coordination chemistry of this ligand.

2.2.1.1 Transmetalation with Coinage Metal Halides

The structure of the triimidosulfite $[\text{Li}_4\{(\text{N}^t\text{Bu})_3\text{S}\}_2]$ and in particular the thf coordinated $[(\text{thf})\text{Li}_4\{(\text{N}^t\text{Bu})_3\text{S}\}_2]$ suggest, that there is not quite enough space for the four lithium cations. The monovalent coinage metal cations should therefore give rise to different coordination polyhedra. In contrast to lithium they prefer linear two fold coordination.

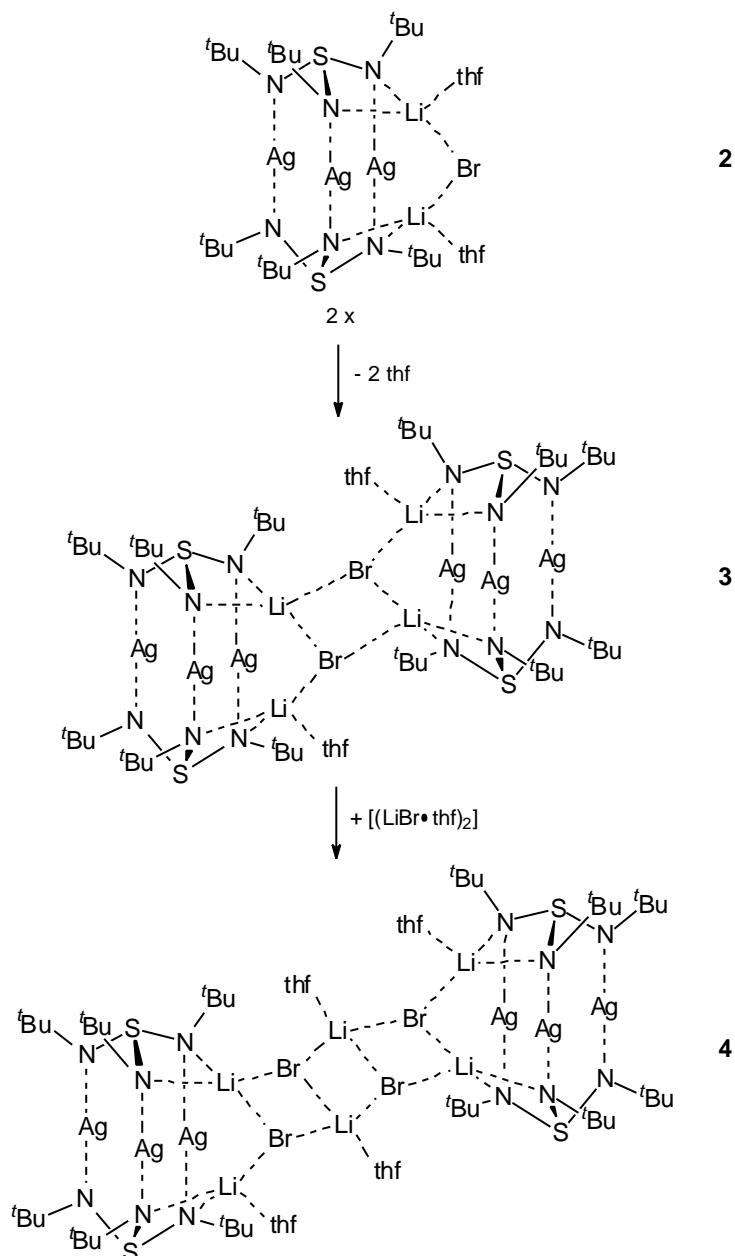
They should force the alkyl groups at nitrogen to be arranged in an eclipsed conformation rather than in a staggered one found in the lithium complexes. Coinage metal halides undergo transmetalation reactions with dilithium triimidosulfite. Although four equivalents of copper iodide were used for complete transmetalation only three of the four present lithium metal centers in the dimer of the starting material are replaced by copper (Scheme 4). In addition, one equivalent of the eliminated lithium halide is co-ordinated to the periphery of the complex $[(\text{thf})_2\text{Cu}_3\text{Li}_2\{\text{(N}^t\text{Bu)}_3\text{S}\}_2]$, (**1**).



Scheme 4: Transmetalation of Triimidosulfite with *CuI* and *AgBr*.

Similar to the reaction of triimidosulfite with copper iodide only three lithium cations in the dimer are replaced by silver atoms in the reaction with silver bromide. The obtained silver complex $[(\text{thf})_2\text{Ag}_3\text{Li}_2\text{Br}\{\text{(N}^t\text{Bu)}_3\text{S}\}_2]$, (**2**), is isotype but not isostructural to **1**. However, **2** is by no means the only product from that reaction. LiBr , the product of the salt elimination, is reasonably well soluble in *thf* to give various $[(\text{thf} \cdot \text{LiBr})_n]$ complexes.^[35] To recover the silver complex from the reaction solution and to suppress formation of soluble lithiumbromide the *thf* has to be removed in vacuum and to be replaced by a non-donating solvent like hexane. In correlation to the time and, hence, to the amount of soluble LiBr is formed, different silver triimidosulfites co-complexed with lithiumbromide are obtained. The longer the complex **2** is exposed to the mother liquor the bigger the co-complexed LiBr moieties are. So far we retrieved three different silver triimidosulfites with ascend content of LiBr and we can't see any

reason way there shouldn't be more to come. While the monomeric complex **2** is isotype to **1**, $[(\text{thf})\text{Ag}_3\text{Li}_2\text{Br}\{(\text{N}^t\text{Bu})_3\text{S}\}_2]_2$, (**3**), can be rationalised as dimerised **2** by removing one donor base and switching the Li–thf contact to a Li–Br contact (Scheme 5). A central Li_2Br_2 four membered ring is formed. Insertion of a $[(\text{thf} \cdot \text{LiBr})_2]$ unit in the Li–Br bond of that four membered ring gives $[(\text{thf})_2\text{Ag}_3\text{Li}_3\text{Br}_2\{(\text{N}^t\text{Bu})_3\text{S}\}_2]$, (**4**).



Scheme 5: Dimerisation of **2** via a Li_2Br_2 square and insertion of $[(\text{thf} \cdot \text{LiBr})_2]$ in **3**.

Unfortunately, the successful synthesis and isolation of the related gold compound has been precluded to date by complex redox processes involving disruption of the triimidosulfite ligand and the formation of a gold mirror and elemental sulfur.

Structure of $[(\text{thf})_2\text{Cu}_3\text{Li}_2\text{I}\{(\text{N}^t\text{Bu})_3\text{S}\}_2]$ (**1**)

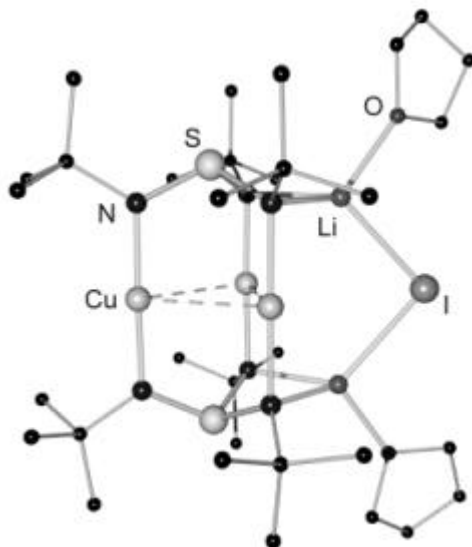


Figure 5: Crystal structure of $[(\text{thf})_2\text{Cu}_3\text{Li}_2\text{I}\{(\text{N}^t\text{Bu})_3\text{S}\}_2]$ (**1**).

Like the starting material $[\text{Li}_4\{(\text{N}^t\text{Bu})_3\text{S}\}_2]$ the structure of $[(\text{thf})_2\text{Cu}_3\text{Li}_2\text{I}\{(\text{N}^t\text{Bu})_3\text{S}\}_2]$, (**1**), consists of two cap shaped triimidosulfite dianions facing each other with their concave site. The ^tBuN -groups are ecliptically arranged with respect to each other. The six nitrogen atoms complex three copper atoms. Each copper atom is linear coordinated to two nitrogen atoms of opposite caps, as one would anticipate from the favoured coordination of Cu(I). The additional η^2 coordination of a lithium cation to each cap forces the involved nitrogen atoms in closer proximity. The persistent linear N–Cu–N coordination causes as a consequence a relatively short distance between Cu2 and Cu3 (251.41(10) pm) compared to the average distance of 269.67(12) pm between the others. The short distance is in the range of $\text{Cu}\cdots\text{Cu}$ distances caused by other A-frame ligands,^[36] but considerably longer than η^2 bridged $\text{Cu}\cdots\text{Cu}$ distances.^[37] As each copper atom is slightly pushed away from the others and the N–Cu–N angle of $177.8(2)^\circ$ indicates electrostatic repulsion rather than metal d^{10} - d^{10} closed shell attraction we don't consider that distance in **1** a bond.^[38]

The peripheral co-complexation of lithium cations induces sever asymmetries in the charge distribution of the triimidosulfite dianion. The S–N bonds coordinated by both metals are elongated because of the competition of both metals with the sulfur atom (av. S–N(Cu,Li) 167.6(5) and av. S–N(Cu) 160.7(5) pm). The same is valid for the

copper nitrogen distances. Additional lithium coordination cause them to elongate by 5 pm from av. 187.6(5) pm in the Cu–N bonds to 192.6(6) pm in the Cu–N(Li) bonds. The longer distances almost exactly match those in the dinuclear copper organyl complex $[\text{CuC}(\text{SiMe}_3)_2\text{C}_5\text{H}_4\text{N}]_2$ ^[39] (191.0(3) pm). The shorter distances are even shorter than those in secondary copper amides $[\text{CuNR}_2]_4$ which are generally close to 191 pm^[40] presumably due to the lower coordination number in **1**. To maintain charge balance both lithium atoms pincer a single iodide anion. A single donating thf molecule is coordinated to each lithium cation to give the preferred fourfold coordination.

Structure of $[(\text{thf})_2\text{Ag}_3\text{Li}_2\text{Br}\{(\text{N}^t\text{Bu})_3\text{S}\}_2]$ (**2**)

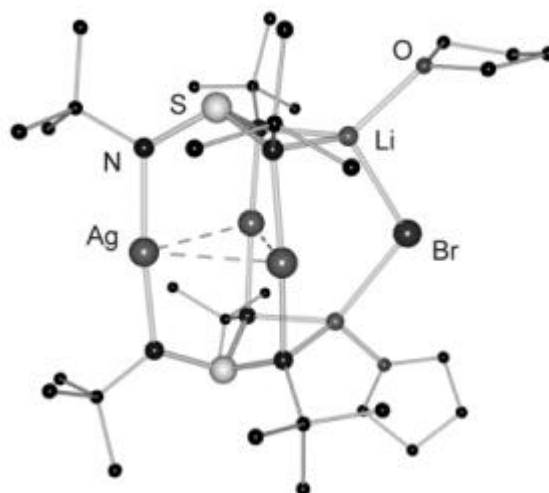


Figure 6: Crystal structure of $[(\text{thf})_2\text{Ag}_3\text{Li}_2\text{Br}\{(\text{N}^t\text{Bu})_3\text{S}\}_2]$ (**2**).

The complex cores $[\text{M}_3\{(\text{N}^t\text{Bu})_3\text{S}\}_2]$ with $\text{M}=\text{Cu}$ in **1** and $\text{M}=\text{Ag}$ in $[(\text{thf})_2\text{Ag}_3\text{Li}_2\text{Br}\{(\text{N}^t\text{Bu})_3\text{S}\}_2]$, (**2**), are very similar. Again, the ecliptically orientated ^tBuN-groups cause a linear coordination of each silver atom and forces them in a Ag_3 triangular arrangement with relatively short $\text{Ag}\cdots\text{Ag}$ distances. (N,N) chelation of a lithium cation to each cap forces the involved nitrogen atoms in closer contact and generates even shorter $\text{Ag}\cdots\text{Ag}$ distances ($\text{Ag}2\cdots\text{Ag}3$ 278.60(7) in comparison to 287.28(7) pm). While the difference between the short and long metal-metal distances is remarkable 18 pm in **1** it is only 9 pm on average in all silver complexes. However, both distances are in the range where $d^{10}\text{-}d^{10}$ interactions in silver complexes are regarded to be important.

Like in **2** these close contacts are mainly supported by A-frame ligands like in $[\text{Ag}_2\{(\text{Py})\text{C}(\text{SiMe}_3)_2\}_2]$, (265.4 pm),^[41] $[\text{Ag}_2\{(\text{Me}_3\text{Si})\text{NC}(\text{Ph})\text{N}(\text{SiMe}_3)\}_2]$, (265.5 pm),^[42] $[\text{Ag}_2\{\text{PhNNNPh}\}_2]$, (266.9 pm),^[43] $[\text{Ag}_2\{(\text{Pyz})_3\text{BH}\}_2]$, (279.6 pm)^[44] and $[\text{Ag}_2\{(\text{O}_2)\text{CPh}\}_2]$, (290.2 pm).^[45] Due to the bigger radius the N–Ag–N angle of $171.83(12)^\circ$ in **2** is more acute than the related angle in **1**. Hence, each silver atom is even more buckled from the centre of the Ag_3 triangle.

Like in **1**, peripheral (N,N) chelation of lithium cations induces asymmetries in the charge distribution of the triimidodisulfite dianion. While the difference in the S–N bond lengths of **2** is only 4.9 pm (6.3 pm in **1**) the Ag–N distance divergence by 8.4 pm is much more pronounced than in **1** (5.0 pm). The softer silver cation tends not to polarise the dianion as much as the harder copper cation.

Structure of $[(\text{thf})\text{Ag}_3\text{Li}_2\text{Br}\{(\text{N}^t\text{Bu})_3\text{S}\}_2]_2$ (**3**)

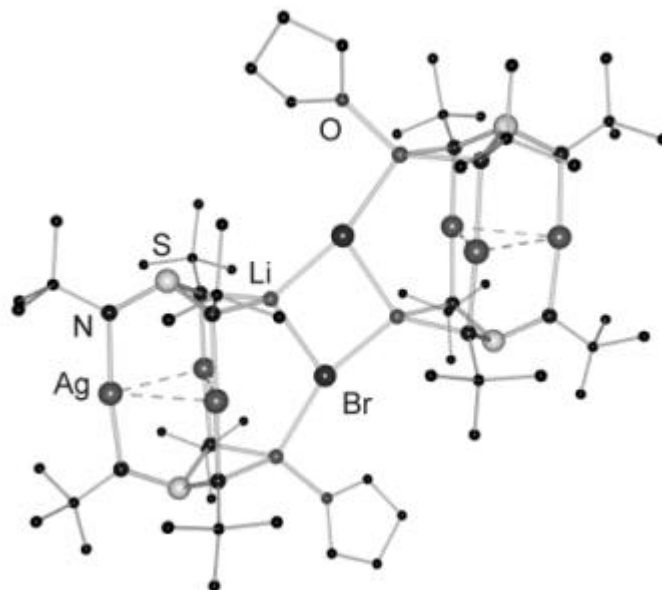


Figure 7: Crystal structure of $[(\text{thf})\text{Ag}_3\text{Li}_2\text{Br}\{(\text{N}^t\text{Bu})_3\text{S}\}_2]_2$ (**3**).

The molecular structure of $[(\text{thf})\text{Ag}_3\text{Li}_2\text{Br}\{(\text{N}^t\text{Bu})_3\text{S}\}_2]_2$, (**3**), consists of a dimer around a Li_2Br_2 four membered ring. Two $[\text{Ag}_3\text{Li}\{(\text{N}^t\text{Bu})_3\text{S}\}_2]$ subunits are connected by opposite sides of that square. The formation of lithium halide squares from *in situ* generated salts is quite common.^[35,46] In thf, lithium bromide forms an infinite ladder. Depending on the nature of donating solvent the Li–X (X = F, Cl, Br, I) bonds from the infinite solid state structures are broken. In a de-integration process, reminiscent to the interconversion process known from the ring stacking and laddering principal of

lithium amides,^[47] isolated squares or cubic structures of LiX are assembled.^[48] The geometrical features of the $[\text{Ag}_3\text{Li}\{(\text{N}^t\text{Bu})_3\text{S}\}_2]$ cages are virtually the same in **2** and **3**. The $\text{Ag}2\cdots\text{Ag}3$ distance in **3** in comparison to the other $\text{Ag}\cdots\text{Ag}$ distances is shortened by 8.8 pm to 278.60(7) pm and the (Li)N-Ag distances are on average 8.4 pm longer than those to the non-metal bridged nitrogen atoms. For further bond lengths and angles see table 2.

Structure of $[(\text{thf})_2\text{Ag}_3\text{Li}_3\text{Br}_2\{(\text{N}^t\text{Bu})_3\text{S}\}_2]_2$ **4**

The crystal structure of $[(\text{thf})_2\text{Ag}_3\text{Li}_3\text{Br}_2\{(\text{N}^t\text{Bu})_3\text{S}\}_2]_2$, (**4**), can be rationalised to be an extension of **3**. A single insertion of a $[(\text{thf}\cdot\text{LiBr})_2]$ square in the Li–Br bond of the four membered ring in **3** gives **4**. Hence, the Li_6Br_4 four-rung ladder is terminated by the $[\text{Ag}_3\{(\text{N}^t\text{Bu})_3\text{S}\}_2]^-$ anionic cages spanning the Li \cdots Li diagonal of the terminal Li_2Br_2 squares. As the central lithium atoms Li3 and Li3a are not linearly coordinated by the two bromide atoms along the ladder spars and are additionally coordinated by a thf molecule each the ladder is folded by an angle of 45.2° (angle between the Li3, Br2, Li3a, Br2a best plane and the Li1, Br1, Li3a, Br2a best plane). Of course, this ladder extension and shift of the silver triimido sulfite moieties has no effect on the geometrical parameters of the cages. The structural features are the same as above. For bond lengths and angles see table 2.

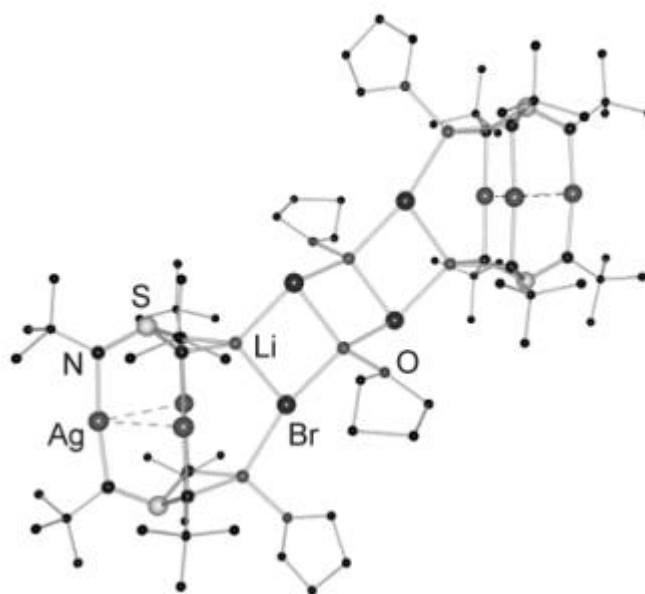


Figure 8: Crystal structure of $[(\text{thf})_2\text{Ag}_3\text{Li}_3\text{Br}_2\{(\text{N}^t\text{Bu})_3\text{S}\}_2]_2$ (**4**).

*Table 2: Selected bond lengths [pm] and angles [°] for 1-4:
The bond lengths and angles of identical subgroups are averaged.*

M = Cu, Ag	1	2	3	4
S – N(M)	160.8(5)	162.5(6)	160.7(8)	162.6(9)
S – N(M,Li)	167.6(6)	167,8(6)	166.9(8)	168.7(9)
(N)M – M(N,Li)	269.75(12)	287.28(7)	286.55(12)	289.25(11)
(N,Li)M – M(N,Li)	251.41(10)	278.60(7)	277.42(11)	279.92(10)
(M)N – M(N)	187.6(5)	209.7(5)	210.8(8)	210.6(8)
(M,Li)N – M(N,Li)	192.6(6)	218.1(6)	214.6(7)	218.3(8)
Li–N(M,Li)	208.0(10)	207.9(13)	206.2(19)	206.4(18)
N-M-N	177.8(2)	171.83(12)	171.9(3)	171.5(3)
(M)N – S – N(M,Li)	109.4(3)	109.9(3)	110.0(5)	110.3(4)
(M,Li)N – S – N(M,Li)	93.0(3)	94.2(3)	94.1(4)	93.5(4)
(N)M – M(N,Li) – M(N,Li)	62.22(3)	61.021(18)	60.99(6)	61.02(3)
(N,Li)M – M(N) – M(N,Li)	55.56(3)	58.010(17)	58.02(3)	57.87(3)

2.2.1.2 Transmetalation with Fe(AcAc)₂

The disposition of the triimidosulfite dianion to facilitate SET processes on one hand and the vast catalytic abilities of iron on the other hand was the motivation to synthesise an iron(II) triimidosulfite complex. A combination of both properties might yield a novel class of oxidation catalysts. Particularly the active sites in metalloproteins like nitrogenases^[49] and Rieske-proteins^[50] witness the synergistic effect between sulfur and iron.

Fleischer in our group previously reported two metathesis reactions of the lithium triimidosulfite with germanium and tin dichloride.^[51] In both reactions complete disintegration of the triimidosulfite to metal *tert*.butylimide and sulfur was observed. Hence, iron dichloride seemed not to be the appropriate metal source in the planned reaction. Because of the strong Lewis acidity of iron dichloride, Fe(AcAc)₂ was used instead in the metathesis reaction to minimise decomposition reactions.

The crystal structure of [Fe₂(μ²-N^tBu)₂((N^tBu)₂S)₂], (**5**), the obtained product, shows two Fe(II) atoms in a central Fe₂N₂ four membered ring containing a centre of inversion. Tetrahedral coordination of each iron atom is completed by (N,N) chelation

of a neutral sulfur diimide molecule. The best planes of both Fe_2N_2 and FeN_2S four membered rings intersect at an angle of 98.8° . The Fe-N(imide) bond lengths of 185.3(4) pm on average are significantly longer than the Fe-N(sulfur diimide) dative bonds of 200.6(4) pm on average. The metal coordination in complex **5** lengthens the S-N bonds by 9.2 pm compared to the parent $\text{S}(\text{N}^t\text{Bu})_2$.^[52]

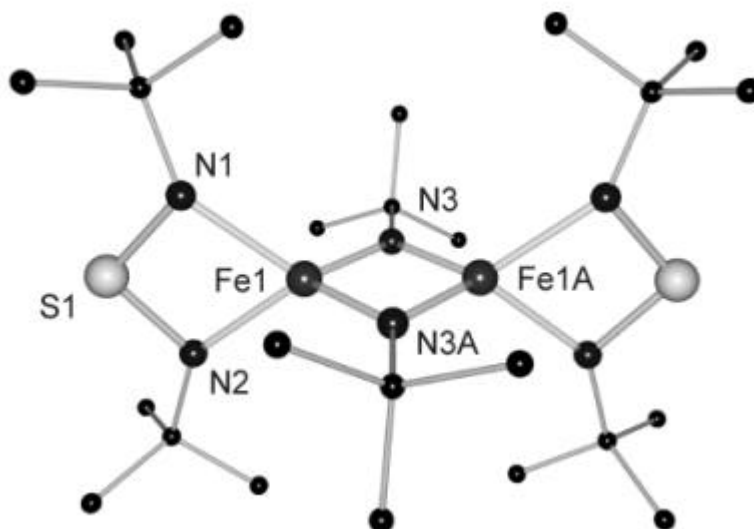


Figure 9: Crystal structure of $[\text{Fe}_2(\eta^2\text{-N}^t\text{Bu})_2\{(\text{N}^t\text{Bu})_2\text{S}\}_2]$ (**5**).

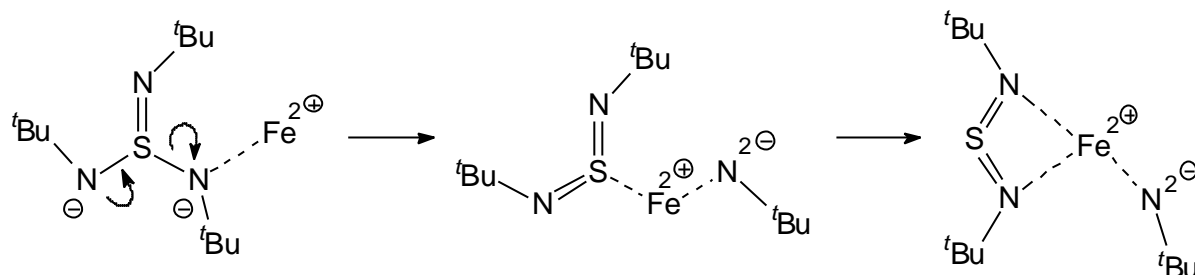
Table 3: Selected bond length [pm] and angles [$^\circ$] of $[\text{Fe}_2(\eta^2\text{-N}^t\text{Bu})_2\{(\text{N}^t\text{Bu})_2\text{S}\}_2]$ (**5**):

S1–N1	162.6(4)	S1–N2	163.3(4)	N1–Fe1	200.7(4)
N2–Fe1	200.5(4)	Fe1–N3	185.4(4)	Fe1–N3A	185.1(4)
N1–S1–N2	93.2(2)	N1–Fe1–N2	72.36(16)	N3–Fe1–N3A	97.50(16)
N1–Fe1–N3	122.89(17)	Fe1–N3–Fe1A	82.50(16)		

The structural motif of a μ bridging imide group is well known in iron imidates like $[\text{Fe}_3(\text{S})_2(\mu_2\text{-N}^t\text{Bu})_2(\text{NO})_4]$,^[53] $[\{(\text{CO})_3\text{Fe}\}_3(\mu_3\text{-NEt})_2]$ ^[54] or $[\{(\text{CO})_3\text{Fe}\}_3(\mu_2\text{-NMe})(\mu_3\text{-NMe})]$ ^[55]. In **5**, each iron atom is η^2 -coordinated with a sulfur diimide. This η^2 coordination mode of sulfur diimide is well established in several d-block metal complexes such as $[(\text{CO})_4\text{W}\{\eta^2\text{-}(\text{N}^t\text{Bu})_2\text{S}\}]$ ^[56] or $[(\text{CO})_5\text{Mn}(\text{CO})_3\text{Mn}\{\eta^2\text{-}(\text{N}^t\text{Bu})_2\text{S}\}]$ ^[57]. Otherwise η^1 coordination is observed in $[(\text{C}_2\text{H}_4)\text{Cl}_2\text{W}\{\eta^1\text{-}(\text{N}^t\text{Bu})_2\text{S}\}]$ ^[58] or $[\{\text{Ph}_3\text{P}\}_2(\text{CO})\text{ClRuH}\{\eta^1\text{-}(\text{NSNPh})\}]$.^[59]

This result confirms ${}^t\text{BuN}^{2-}$ abstraction from the triimidosulfite to give sulfur diimide. The iron compound **5** is the intermediate missing link in the metal imide formation from triimidosulfite (Scheme 6). The first step might be an insertion of the iron

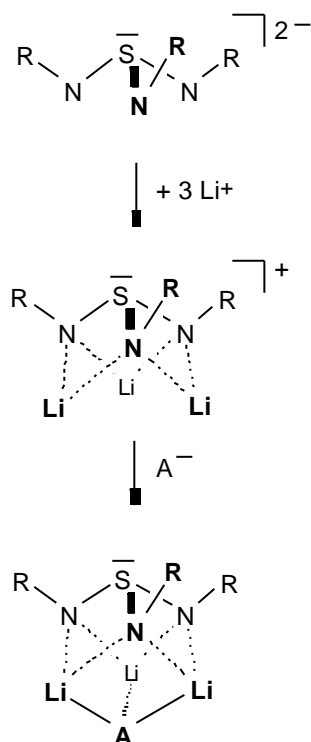
dication into the S-N bond followed by 1-2 migration of the iron atom from sulfur to nitrogen. The coordination sphere is completed by the second nitrogen atom of the sulfurdiimide. This imide formation might turn out to be a useful reaction in imidation or transimidation.



Scheme 6: Abstraction of $t\text{BuN}^{2-}$ from triimidosulfite.

2.2.2 Anion-Solvation

From our earlier work on the dilithium triimidosulfite, it is known to be capable to coordinate various salts like LiHal in $[(\text{thf})_3\text{Li}_3\{\text{I}(\text{N}^t\text{Bu})_3\text{S}\}]_2^{[13]}$ and $[(\text{thf})_3\text{Li}_3\text{Br}\{\text{N}^t\text{Bu}\}_3\text{S}\}]_2^{[13]}$ LiN_3 in $[(\text{thf})_3\text{Li}_3\text{N}_3\{\text{N}^t\text{Bu}\}_3\text{S}\}]_\infty^{[60]}$ or KO^tBu in $[(\text{thf})_2\text{Li}_2\text{K}(\text{O}^t\text{Bu})\{\text{N}^t\text{Bu}\}_3\text{S}\}]_2^{[61]}$

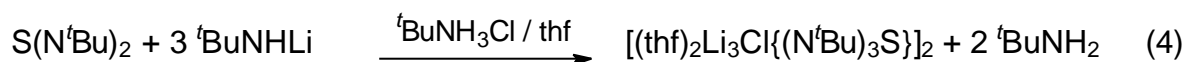


Scheme 7: Conversion of the cap shaped $\text{S}(\text{NR})_3^{2-}$ dianion to a cationic $\text{Li}_3(\text{NR})_3\text{S}^+$ ligand capable of anion solvation.

The coordination of three lithium atoms to the cap shaped $\text{S}(\text{N}^t\text{Bu})_3^{2-}$ dianion leads to a cationic $[\text{Li}_3(\text{N}^t\text{Bu})_3\text{S}]^+$ ligand, which describes a conversion of a tripodal coordinating dianion to a tripodal coordinating cation capable of anion solvation. The $\text{Li}\Delta\text{Li}$ distances in this cap shaped $[\text{Li}_3(\text{N}^t\text{Bu})_3\text{S}]^+$ cation (mid Scheme 7) are quite variable and depend on the radius of the coordinated anion (275 (S^{2-}),^[62] 285 (N^{3-}),^[60] 293 (Br^-),^[13] 300 pm (Γ),^[13]). The dilithium triimidoseleinite $[\text{Li}_2\{(\text{N}^t\text{Bu})_3\text{Se}\}]_2$ ^[21] shows a similar property to co-coordinate lithiumhalides.^[63]

2.2.2.1 Halide-Addition

Fleischer in our group isolated the bromide and iodide adduct as an intermediate in the oxidation reactions of triimidosulfite with bromine or iodine. In both cases the halogen anion is η^3 coordinated to the three lithium atoms. The coordination sphere of the lithium atoms is completed by the η^2 coordination of the triimidosulfite dianion and one thf. Since the oxidation reaction with chlorine could not be controlled exact enough, the chloride adduct was not identified. Hence another synthetic route was adopted. The syntheses of triimidosulfite from sulfur diimide with two equivalents of lithium *tert*butylamide was attempted in the presence of *tert*butylammoniumchloride.



6

Storing of the reaction solution for several days at -36°C affords colourless crystals of **6** suitable for X-ray structure determination. The crystal structure shows in contrast to the bromide or iodide adduct a dimerisation via a distorted Li_2Cl_2 square. Like for the heavier congeners the lithium atoms are η^2 coordinated by the triimidosulfite dianion, but only two lithium cations are coordinated to a thf molecule each, whereas the third lithium cation provides the link to a second chloride anion in the dimer. Thus coordination mode is known from the N_3^- -adduct.^[60] Consequently, the coordination sphere of Li1 and Li2 is tetrahedral while Li3 is almost located in the base of a trigonal pyramid together with N2, N3 and Cl1A. Cl1 is the apex of that pyramid.

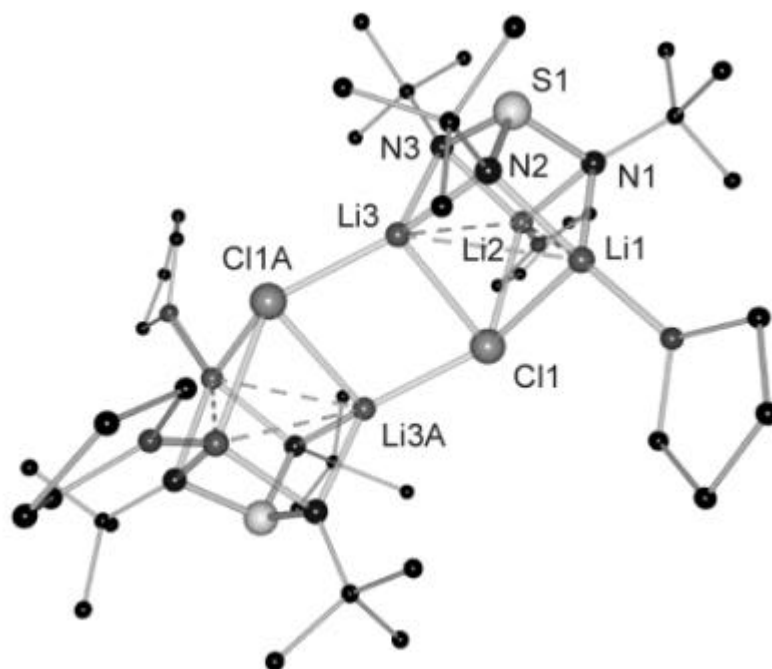


Figure 10: Crystal structure of $[(\text{thf})_2\text{Li}_3\text{Cl}\{(\text{N}^t\text{Bu})_3\text{S}\}]_2$ (**6**).

Table 4: Selected bond length [pm] and angles [$^\circ$] of $[(\text{thf})_2\text{Li}_3\text{Cl}\{(\text{N}^t\text{Bu})_3\text{S}\}]_2$ (**6**):

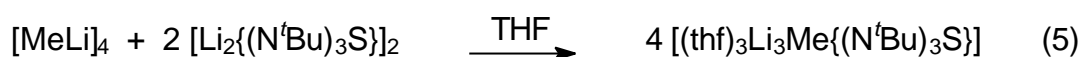
S1–N1	166.4(2)	S1–N2	165.5(2)	S1–N3	165.8(2)
N1–Li1	200.7(5)	N1–Li2	207.3(5)	N2–Li1	208.4(6)
N2–Li3	199.1(5)	N3–Li3	210.0(5)	N3–Li2	199.1(5)
Li1–Cl1	248.4(5)	Li2–Cl1	253.2(5)	Li3–Cl1	253.2(5)
Li3–Cl1A	235.5(5)				
N1–S1–N2	100.76(12)	N2–S1–N3	100.55(12)	N3–S1–N1	99.49(11)
Cl1A–Li3–Cl1	101.45(17)	Li3–Cl1–Li3A	78.55(18)		

Thus formation of a dimeric structure in **6** is not an unusual feature. In comparison to its heavier homologues the chloride anion is a stronger Lewis base and prefers a coordination of four lithium cations.

2.2.2.2 Carbanion-Addition

In general the Li \cdots Li distances in $[\text{Li}_3(\text{N}^t\text{Bu})_3\text{S}]^+$ are larger than those found in parent tetrameric lithium organics (241 pm ($[\text{tBuLi}]_4$),^[64] 253 pm ($[\text{EtLi}]_4$),^[65] 259 pm ($[\text{MeLi}]_4$),^[66]) but similar distances can be found in hexameric aggregates (294 pm in $[\text{nBuLi}]_6$)^[64] or 296 pm in $[\text{iPrLi}]_6$),^[67].

With this in mind the dilithium triimidosulfite $[\text{Li}_2\{(\text{N}^t\text{Bu})_3\text{S}\}]_2$ should be a suitable synthon to achieve disintegration of the parent $[\text{MeLi}]_4$ tetramer and stabilisation of a MeLi monomer in a $[(\text{thf})_3\text{Li}_3\text{Me}\{(\text{N}^t\text{Bu})_3\text{S}\}]$ complex, similar to the halide adduct species mentioned above. $[\text{MeLi}]_4$ reacts smoothly with a triimidosulfite solution when warmed to slightly above room temperature for a couple of minutes. Both, the $[\text{MeLi}]_4$ tetramer and the $[\text{Li}_2\{(\text{N}^t\text{Bu})_3\text{S}\}]_2$ dimer disintegrate and recombine to give $[(\text{thf})_3\text{Li}_3\text{Me}\{(\text{N}^t\text{Bu})_3\text{S}\}]$ (**7**), (eq. 5).



5 is a white solid which turns blue instantaneously when it is exposed to air. It is as pyrophoric as parent $[(\text{MeLi})_4]_\infty$. The compound is readily soluble in thf but also in hexane once it is thf coordinated.

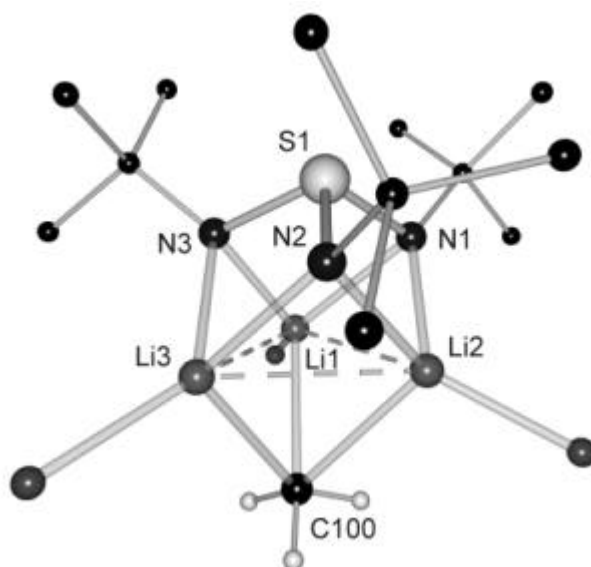


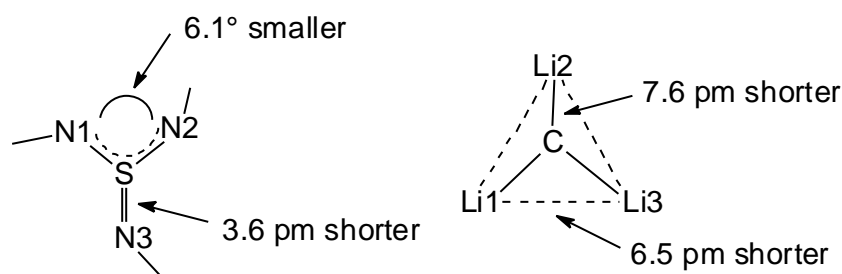
Figure 11: Solid state structure of $[(\text{thf})_3\text{Li}_3\text{Me}\{(\text{N}^t\text{Bu})_3\text{S}\}]$ (**5**) (hydrogen atoms at the *t*Bu substituents and thf carbon atoms are omitted for clarity).

Equation 5 describes the recombination of one tetrameric methyllithium and two dimeric triimidosulfites to give four methanide-tri-lithium-triimidosulfite monomers. $[(\text{thf})_3\text{Li}_3\text{Me}\{(\text{N}^t\text{Bu})_3\text{S}\}]$ (**7**) was crystallised from hexane solution at $-36\text{ }^\circ\text{C}$. The colourless crystals were of sufficient quality for X-ray crystallographic studies.

Table 5: Selected bond length [pm] and angles [°] of [(thf)₃Li₃Me{(N^tBu)₃S}] **7**:

S1–N1	166.7(3)	S1–N2	167.1(3)	S1–N3	163.2(3)
N1–Li1	205.9(7)	N1–Li2	202.8(7)	N2–Li2	212.4(7)
N2–Li3	197.5(7)	N3–Li3	215.4(7)	N3–Li1	199.2(7)
Li1–Li2	263.5(8)	Li2–Li3	267.0(9)	Li3–Li1	257.4(8)
C100–Li1	232.5(8)	C100–Li2	224.0(7)	C100–Li3	230.6(8)
N1–S1–N2	96.84(15)	N2–S1–N3	101.03(14)	N3–S1–N1	104.26(15)

The crystal structure of **7** (Figure 11) shows a triimidosulfite, coordinated to three lithium atoms η^2 arranged at every SN₂ bisection to form a Li₃ triangle known from lithium organics. The triimidosulfite dianion caps the upper face of the triangle, while the lower face is capped by the methanide anion.^[68] The Li–C distances in **7** range from 224.0(7) to 232.5(8) pm and matches with those found in lithium organics (224.6(14) in [^tBuLi]₄,^[64] 225.6(6) in [MeLi]₄,^[66] 228.1 pm in [EtLi]₄^[65]). The Li Δ Li distances in **7** range from 257.4(8) to 267.0(9) pm and the shortest is almost identical to the related distance in [MeLi]₄. The three thf molecules coordinated to the lithium atoms form a suitable cavity and provide sufficient shielding to the methanide anion. At first sight one anticipates a C₃ axis in the molecule along the S1 \cdots C100 vector. But apart from the non isosceles Li₃ triangle the S–N bonds of the triimidosulfite are not equal. The S1–N3 bond (163.2(3) pm) is 3.6 pm shorter than the other two (av. 166.8(3) pm). N3 is coordinated to the shorter Li1 Δ Li3 side of the Li₃ triangle (257.4(8) pm; 6.5 pm shorter than the two others). To counterbalance this N3-shift, the methanide C100 is more shifted towards Li2. The C100–Li2 distance (224.0(7) pm) is 7.6 pm shorter than the C100–Li1,3 distances (av. 231.6(8) pm) (Scheme 8).



Scheme 8: Bonding in the triimidosulfite moiety: N3 is coordinated to the shorter Li1 \cdots Li3 side of the Li₃ triangle while the methanide C is shifted towards Li2.

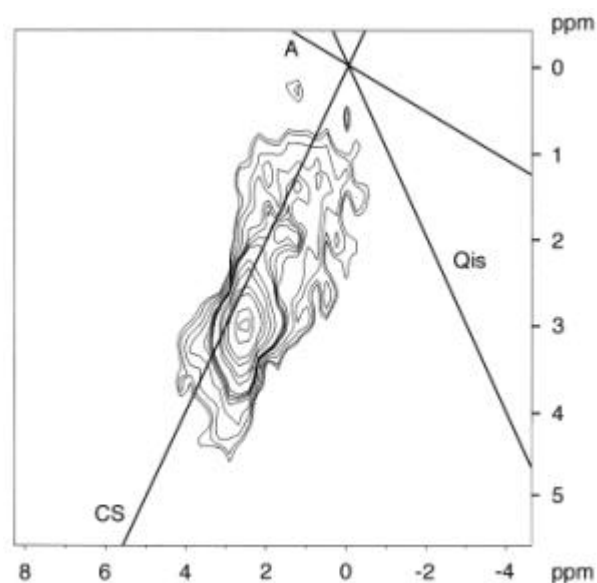


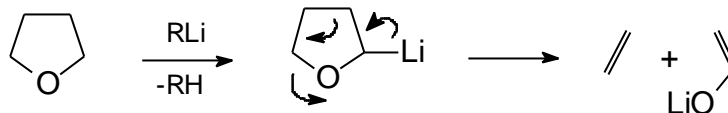
Figure 12: The unsheared 3Q MQMAS ${}^7\text{Li}$ solid-state NMR spectrum of **5** shows two ${}^7\text{Li}$ sites with an intensity ratio of nearly 2 for the two signals (sharp peak, assigned to Li1 and Li3 of the solid state structure): 1 (broad peak, assigned to Li2 of the solid state structure). Additional axes are included for interpretation: **A** is the anisotropic axis with the slope of $-7/27$. **Qis** is the quadrupolar induced shift axis and **CS** is the chemical shift axis.

The unsheared 2D ${}^7\text{Li}$ MQMAS NMR spectrum of **5** shows a sharp and a broad signal at isotropic shifts of $\delta_{\text{iso}} = 1.55$ and 2.75 , respectively, with the area ratio of 2:1. The shape of the contour plot in Figure 12 indicates that the site at $\delta_{\text{iso}} = 1.55$ is well defined because the signal shows neither a distribution of chemical shifts nor of quadrupolar couplings. This peak can be assigned to the two sites Li1 and Li3, because they have the same distance to the methanide anion. Hence, the broad signal of the 2D MQMAS has to be assigned to the Li2 site and shows a small distribution of chemical shifts. The result of the ${}^7\text{Li}$ MQMAS is consistent with the single pulse high power decoupled ${}^6\text{Li}$ MAS NMR experiment, which also exhibits two sites for **5** in the ratio 2:1.

2.2.2.3 Ethylenoxidadduct

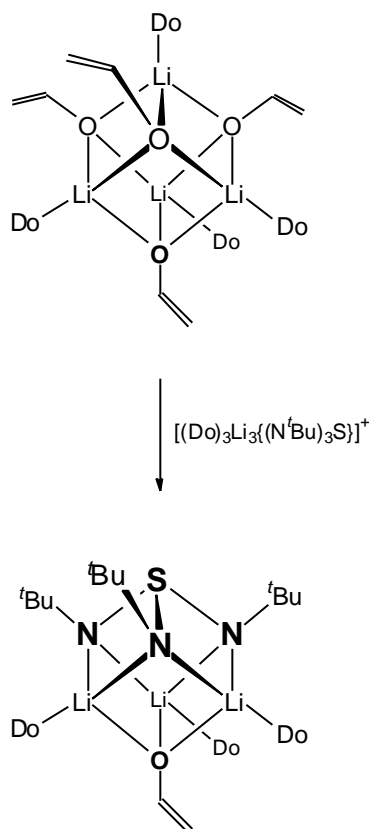
The ether cleavage reaction is one of the most common side reactions in organometallic chemistry as the RLi starting material is often dissolved in ethers.^[69] Apart from the mostly unintended reaction to side products, cyclic ethers are

deliberately employed in this reaction^[70] as they give synthetically important lithium enolates^[71] by α -metalation followed by a $[\pi 4s+\pi 2s]$ -cycloreversion. In this reaction the most common cyclic ether tetrahydrofuran (thf) gives lithium ethyleneoxide and ethene.



Scheme 9: Ether cleavage reaction of thf by lithium organics: α -metalation is followed by a $[\pi 4s+\pi 2s]$ -cycloreversion to give lithium ethyleneoxide and ethene.

Recently it was found that ethene can insert in the Li–C bond of unreacted ^tBuLi, to give *n*-hexyllithium [(thf)LiCH₂CH₂^tBu]₄.^[72] Because the ionic character of the Li–O bond lithium enolates tend to aggregate in the solid state as solvated dimers, tetramers or even hexamers.^[71]



Scheme 10: The computed S_4 symmetric cubic tetramer $[(Do)(LiOCH=CH_2)]_4$ is the most stable lithium enolate solvate (top). $[(thf)_3Li_3(OCH=CH_2)\{(N^tBu)_3S\}]$ **8** mimics the same aggregation by replacement of the top $[(Do)(LiOCH=CH_2)]_3^{2-}$ dianionic fragment by the triimido sulfite dianion $[S(N^tBu)_3]^{2-}$ (bottom).

Although heteroatoms, like in the mixed lithium enolate/chiral amide structures^[73] or adjacent double bonds,^[74] help to coordinate the lithium atoms and to decrease the degree of aggregation, structurally characterised ethyleneoxides generally form complex cage like structures.^[70,75] The S_4 symmetric tetrasolvated tetramer $[(Me_2O)(LiOCH=CH_2)]_4$ was computed to be the most stable oligomer (Scheme 2-7, top).^[76]

$[(thf)_3Li_3(OCH=CH_2)\{(N^tBu)_3S\}]$, (**8**), formally derives from the tetramer $[(Me_2O)(LiOCH=CH_2)]_4$ by replacement of the top $[(Me_2O)(LiOCH=CH_2)_3]^{2-}$ dianionic fragment by the diimido sulfite dianion $[S(N^tBu)_3]^{2-}$ (Scheme 10, bottom). This tripodal dianion templates the Li_3 triangle required for the oxygen atom of the single ethyleneoxide ion to be η^3 metal coordinated.

By analogy to Mulveys inverse crowns^[77] like $[M_2Mg_2(NR_2)_4]^{2+}$, $M = Li, Na, K$ the $[Li_3(N^tBu)_3S]^+$ cationic motif in **8** can be regarded an inverse podant, capable of single-anion coordination to e.g. methanide.^[78] In the attempted coordination of *tert*butanide from $tBuLi$ we isolated and crystallised **8** in a high-temperature (**8a**; $r_{cal.} = 1.036 \text{ Mg/m}^3$) and a low-temperature phase (**8b**; $r_{cal.} = 1.073 \text{ Mg/m}^3$). For the first time an *in situ* generated, industrial important product is stabilised by the diimido sulfite dianion.

Both phases contain the cap shaped triimido sulfite dianion coordinated to three lithium atoms close to the SN_2 bisectors. The single ethyleneoxide anion is η^3 coordinated via the oxygen atom to those three metal centres (Figure 13). Thus, the oxygen atom forms one corner of a SN_3Li_3O cube. In both polymorphs the $H_2C=CHO$ group is disordered.

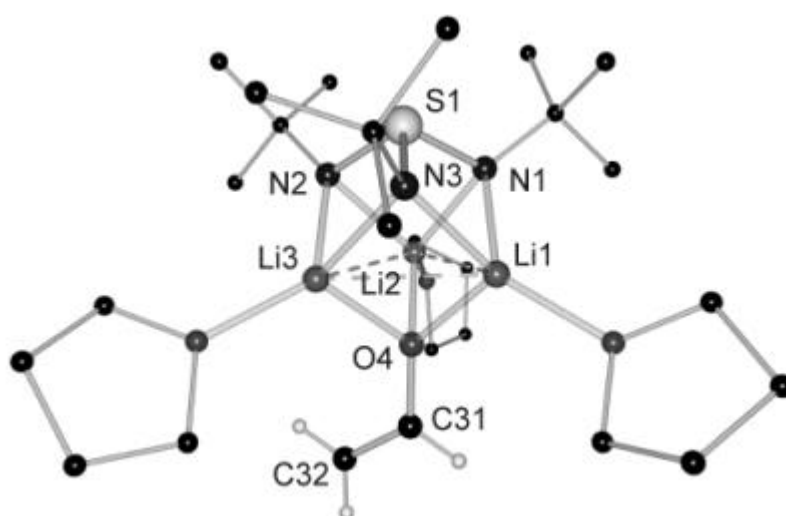


Fig. 13: Solid-state structure of $[(thf)_3Li_3(OCH=CH_2)\{(N^tBu)_3S\}]$ **8**.

Table 6: Selected average bond lengths (pm) and angles (°) of **8a** and **8b**:

	8a	8b		8a	8b
S–N	165.3(3)	166.4(2)	Li Δ Li	264.3(10)	265.5(6)
Long Li–N	210.9(7)	211.0(5)	C31–O4	135.8(6)	133.1(6)
short Li–N	202.3(7)	200.4(5)	C31–C32	136.5(13)	132.1(5)
Li–OCH=CH ₂	195.7(8)	196.4(11)	N–S–N	100.4(2)	100.38(11)

In **8a** it slots in between the three thf molecules with a 0.8/0.1/0.1 site occupation factor (sof) each. In **8b** the ethylene group is only disordered over two positions: staggered between Li2 and Li3 (0.8 sof) and eclipsed to Li1 (0.2 sof). The av S–N bond lengths of 165.3 and 166.4 pm for **8a** and **8b**, respectively, are almost identical. The Li₃N₃ array is not a regular chair-shaped ring but shows alternating long and short Li–N bonds. The av Li Δ Li distances in the cap shaped [Li₃(N^tBu)₃S]⁺ cation are 264.3 pm in **8a** and 265.5 pm in **8b** and are only marginally longer than the distances found in parent tetrameric lithium organics (241 ([^tBuLi]₄),^[64] 253 ([EtLi]₄),^[65] 259 pm ([MeLi]₄),^[66]). The similarities in the bond lengths of both structures indicate that the different phases are not a result of severe changes in bond distances. However, the conformation of both molecules changes quite dramatically.

The most obvious difference between **8a** and **8b** is the more dense packing of the molecules in the low-temperature phase compared to the high-temperature polymorph. The average intermolecular distances in **8a** give the molecules considerably more room than in **8b**. Virtually no interlocking of the molecular periphery in the packing of **8a** tolerates the disordered orientation of the ethyleneoxide over three positions, although the depicted one is favoured by eight of ten molecules (Figure 14). In the packing of **8b** the molecular rods are zipped together by interlocking thf molecules (Figure 15). This causes the ethyleneoxide to be trapped in the groove formed by two *tert*butyl groups of an adjacent rod. The channel permits only two disordered orientations of the ethyleneoxide group in **8b**. The position with the smaller sof is disfavoured by the orientation of the CH₂ group eclipsed towards Li1.

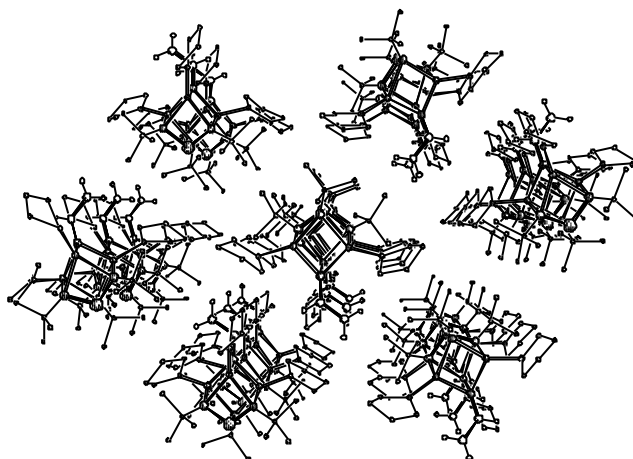


Fig. 14: Wide packing of the molecules in the high-temperature polymorph of **8a** with no interlocking at the periphery.

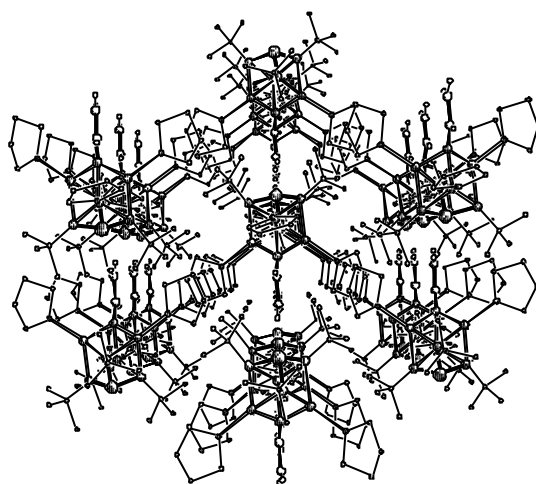


Fig. 15: Dense packing of the low-temperature polymorph **8b**, with the thf donors zipping the molecular rods. The ethyleneoxide moiety is locked in a groove provided by an adjacent rod.

Evidently the beginning of the chain of cause and effect between the change in conformation and different packing can not be identified. The question whether the different packing causes the conformation or *vice versa* remains open. However, at temperatures lower than -36°C the ethyleneoxide group clicks into the space between two thf molecules while it has more rotational freedom at higher temperatures.^[79]

2.2.2.4 Conclusion

A completely new chemical feature in the triimidosulfite dianion chemistry is the conversion of the tripodal coordinating dianion to a tripodal coordinating cation. In analogy to Mulveys inverse crowns^[77] like $[M_2Mg_2(NR_2)_4]^{2+}$, $M = Li, Na, K$, it is capable of anion solvation. It is not only possible to solvate a carbanion like methanide, it is also possible to stabilise reactive intermediates or products e.g. ethyleneoxide, formed by the decomposition reaction of thf with *tert*butyllithium.

In all known complexes of this type the anion is η^3 coordinated by three lithium cations. In the azide and the chloride adduct further dimerisation (Cl^-) or polymerisation (N_3^-) is observed (Figure 16).

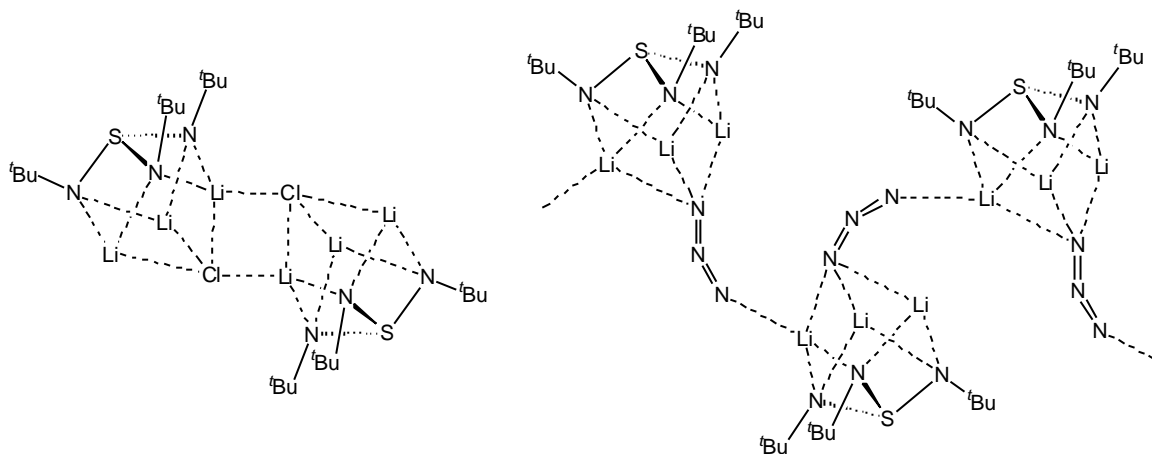


Figure 16: Dimerisation or polymerisation via the coordinated anion.

The $Li\Delta Li$ distances in the cap shaped $[Li_3(N^tBu)_3S]^+$ cation are quite variable and depend on the radius of the coordinated anion (263 (H_3C^-) **7**, 265 (H_2CCH^-) **8**, 275 (S^{2-}),^[62] 285 (N^{3-}),^[60] 292 (Cl^-) **6**, 293 (Br^-),^[13] 300 pm (Γ),^[13]). This flexibility demonstrates impressively the great application of the cationic ligand.

In **3**, **4** and **6** lithium halide ladders of various extensions are formed. The $(LiCl)_2$ subunit in **6** is terminated by a neutral $Li_2(N^tBu)_3S$ moiety at opposite sites. In **3** and **4** the terminating group is a $LiM_3\{(N^tBu)_3S\}_2$ unit. The first suits the requirements of the cubic $LiCl$ solid state lattice quite well by forming a SN_3Li_3Cl terminating group while the S bicapped trigonal prismatic coinage metal complex in **3** and **4** is inappropriate to mimic the $LiBr$ solid state structure. This might be the reason for $LiBr$ ladder extension different to $LiCl$ ladder termination.

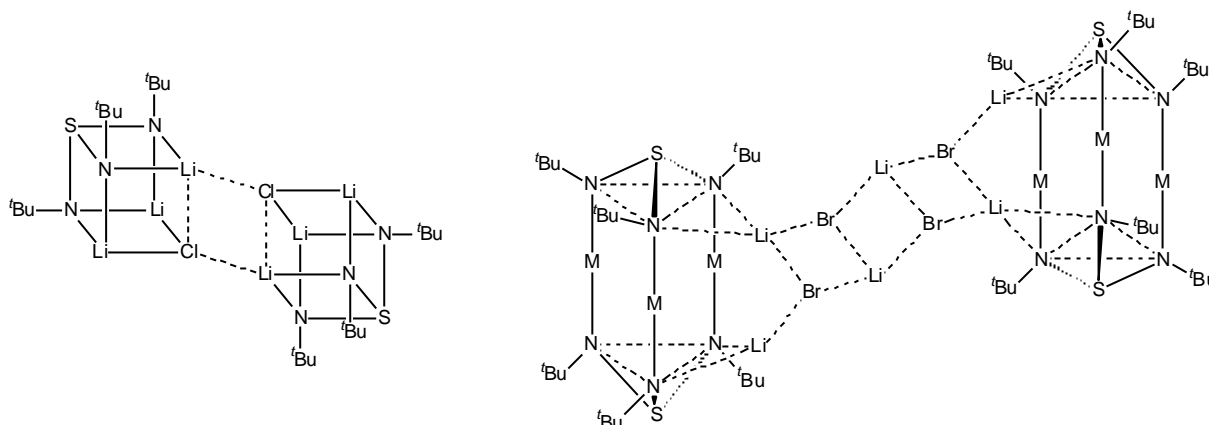


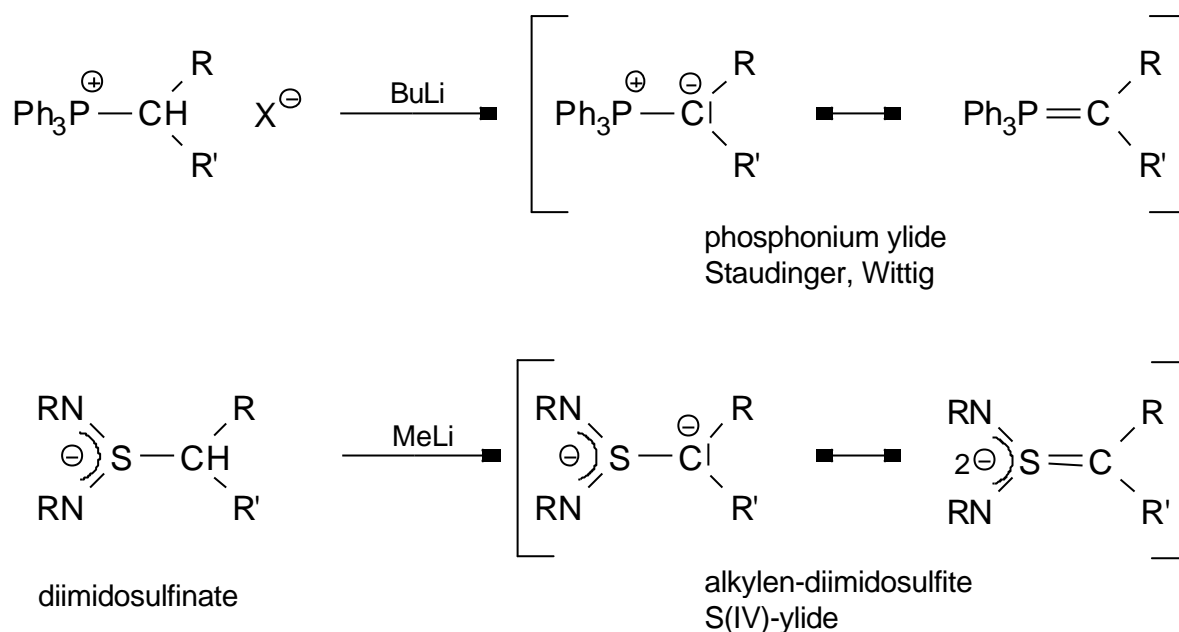
Figure 17: Terminating groups for lithium halide ladders.

2.3 Alkylendiimidosulfites

Over the last years work was generally focused on the replacement of the oxygen atoms of simple sulfur oxygen compounds by a NR group. The main focus of this thesis is on isoelectronic replacement of the oxygen atoms by $C^{\ominus}R_2$ groups.



The synthetic access to carba/imido analogues of the sulfur oxoanions has been elaborated in the course of this thesis. The direct chemical replacement of an oxygen atom or an imido group by a $C^{\ominus}R_2$ group is not practicable. A route to such compounds is the following synthetic pathway. In a first step addition of a lithiumalkyl to sulfur diimide leads to the alkylendiimidosulfates $[RS(N^tBu)_2]^{-}$ ($R = Me, sec.Bu$). In the second step the α -carbon atom in R is metalated with one equivalent of methyllithium to obtain the dianionic S-ylides. This new class of compounds can be rationalised as sulfite analogues, where two oxygen atoms are isoelectronically replaced by a N^tBu group and the remaining oxygen atom is replaced by a CR_2 group. Similar to Corey's S-ylides ($R_2(O)S^{+}-CR_2$) and Wittig's phosphonium ylides ($R_3P^{+}-CR_2$) these molecules contain a positively charged sulfur atom next to a carbanionic centre.

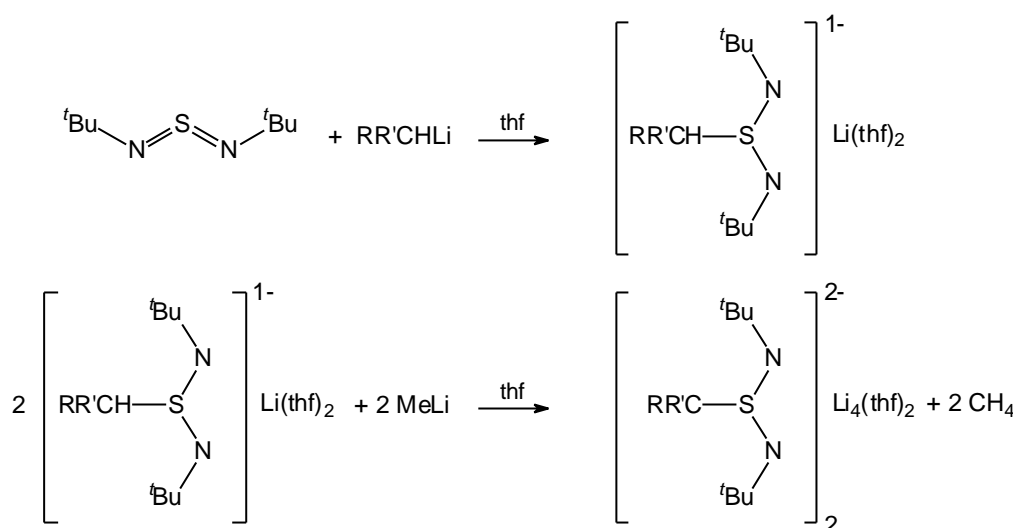


Scheme 11: Synthetic path to the phosphonium ylides and the novel dianionic S(IV)-ylides.

2.3.1 Synthesis of $[(\text{thf})\text{Li}_2\{(\text{H}_2\text{C})\text{S}(\text{N}^t\text{Bu})_2\}]_2$ (**9**) and $[(\text{thf})\text{Li}_2\{(\text{Et})(\text{Me})\text{CS}(\text{N}^t\text{Bu})_2\}]_2$ (**10**)

$[(\text{thf})\text{Li}_2\{(\text{H}_2\text{C})\text{S}(\text{N}^t\text{Bu})_2\}]_2$ (**9**) and $[(\text{thf})\text{Li}_2\{(\text{Et})(\text{Me})\text{CS}(\text{N}^t\text{Bu})_2\}]_2$ (**10**) can be synthesised in a two step reaction: firstly the alkyl diimidosulfinate is generated in an addition reaction of the corresponding lithium organic to N,N'-di(*tert*butyl)sulfurdiimide. In a second step the α -carbon atom is deprotonated by one equivalent of methyl lithium to give the sulfite analogues in good yields (60 – 80%).

Deprotonation reactions of an α -carbon atom next to a sulfur atom in general are well established. Most widespread is the synthesis of sulfur ylides,^[80] but also employed in the synthesis of sulfines and sulfenes by HCl elimination from $\text{RCH}_2\text{S}(\text{O})\text{Cl}$ ^[81] or, more recently, in asymmetric C-C coupling reactions with sulfoximines.^[82] In all these known compounds the sulfur atom is neutral or positively charged. The alkyl diimidosulfinate are the first examples of anions capable of generating S-ylides. Unlike in the carboxylates with α -CH functions, where the negative charge prevents the formation of enolates, the negative alkyl diimidosulfinate can be deprotonated with the strong base MeLi to give the S-methylene-N,N'-di(*tert*butyl) diimidosulfite $[\text{H}_2\text{CS}(\text{NR})_2]^{2-}$ in **9** and the S-sec.butylene-N,N'-di(*tert*butyl)diimidosulfite in **10**.

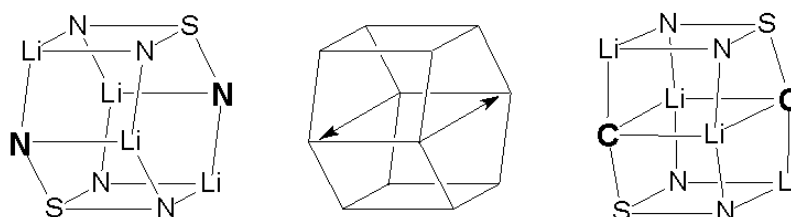
**9 and 10**

	R	R'
9	H	H
10	Et	Me

Attempts to deprotonate the alkyl diimidosulfonates with metal amides or metal alkoxides failed. This seems to be more a kinetic effect rather than the lack of basicity.

2.3.2 Crystal Structures of $[(\text{thf})\text{Li}_2\{\text{H}_2\text{CS}(\text{N}^t\text{Bu})_2\}]_2$ (**9**) and $[(\text{thf})\text{Li}_2\{(\text{Et})(\text{Me})\text{C}-\text{S}(\text{N}^t\text{Bu})_2\}]_2$ (**10**):

By isoelectronic replacement of an imido group from the triimidosulfite $[\text{Li}_4\{(\text{N}^t\text{Bu})_3\text{S}\}]^{[2\text{h}]}$ by a CH_2 group in $[(\text{thf})\text{Li}_2\{\text{H}_2\text{CS}(\text{N}^t\text{Bu})_2\}]_2$ (**9**) the degree of aggregation is maintained in the solid state (Scheme 12). Both structures are dimers.



Scheme 12: Degree of aggregation via displacement of an imido with a carbanionic group.

Like in the S–N bond lengths of av. 165.8(2) pm in **9**, which are in the same range as in $\text{S}(\text{NR})_3^{2- [2\text{h}]}$ (~167 pm) or $\text{RS}(\text{NR})_2^{- [12]}$ (~165 pm), the S–C bond length seems to

be not affected by the additional charge either. The S–C bond length of 178.6(3) pm in **9** is as long as a S–C single bond found in alkyl diimidosulfonates^[12] (~181 pm) or alkyl triimidosulfonates^[22] (~179 pm).

No bond shortening, anticipated from a Lewis diagram with a S=C double bond is detected. This findings favour the ylidic **B**-type resonance formula in Scheme 13. The S–N and S–C bond lengths indicate that one negative charge is delocalized over the SN₂ backbone while one negative charge is localised at the carbon atom. The contribution of the ylenic form **C** is insignificant.

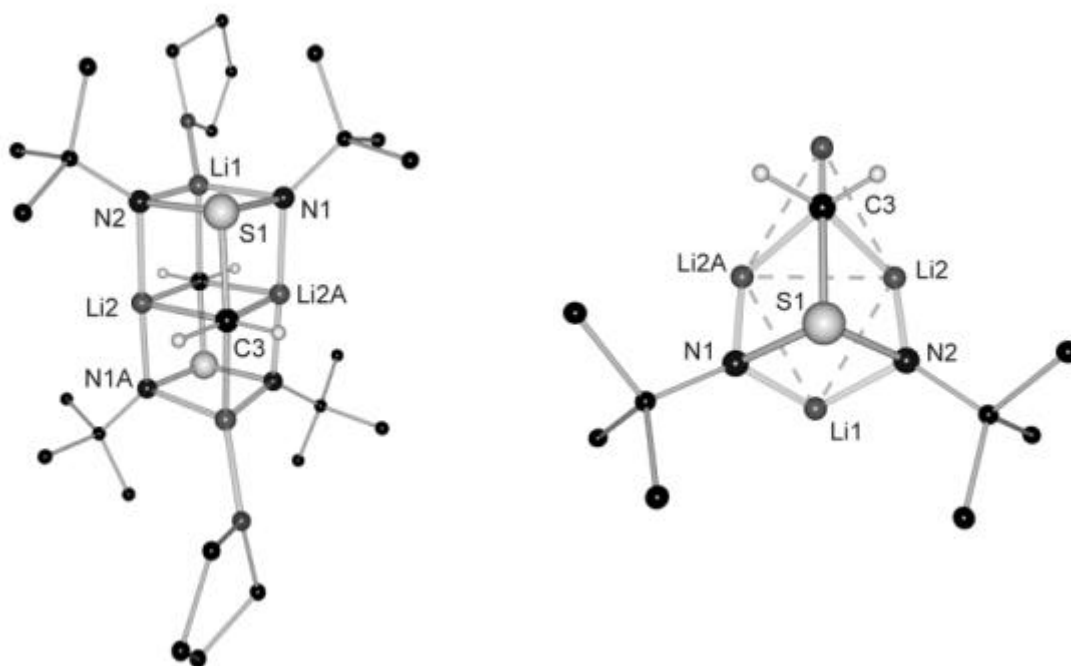


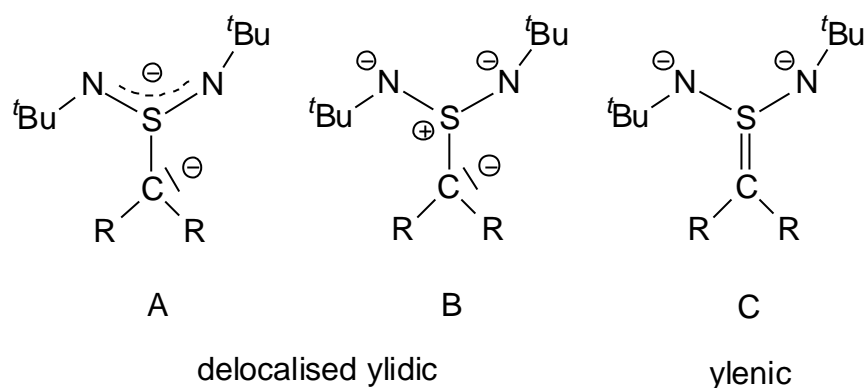
Figure 18: Solid state structure of $[(thf)Li_2\{(H_2C)S(N^tBu)_2\}]_2$ (**9**) (left) and the coordinating features of the ligand (right).

Table 7: selected bond lengths [pm] and –angles [°] of $[(thf)Li_2\{(H_2C)S(N^tBu)_2\}]_2$ (**9**):

S1–N1	165.9(2)	S1–N2	165.6(2)	S1–C3	178.6(3)
N1–Li1	203.4(5)	N1–Li2A	202.6(6)	N2–Li1	210.1(6)
N2–Li2	198.4(6)	C3–Li2	237.2(6)	C3–Li2A	235.1(6)
N1–S1–N2	103.0(1)	N1–S1–C3	100.7(1)	N2–S1–C3	99.2(2)
N2–Li2–N1A	177.8(3)				

The carbanion C3 is coordinated to the centre of a triangle made up by three lithium atoms, a structural motif well known from lithium alkylides (Figure 18, right).^[65–67] All lithium atoms are coordinated by four atoms. Li1 and Li1A are coordinated

tetrahedrally by two nitrogen atoms, one carbon atom and one thf donor molecule. Li2 and Li2A are located at the apical position of a distorted square pyramid with two nitrogen atoms and two carbon atoms in the basal positions.



Scheme 13: Resonance formulas of compound 9 and 10.

The 2D ^7Li MQMAS NMR spectrum of **9** clearly shows two well resolved peaks at isotropic shifts of $\delta_{\text{iso}} = 2.4$ and 3.1. The shape of the contour plot in Fig. 19 indicates that the sites are well defined because the signals show neither a distribution of chemical shifts nor of quadrupolar couplings.

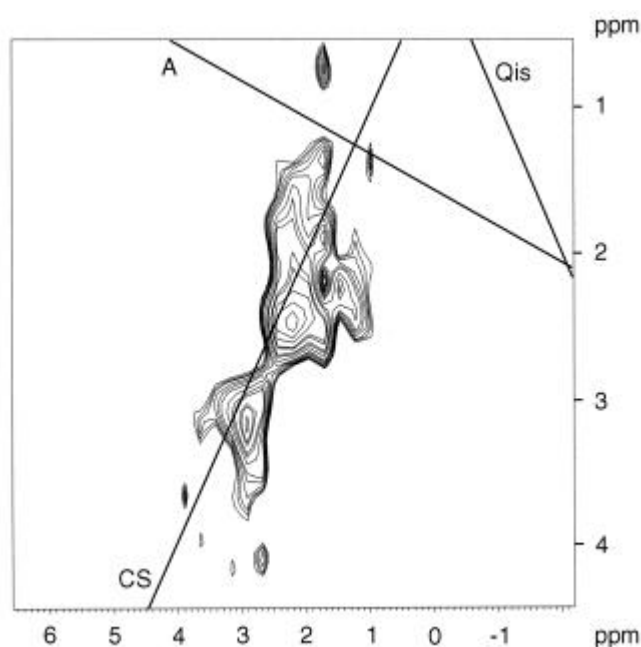


*Figure 19: Unsheared 3Q MQMAS ^7Li solid-state NMR spectrum of **9** showing two ^7Li sites with an intensity ratio of approximately 1:1. Additional axes are included for interpretation: **A** is the anisotropic axis with the slope of $-7/27$. **Qis** is the quadrupolar induced shift axis and **CS** is the chemical shift axis.*

The result of the ^7Li MQMAS is consistent with the single pulse high power decoupled ^6Li MAS NMR experiment, which also exhibits two well defined sites for sample **9** in the ratio 1:1.

The structure of $[(\text{thf})\text{Li}_2\{(\text{Et})(\text{Me})\text{CS}(\text{N}^t\text{Bu})_2\}]_2$ (**10**) is isomorphous, but not isostructural to **9**. The main structural features of both are the same. The av. S–N bond length of 165.0(2) pm is almost identical to that found in **9** (165.8(2) pm). The replacement of the methylene group in **9** by the much bulkier secbutylene group in **10** induces a 3 pm elongated S–C bond length (S–C 181.7(3) in **10** vs. 178.6(3) pm in **9**). The $\text{Li}_3\Delta\text{CR}_2$ structural motif from lithium organics is present and the mesomeric form **B** from Scheme 13 describes the bonding best.

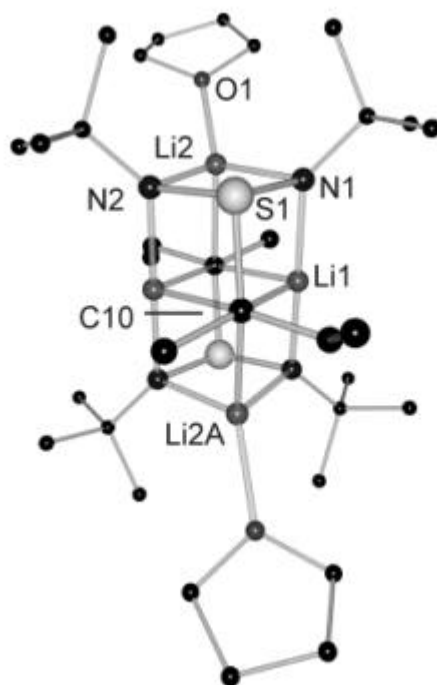


Figure 20. Solid state structure of $[(\text{thf})\text{Li}_2\{(\text{Et})(\text{Me})\text{CS}(\text{N}^t\text{Bu})_2\}]_2$ (**10**).

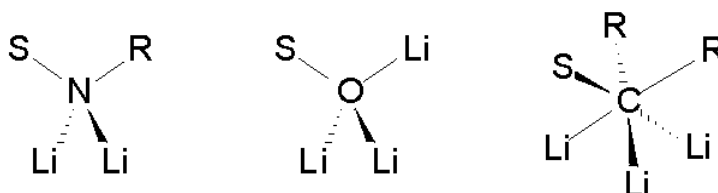
Table 8: selected bond lengths [pm] and –angles [°] of **10**:

S1–N1	165.2(2)	S1–N2	164.9(2)	S1–C10	181.7(3)
N1–Li1	201.2(5)	N1–Li2	209.4(5)	N2–Li2	207.5(5)
N2–Li1A	201.9(5)	C10–Li1	237.2(5)	C10–Li1A	241.0(6)
C10–Li2A	236.8(5)				
N1–S1–N2	104.48(11)	N1–S1–C10	99.88(11)	N2–S1–C10	99.64(12)
N1–Li1–N2A	178.8(3)				

One negative charge is delocalized over the SN_2 backbone and one is localised at the α -carbon atom. Similar to $[\text{Li}_4\{(\text{N}^t\text{Bu})_3\text{S}\}_2]$ both crystal structures of **9** and **10** are dimeric. The first adopts a distorted hexagonal prismatic arrangement, made up from two stacked SN_3Li_2 six membered rings (Scheme 12, left).^[2h] Replacement of a NR group by a CR_2 (bolt) group causes two additional Li–C bonds across that six-membered rings to be formed. Hence the hexagonal prismatic structure changes to two distorted $\text{SN}_2\text{C}_2\text{Li}_3$ cubes with a common C_2Li_2 face (Scheme 12, right).

Chivers et al. recently reported the syntheses and structure of the heteroleptic oxodiimidosulfite $[\text{Li}_2\{(\text{N}^t\text{Bu})_2\text{SO}\}]$.^[83] The replacement of one NR group by a single oxygen atom results in complete structural rearrangement. The hexagonal prismatic structure in the triimidosulfite is opened and trimerisation to a hexameric array is detected. All oxygen atoms in this aggregate are coordinated to three lithium atoms.

A comparison of the structures of the imido-, imido/oxo- and imido/carba-sulfites reveals that the structures are determined by the preferred coordination mode of the corresponding heteroatom. Nitrogen prefers a tetrahedral coordination mode with two lithium atoms. Oxygen also prefers a tetrahedral environment resulting in the coordination of three lithium atoms. By contrast, the carbon atom prefers a distorted octahedral coordination sphere. Like in the lithium organics one triangular face of the octahedron is formed by three lithium atoms (Scheme 14).



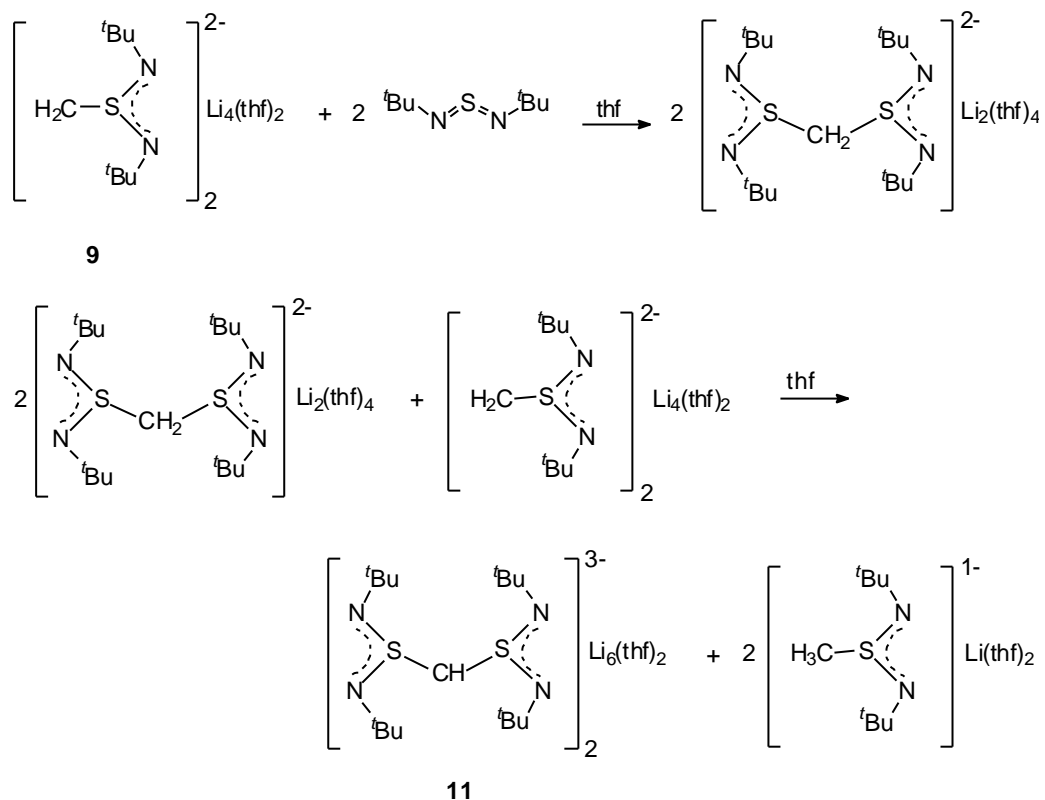
Scheme 14: Different coordination modes of the imido-, imido/oxo- and imido/carba-sulfites.

2.4 Alkylen-bis-diimidosulfites

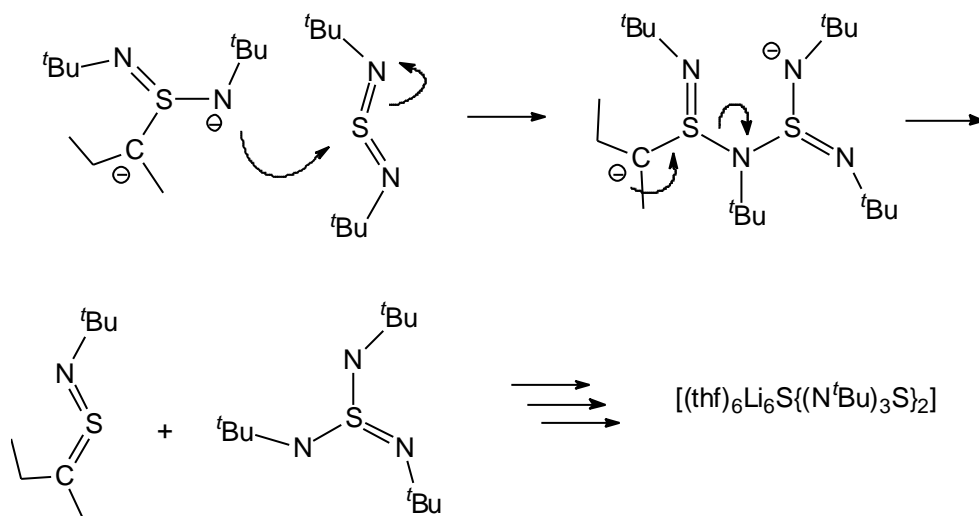
2.4.1 Addition Reactions of $[(\text{thf})\text{Li}_2\{\text{H}_2\text{CS}(\text{N}^t\text{Bu})_2\}]_2$ (**9**) and $[(\text{thf})\text{Li}_2\{(\text{Et})(\text{Me})\text{C}-\text{S}(\text{N}^t\text{Bu})_2\}]_2$ (**10**) to a Sulfurdiimide:

To elucidate the reactivity of $[(\text{thf})\text{Li}_2\{\text{H}_2\text{CS}(\text{N}^t\text{Bu})_2\}]_2$ (**9**) and $[(\text{thf})\text{Li}_2\{(\text{Et})(\text{Me})\text{C}-\text{S}(\text{N}^t\text{Bu})_2\}]_2$ (**10**), addition reaction of the nucleophilic carbanionic centre to the

electrophilic sulfur atom in sulfur diimide is elucidated. With **9** this addition reaction works. In the first step the addition leads to the intermediate $[(\text{thf})_4\text{Li}_2\{((\text{N}^t\text{Bu})_2\text{S})_2\text{CH}_2\}]$. The acidity of the hydrogen atoms of the bridging CH_2 group is so high that this product is deprotonated by $[(\text{thf})\text{Li}_2\{\text{H}_2\text{CS}(\text{N}^t\text{Bu})_2\}]_2$ (**9**) before the addition of **9** to the sulfur diimide is completed.



As a result $[(\text{thf})\text{Li}_3\{((\text{N}^t\text{Bu})_2\text{S})_2\text{CH}\}]_2$ (**11**), containing the $[(\text{N}^t\text{Bu})_2\text{SCHS}(\text{N}^t\text{Bu})_2]^{3-}$ trianion and the known methyl diimidodisulfinate $[(\text{thf})_2\text{Li}\{(\text{N}^t\text{Bu})_2\text{SCH}_3\}]$ is obtained.



In $[(\text{thf})\text{Li}_2\{(\text{Et})(\text{Me})\text{CS}(\text{N}^t\text{Bu})_2\}]_2$ (**10**) the nucleophilic carbon atom is sterically hindered and the addition reaction is prevented. Instead a sterically less crowded, but also negatively charged, nitrogen atom adds in a first step to the electrophilic sulfur atom of the sulfur diimide. In the subsequent step the imido group is completely transferred to the sulfur diimide and the triimidosulfite is formed. The initially present sulfur carbylenimine decomposes in a complex redox process to give sulfide anions and other unidentified products. However, from the solution the lithiumsulfide adduct of the triimidosulfite $[(\text{thf})_6\text{Li}_6-\mu_6\text{S}-\{(\text{N}^t\text{Bu})_3\text{S}\}_2]$, as described earlier,^[62] crystallises at -20°C in 35% yields.

2.4.2 Crystal Structure of $[(\text{thf})\text{Li}_3\{((\text{N}^t\text{Bu})_2\text{S})_2\text{CH}\}]_2$ (**11**)

The $[(\text{thf})\text{Li}_3\{((\text{N}^t\text{Bu})_2\text{S})_2\text{CH}\}]_2$ (**11**) could only be crystallised by the addition of lithium chloride to the thf solution. The deliberate addition of LiCl to promote crystallisation is a widely used technique.^[84] In the structure one equivalent of LiCl is co-coordinated to the dimer (Figure 21). In the structure both $[(\text{N}^t\text{Bu})_2\text{SCHS}(\text{N}^t\text{Bu})_2]^{3-}$ trianions facing each other with their biconcave sites, accommodating the six lithium cations between them.

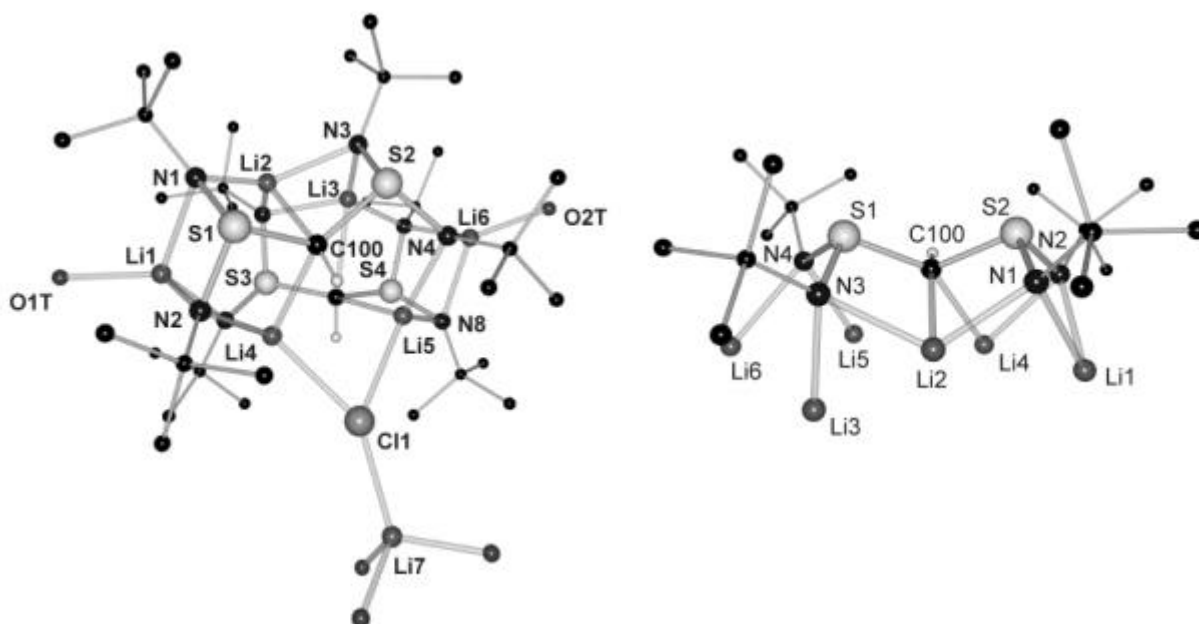


Figure 21: Solid state structure of $[(\text{thf})\text{Li}_3\{((\text{N}^t\text{Bu})_2\text{S})_2\text{CH}\}]_2 \cdot \text{LiCl}(\text{thf})_3$, (**11**· $\text{LiCl}(\text{thf})_3$, left) and view of the coordination mode of one ligand (right), carbon atoms of the coordinated thf molecules are omitted for clarity.

Table 9: selected bond lengths [pm] and –angles [°] of **11**

S1–N1	163.8(3)	S1–N2	165.4(3)	S2–N3	163.8(3)
S2–N4	166.9(3)	S1–C100	179.4(3)	S2–C100	178.7(3)
C100–Li2	230.1(6)	C100–Li4	223.2(6)	Li–Cl	247.4(5)
N1–S1–N2	105.74(14)	N1–S1–C100	100.77(15)	N2–S1–C100	95.59(12)
N3–S2–N4	109.48(13)	N3–S2–C100	99.84(15)	N4–S2–C100	100.44(14)
S1–C100–S2	121.20(18)				

The ligand coordinates like the two tripodal ligands coupled via C100 gives a pentacoordinated system. The addition reaction of **9** to sulfur diimide is carried out in several solutions (thf, hexane/thf and DEM/thf). Depending onto the reaction conditions, different lattice solvent is found in the crystal structure. As well each crystallised in different cells. In the thf solution a disordered lattice thf molecule is found (**11a**; $P\bar{1}$, 1521.27(10), 1537.61(10), 1934.79(10), 83.588(10), 79.912(19), 68.434(10)). In the hexane/thf solution a hexane molecule is found (**11b**; $P\bar{1}$, 1392.6(3), 1573.2(3), 1808.4(4), 80.89(3), 75.09(3), 86.63(3)) and in the DEM/thf solution a lattice DEM molecule is found (**11c**; $P2_1/n$, 1400.8(3), 1571.8(3), 3495.3(7), 90.00(3), 95.99(3), 90.00(3)).

In the two SN_2C tripods of the corner shared caps the lithium coordination is quite different. While three lithium cations adopt an almost ideally staggered arranged relative to the two nitrogen atoms and the CH function (relative to S1 in Figure 21, right) they are much more distorted in the second cap (relative to S2 in Figure 21, right). All nitrogen atoms as well as the two carbanionic bridging CH group are coordinated to two lithium atoms each. While Li1, Li4, Li5 and Li6 are coordinated tetrahedrally, Li2 and Li3 are coordinated trigonal pyramidally. The chlorine atom is coordinated by Li4 and Li5 from the complex and by Li7 from the pending $Li(thf)_3$ fragment. The av. S–N bond length of 165.0(3) pm in **11** is identical to that one in **10**. The S–C bond of 179.1(3) pm on average again is fairly long, indicating insignificant double bond character. This ligand together with the recently prepared imidodisulfite^[85] dianion $[O_2S(\mu-NPh)SO_2]^{2-}$ is of potential interest as a multidentate ligand.

3 S(VI)-Compounds

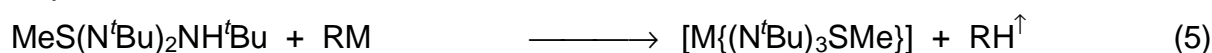
3.1 Introduction

Established S(VI) polyimido compounds are the sulfurtriiimides $S(NR)_3$, tetraimidosulfates $S(NR)_4^{2-}$, and S-methyltrimidosulfonates $RS(NR)_3^-$. In the field of S(VI) polyimido compounds we focused our interest on the alkyltriiimidosulfonates. Some new preparation methods for several metal triimidosulfonates are presented and the nature of the S–N bond concerning to the different metal complexes is discussed. A second emphasis lies on the preparation of CR_2 substituted S(VI) compounds in analogy to the alkylendiimidosulfites described in chapter 2.3. A convenient synthetic route to such compounds is presented and the reactivity of the carbanionic centre is described.

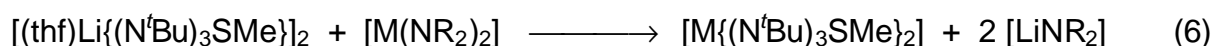
3.2 Alkyltriiimidosulfonates

In this thesis three different routes to S-alkyltriiimidosulfonate metal complexes are presented: the first involves deprotonation of the S-methyl-tri(*tert*-butyl)triiimidosulfonic acid $MeS(N^tBu)_2NH^tBu$ (**12**). The deprotonation reagent need not to be an alkali metal organic compound but metal amides can also be employed (eq 5).^[22] Secondly, lithium-S-methyl-tri(*ter*-butyl)triiimidosulfonate $[(thf)Li\{(N^tBu)_3SMe\}]_2$ is a suitable starting material for transmetalation reactions with metal amides like $[M\{N(SiMe_3)_2\}_2]$ ($M = Ba, Zn, Sn, Fe$) (eq 6).^[34] Another possibility is the insertion reaction of sulfur triimide into the metal-carbon bond of dimethylzinc and trimethylaluminum to give the aluminum- (**13**) and zinc-S-methyl-tri(*ter*-butyl)triiimidosulfonates (**14**) (eq 7).

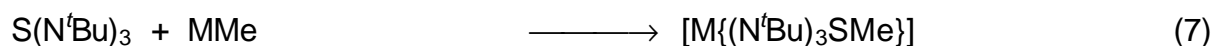
Deprotonation:



Transmetalation:

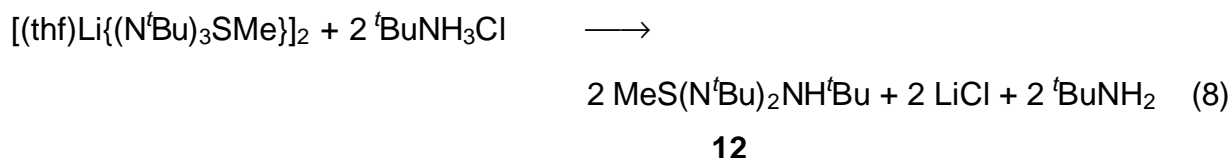


Insertion:



3.2.1 Synthesis and Structure of the S-methyl-tri(*tert*butyl)triimidosulfonic Acid MeS(N^tBu)₂NH^tBu (**12**)

Protonation of lithium-S-methyl-tri(*tert*butyl)triimidosulfonate with *tert*butylammonium chloride in thf at -5°C gives **12** (eq 8).



Recently it was found that two molecules of the triimidosulfonic acid **12** rearrange to one di(*tert*butyl)imin and two S-methyl-di(*tert*butyl)diimidosulfonic acid molecules MeS(N^tBu)NH^tBu at room temperature.^[22] However, handling the reaction solution at -5°C , filtering from the lithium chloride, and storage of the very concentrated pentane solution at -36°C for several days gives pure **12** in 76% yield. Colorless crystals of the pure S-methyl-tri(*tert*butyl)triimidosulfonic acid with a decomposition point at ca. 80°C could be obtained.

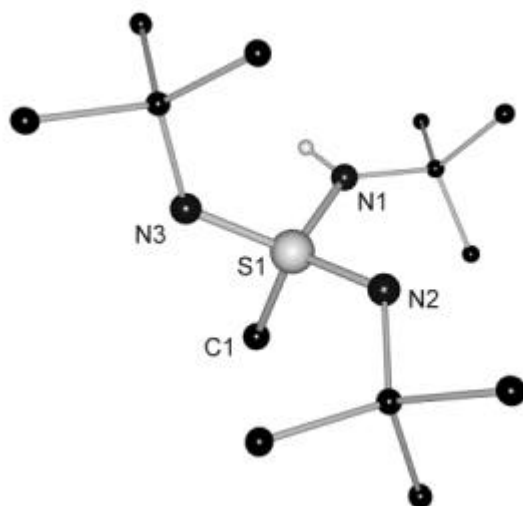


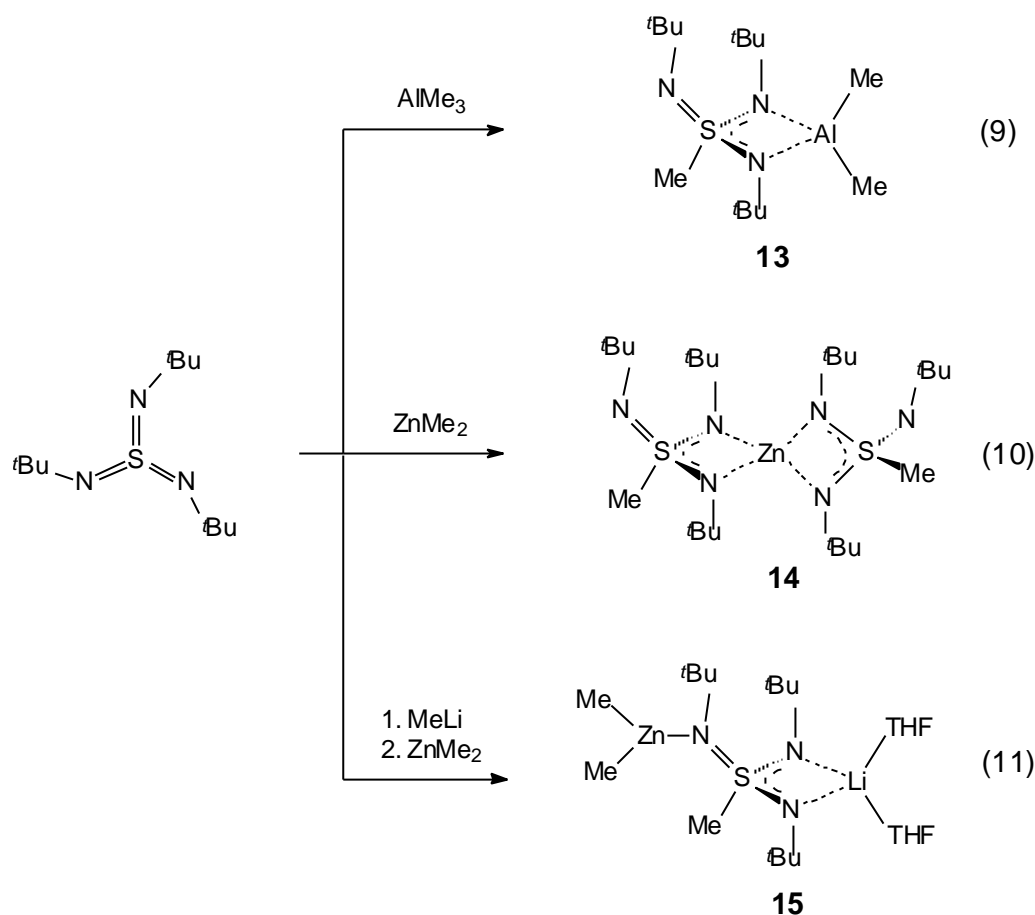
Figure 22: Solid-state structure of MeS(N^tBu)₂NH^tBu (**12**); Selected bond lengths [pm] and angles [°] are presented in Table 10.

Surprisingly, the crystal structure shows independent molecules (Figure 22), although a N \cdots HN hydrogen bonded network was anticipated. The central sulfur atom is tetrahedrally coordinated and slightly displaced from the center of the tetrahedron

toward the N₃ face (av N–S–N 112.9; av C–S–N 105.4°). The C2–N1(H1)–S1–N2 – C6 moiety is almost ideally planar (mean esd from best plane 9.17 pm) and arranged in an E/Z type of orientation to minimize steric strain between the N3 lone pair and the N1 bonded hydrogen atom. The third ^tBu group points away from the methyl group down toward the N3 plane. The S1–N1 bond of 164.77(11) pm is 12.9 pm longer than the two others (S1–N2 152.24(12) and S1–N3 151.57(11) pm). Both SN distances match the range normally defined for a S–N single and a S=N double bond. The position of the N(H1) hydrogen atom was taken from the difference Fourier map and refined freely. There is no sign of any disorder. The S1–C100 distance of 179.04(13) pm is also typical for a S–C single bond.

3.2.2 Insertion of Sulfur Triimide into the Metal Carbon Bond of Trimethyl Aluminum and Dimethyl Zinc

Addition of ionic methyllithium to the formal S=N double bond in sulfur triimides S(NR)₃ yields the lithium-S-methyl-triimidodisulfonate. When the S^{δ+} charge is considered this reactivity to the methanide is not surprising. Presumably because of steric crowding in the afforded sulfonates addition of other lithium organics like ⁿBuLi, ^tBuLi or PhLi failed. To generate others than lithium triimidodisulfonates the electrophily of the central sulfur atom should be high enough to be substituted by even more covalent bonded methyl groups derived from organometallics like AlMe₃ or ZnMe₂. Formally this could be described as an insertion to a metal carbon bond rather than an addition of ionic MeLi across the formal S=N double bond. In fact, AlMe₃ reacted with S(N^tBu)₃ in a 1:1 ratio (eq 9) while one equivalent of ZnMe₂ reacted with two equivalents of sulfur triimide (eq 10). The triimide inserts into only one of the three present Al–C bonds while in both of the Zn–C bonds. With AlMe₃ other stoichiometries always result in the same product [Me₂Al(N^tBu)₃SMe] (**13**). In [Zn{(N^tBu)₃SMe}₂] (**14**), the central zinc atom is exclusively coordinated by four nitrogen atoms. In the reaction sequence of first adding MeLi and secondly ZnMe₂, the lithium organic first adds across the formal S=N double bond to give the lithium-S-methyl-triimidodisulfonate. The third available ^tBuN group coordinates to the ZnMe₂ to afford the mixed metal triimidodisulfonate [(thf)₂Li{(N^tBu)₃SMe}·ZnMe₂] (**15**), according to eq 11.



3.2.3 Structures of $[\text{Me}_2\text{Al}(\text{N}^t\text{Bu})_3\text{SMe}]$ (**13**), $[\text{Zn}\{(\text{N}^t\text{Bu})_3\text{SMe}\}_2]$ (**14**) and $[(\text{thf})_2\text{Li}\{(\text{N}^t\text{Bu})_3\text{SMe}\} \text{ZnMe}_2]$ (**15**)

After 3 days storage at -26°C , X-ray suitable crystals of **13** were obtained from a thf/hexane solution. In the structure, depicted in Figure 23, the S-methyl-tri(*tert*butyl)triimidosulfonate chelates the cationic dimethyl aluminium moiety with two nitrogen atoms of the N^tBu groups. The negative charge is delocalized over the chelating SN_2 backbone, indicated by the almost ideal planar arrangement of the C1–N1–S1–N2–C5–Al1 part (mean deviation from best plane only 9 pm). Both S–N bond distances in the SN_2Al four membered ring are equal within esd's (160.3(2) pm) and significantly longer than the S–N distances to the pending N^tBu group of 150.8(2) pm. The latter is the shortest known S–N bond length in triimidosulfonates and is even shorter than the S–N distances in sulfur diimides ($\text{S}(\text{=N}^t\text{Bu})_2$ ^[86a] av 153.8 pm; $\text{S}(\text{=NSiMe}_3)_2$ ^[86b] av 152.0 pm) and as short as in sulfur triimides ($\text{S}(\text{=N}^t\text{Bu})_3$ ^[86c] 150.4 pm; $\text{S}(\text{=NSiMe}_3)_3$ ^[86c] av 151.5 pm). In the lithium^[2k] and barium^[22] triimidosulfonates, the S–N(M) and S=N distances are on average 157.3 and 153.7 pm, respectively. The av Al–N bond lengths in **13** of 191.0(2) pm are significantly longer than in

aluminum amides like $[\text{Al}\{\text{N}(\text{SiMe}_3)_2\}_3]^{[87]}$ (178.0 pm) or $[(\text{Et}_2\text{O})_2\text{LiAlH}_3\{\text{N}(\text{SiMe}_3)_2\}]^{[88]}$ (185.8 pm) but fit the distances where the Me_2Al^+ cationic moiety is additionally chelated by two nitrogen atoms.^[89] In the dimeric metallacycle $[\text{Me}_2\text{AlN}\{(\text{CF}_3)_2\text{C}_6\text{H}_3\}\text{S}(\text{O})^t\text{Bu}]_2$ the dimethyl aluminum atoms are coordinated by a nitrogen atom next to a sulfur atom and an oxygen atom with S–N and Al–N bond lengths of 161.5(2) and 193.2(2) pm, respectively.^[90] Further bond lengths and angles in comparison to the structures **14** to **16** are presented in Table 10.

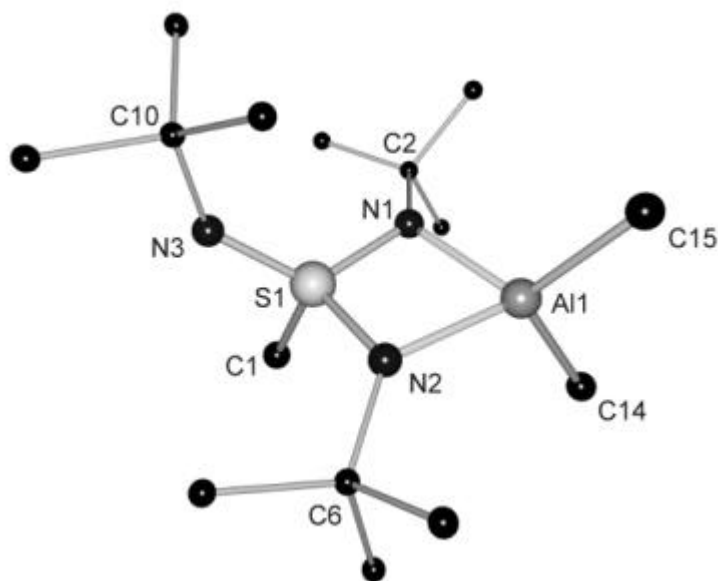


Figure 23: Solid-state structure of $[\text{Me}_2\text{Al}\{(\text{N}^t\text{Bu})_3\text{SMe}\}]$ (**13**); Selected bond lengths [pm] and angles [$^\circ$] are presented in Table 3-1.

The aluminum atom in $[\text{Me}_2\text{Al}(\text{N}^t\text{Bu})_3\text{SMe}]$ (**13**) is coordinated distorted tetrahedral by two methyl groups and two nitrogen atoms of the S-methyltriimidosulfonate. The methyl groups at the aluminum atom are neither chemically nor magnetically equivalent, which is reflected in the marginally different aluminum–carbon bond lengths (196.8(3) and 195.8(3) pm) and two single resonances in the $^1\text{H-NMR}$ spectrum at $\delta = -0.921$ and -0.915 ppm. There is considerable steric interaction between the pending ^tBuN group and the aluminum bonded methyl group (C14, Figure 2) at the same side of the N_3 plane causing different S1–Al1–C angles of 127.3° (C14) and 117.8° (C15), respectively.

X-ray suitable crystals of $[\text{Zn}\{(\text{N}^t\text{Bu})_3\text{SMe}\}_2]$ (**14**) were obtained after 3 days storage at -26°C from thf solution. The structure is shown in Figure 24 and selected bond lengths and angles are compiled in Table 10. The zinc atom is coordinated tetrahedral by four nitrogen atoms of two chelating sulfonate anions while both methyl

groups of the ZnMe_2 starting material are transferred to the electrophilic sulfur atom. Like in **13** the C2–N1–S1–N2–C6–Zn1 group in **14** is almost ideally planar with a mean deviation from the best plane by only 3.4 pm. Both symmetry independent S–N bond distances in the four membered SN_2Zn rings are equal within esd's (av. 159.2(3) pm). The S1–N3 bond is 7.9 pm shorter and is closer to the distance defined as a S=N double bond. The two symmetry independent Zn–N bond distances in the two orthogonal four membered SN_2Zn rings are only marginally different (Zn1–N1 201.86(18) and Zn1–N2 200.38(18) pm). They are located halfway between those in zinc amides like $[\text{Zn}\{\text{N}(\text{SiMe}_3)_2\}_2]^{[91]}$ (182 pm in the gas phase) and Zn←N dative bonds^[92] (212–216 pm) and match the values found in $[\text{MeZnPy}_2\text{CH}]_2^{[93]}$ (204 pm). In $[\text{EtZnN}(\text{Me})\text{S}(\text{O})\text{PhCH}_2\text{O}]_2^{[94]}$ the Zn–N bond distance is 210.0 while the S–N bond is 152.8 pm long. It is important to mention that each single molecule of **14** is chiral along the S1–Zn1–S1A axis. According the Cahn-Ingold-Prelog rules it adopts P chirality. However, the compound crystallizes in a centrosymmetric space group as a racemate.

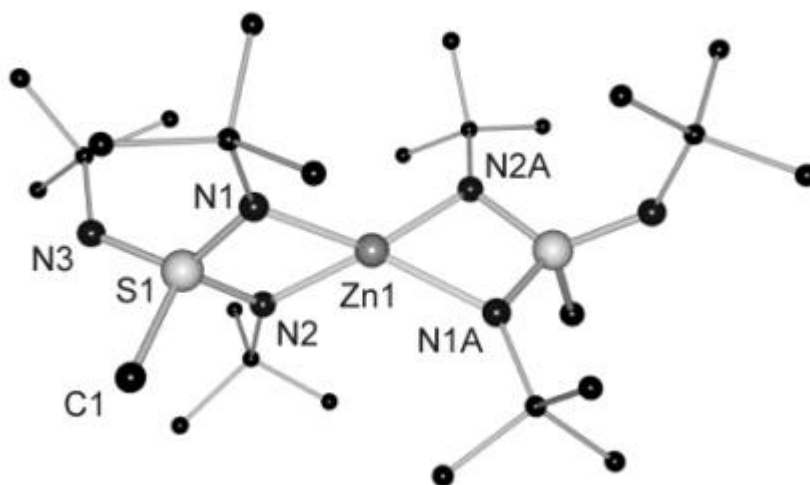


Figure 24: Solid-state structure of $[\text{Zn}\{(\text{N}^t\text{Bu})_3\text{SMe}\}_2]$ (**14**); Selected bond lengths [pm] and angles [$^\circ$] are presented in Table 3-1.

Colorless crystals of $[(\text{thf})_2\text{Li}\{(\text{N}^t\text{Bu})_3\text{SMe}\}\cdot\text{ZnMe}_2]$ (**15**) were obtained after 3 days storage at -38°C from a hexane/thf solution. The structure is shown in Figure 25 and selected bond lengths and angles are listed in Table 10. Similar to the coordination pattern in **13** and **14** the triimidosulfonate chelates the lithium cation via two nitrogen atoms of the imido groups. The C2–N1–S1–N2–C6–Li1 moiety is planar (mean deviation from best plane only 8.13 pm). Both S–N bond distances of the chelating SN_2 backbone in the SN_2Li four membered ring are equal within esd's (156.1(2) pm)

and almost identical to those found in the dimeric $[(\text{thf})\text{Li}\{(\text{N}^t\text{Bu})_3\text{SMe}\}]_2$.^[22] The third imido group in **15** is no longer a pending spectator ligand but involved in donation to the neutral ZnMe_2 organometallic group. Like the lithium cation the zinc atom is located at the N1–S1–N2 bisection. The bridging of the N3 nitrogen atom between the electropositive Zn metal and sulfur atoms causes charge density to shift from the sulfur to the metal and results in a substantial S1–N3 bond lengthening. Was the short S–N bond to the pending imido nitrogen atom N3 in **13** and **14** (av. 151 pm) suggesting some double bond character the related bond in **15** is 158.06(18) pm long and almost as long as the S–N(M) bonds in **13** and **14**. The $\text{Zn1}\leftarrow\text{N3}$ dative bond of 213.74(17) pm is about 13 pm longer than the Zn–N contacts in **14** although the coordination number decreases to three. In the known structures of ZnMe_2 with bidentate nitrogen donor bases the Zn atom is tetrahedrally coordinated and the $\text{Zn}\leftarrow\text{N}$ bond length span the range from 220 in $[\text{Me}_2\text{Zn}\{\text{N}^t(\text{Bu})\text{CH}\}_2]$ ^[95] to 228 pm in $[\text{Me}_2\text{Zn}\{\text{N}(\text{Me}_2)\text{CH}_2\}_2]$.^[96] $[(\text{thf})_2\text{Li}\{(\text{N}^t\text{Bu})_3\text{SMe}\}\cdot\text{ZnMe}_2]$ (**15**) is the first structural example containing a tricoordinated zinc atom in a dimethyl zinc adduct with only one $\text{Zn}\leftarrow\text{N}$ bond.^[97]

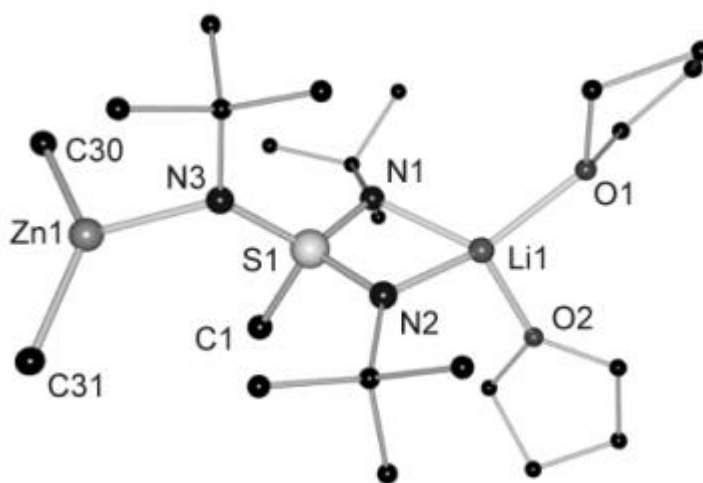


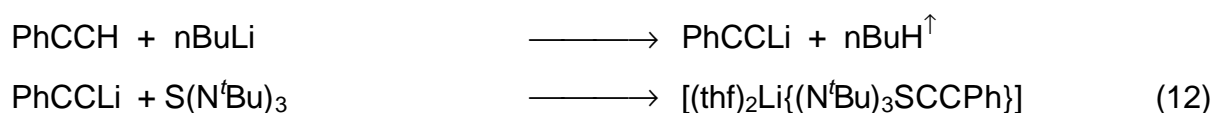
Figure 25: Solid-state structure of $[(\text{thf})_2\text{Li}\{(\text{N}^t\text{Bu})_3\text{SMe}\}\cdot\text{ZnMe}_2]$ (**15**); Selected bond lengths [pm] and angles [$^\circ$] are presented in Table 3-1.

3.2.4 Lithium-S-phenylalkynyl-N,N',N''-tri(*tert*butyl)triimidosulfonate $[(\text{thf})_2\text{Li}\{(\text{N}^t\text{Bu})_3\text{SCCPh}\}]$ (**16**)

In all known metal complexes the methyltriimidosulfonate chelates as a bidentate ligand, although tripodal coordination occurs with the triimidosulfite^[98] $[\text{S}(\text{N}^t\text{Bu})_3]^{2-}$ and the triimidosulfate^[13] $\text{OS}(\text{N}^t\text{Bu})_3^{2-}$. In these dianions, tripodal coordination is

facilitated by all *tert*butyl groups pointing towards the lone pair of the sulfur atom, leaving all lone pairs of the nitrogen atoms pointing in the opposite direction. The same is valid for the $\text{MeSi}(\text{N}^t\text{Bu})_3^{3-}$ trianion. All *tert*butyl groups are oriented towards the methyl group at the silicon atom. Hence all nitrogen atoms are exposed to lithium coordination in the dimeric cage structure of $[\text{Li}_6\{(\text{N}^t\text{Bu})_3\text{SiMe}\}_2]$. This arrangement is suitable because the Si–N bonds are considerably longer (174 pm) than the S–N bonds in the systems reported here (160 pm). Furthermore, the Si–N–C angles are wider (av. 130°) than the S–N–C angles in $\text{MeS}(\text{N}^t\text{Bu})_3^-$ ($120\text{--}125^\circ$). This gives the methyl group at the central silicon atom sufficient space. Such a hypothetical orientation of the *tert*butyl groups in $\text{MeS}(\text{N}^t\text{Bu})_3^-$ is not possible due to steric crowding. The anion minimizes steric strain by turning one *tert*butyl group away from the methyl group down to the N_3 face and blocking one nitrogen atom from tripodal metal coordination.

To achieve tripodal coordination, the steric demand of the sulfur bounded organic group was minimized. An alkynyl group $\text{R}-\text{C}\equiv\text{C}-$ seemed to be a good choice to achieve this, since a sp hybridized carbon atom is smaller in radius than a sp^3 carbon atom and the linear C_2 chain should shift the substituent R out of reach of the ^tBuN -groups. To synthesize the target molecule, in the first step phenylacetylene is lithiated *in situ* with butyllithium. To this solution tri(*tert*butyl)sulfurtriimide $\text{S}(\text{N}^t\text{Bu})_3$ is added slowly at -78°C . The reaction temperature has to be maintained below -20°C . At slightly higher temperature the product decomposes and mainly polymerization occurs. In addition, the product $[(\text{thf})_2\text{Li}\{(\text{N}^t\text{Bu})_3\text{SCCPh}\}]$ (**16**) is extremely air sensitive (eq 12).



16

Storage of the cold filtered reaction solution at -36°C for 3 days yields green-yellow crystals. The solid state structure (Figure 26) of the lithium S-phenylalkynyl-tri(*tert*butyl)triimidodisulfonate **16** shows that tripodal coordination does not occur to the lithium cation. Like the methyl derivatives this anion coordinates also bidentate with only two nitrogen atoms to the metal. A comparison with the tripodal $\text{OS}(\text{N}^t\text{Bu})_3^{2-}$ dianion proves, that tripodal coordination is primarily caused by the higher negative

charge rather than by steric effects. Obviously for a single negative charge in the triimidosulfonates it is sufficient to be delocalized in two S–N bonds while for a double negative charge in the triimidosulfites and -sulfates three S–N bonds are required. The intriguing structure of $[(\text{thf})_2\text{Li}\{(\text{N}^t\text{Bu})_3\text{SCCPh}\}]$ (**16**) sheds light upon the charge density distribution in the SN_2Li kite shaped four membered ring. While the four S–N(Li) bonds in the lithium-S-methyl-tri(*tert*butyl)triimidosulfonate dimer $[(\text{thf})\text{Li}\{(\text{N}^t\text{Bu})_3\text{SMe}\}]_2$ are equal and on average 157.2 pm long the two related distances in **16** differ by 15.7 pm (S1–N1 151.3(2) and S1–N2 167.0(3) pm).

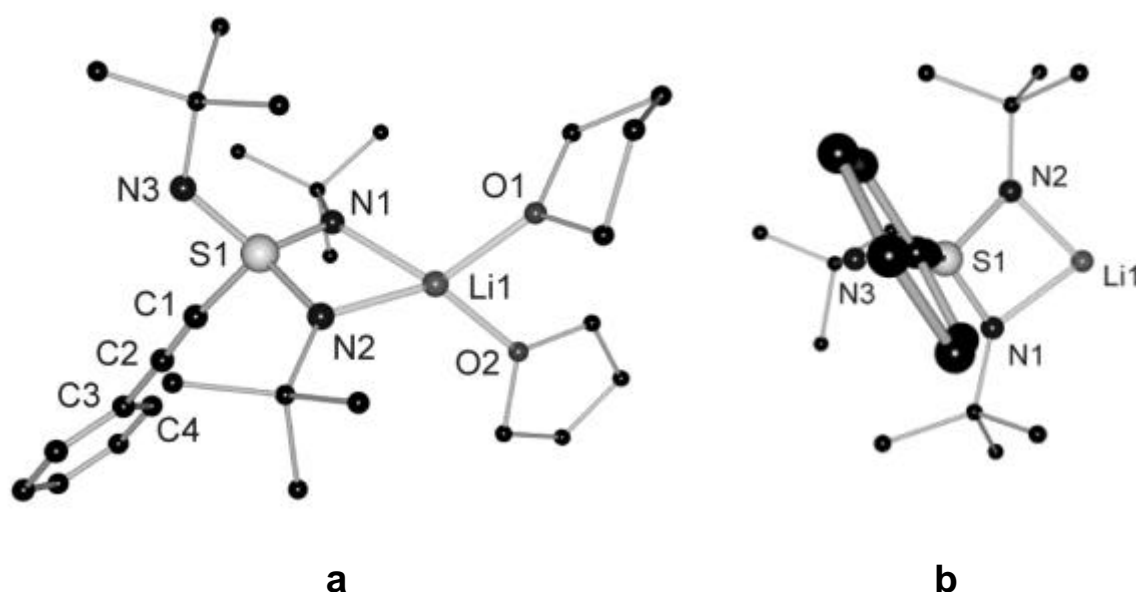


Figure 26: Solid-state structure of $[(\text{thf})_2\text{Li}\{(\text{N}^t\text{Bu})_3\text{SCCPh}\}]$ (**16**); (a) shows the molecule similar to the projections of **11-15**, (b) shows the N_3 face in the paper plane and the orientation of the phenylalkynyl substituent in conjugation to the S1–N1 bond. Selected bond lengths [pm] and angles [$^\circ$] are presented in Table 10.

Although N1 is coordinated to a lithium cation the S1–N1 distance in **16** is as short as the S–N3 bonds in the pending non-coordinated $^t\text{BuN}^-$ groups in **13** and **14** and as in sulfurdiimides.^[86] The S1–N2 bond in the metallacycle of **16** is even longer than the S–N(H) ^tBu single bond in **12** (164.77(11) pm). This asymmetry is reflected in the Li–N bonds. In the methyl derivative they were equally and on average 199.3 pm long.

Tab. 10: Selected bond length [pm] and angles [°] of **12-16**:

	12	13	14	15	16
	,M' = H	M = Al	M = Zn	M = Li, Zn	M = Li
S1–C1	179.04(13)	178.1(2)	178.3(4)	180.0(2)	171.8(3)
C1–C2					116.9(4)
C2–C3					140.7(4)
S1–N1	164.77(11)	160.52(19)	160.2(3)	156.07(17)	151.3(2)
S1–N2	151.57(11)	160.12(18)	159.3(3)	156.22(17)	167.0(3)
S1–N3	152.24(13)	150.72(18)	151.9(3)	158.06(18)	154.4(3)
M–N1	84.4(19)	190.95(19)	201.9(3)	201.4(4)	214.6(7)
M–N2		191.0(2)	200.4(3)	200.0(4)	196.7(6)
M–N3				213.74(17)	
M–C		195.8(3)		199.1(3)	
M–C		196.8(3)		198.6(3)	
N1–S1–N2	101.87(6)	91.38(9)	94.35(14)	98.23(9)	96.97(14)
N2–S1–N3	127.43(6)	122.76(10)	122.69(17)	119.70(9)	127.98(13)
N1–S1–N3	109.41(6)	122.68(10)	123.21(17)	119.92(9)	117.99(14)
C1–S1–N1	104.05(6)	110.32(10)	108.59(18)	110.45(10)	113.34(13)
C1–S1–N2	112.92(6)	108.89(10)	108.53(18)	109.70(10)	109.20(15)
C1–S1–N3	99.28(6)	100.55(10)	98.94(16)	98.89(10)	91.75(13)
N1–M–N2		73.83(8)	71.27(11)	72.05(14)	70.8(2)
C–M–C		115.21(13)		131.64(13)	

In **16**, however, they differ by 17.9 pm (Li1–N1 214.6(7) and Li1–N2 196.7(6) pm). The lithium cation is considerably shifted toward N2 which is remote from the sulfur. The orientation of the phenylalkynyl substituent relative to the SN₂Li four membered ring explains the asymmetry. The phenyl group is in plane with the short N1–S1 bond (see Figure 26b) and, consequently, couples electronically in *via* the C1≡C2 triple bond to the negative charge at the N1 nitrogen atom. Conjugation to the phenylalkynyl substituent results in S–N bond shortening. While the short S–C1 bond

in **16** (171.8(3) pm) has to be attributed to the about 8 pm smaller radius of the sp carbon atom compared to the sp³ carbon atom in **12-15** (av. S–CH₃ 179.2 pm), the C1≡C2 bond of 116.9(4) pm is significant shorter than a standard C≡C triple bond (120.2 pm). The same is valid for the C2–C3 distance of 140.7(4) pm (standard C(sp²)–C(sp) single bond: 143.2 pm). The C_{ipso}–C_{ortho} bond above the S1–N1 bond is 8.4 pm shorter than the other. All this indicates that the electron density is shifted from the N1 nitrogen atom toward the phenylalkynyl substituent. This leaves N1 unattractive to the lithium cation resulting in a long Li–N bond. To get electronically saturated the lithium cation needs closer contact to N2 but this obviously causes elongation of the S1–N2 bond. As the negative charge density of N2 is required by the metal it can not result in electrostatic S^{δ+}–N^{δ-} bond shortening. Electronic deficiency at sulfur is substituted by N3 of the pending ^tBuN group. The S1–N3 distance is as short as the related distance in [(thf)Li{(N^tBu)₃SMe}]₂.

3.2.5 Structural Comparison of the known Triimidosulfonates

In all complexes known to date the triimidosulfonate monoanion exclusively chelates the metal fragments rather than coordinating in a tripodal way. The two adjacent ^tBu substituents are in plane with the SN₂M four membered ring, while the third is twisted towards the open N₃ face. From this studies it can be excluded that the reason is sterical crowding induced by the S-bound substituent. The phenylalkynyl group in **16** gives enough space for the third ^tBuN- group to flip toward the S-bonded substituent and release the N3 plane for tripodal metal coordination. It is obvious now that two S–N bonds are sufficient to delocalize a single negative charge. The two involved S–N bonds are elongated relative to that one of the pending ^tBuN- group as the metal and the electropositive sulfur atom compete for the negative charge of the imido nitrogen atom. Consequently, the third is shortened by emphasized electrostatic attraction. However, the Lewis basicity of the lone pair at the pending imido nitrogen atom is high enough to be employed in N→M dative bonding in mixed metal complexes as shown in **15**. The sulfur/metal competition lengthens the bond almost to the S–N(H)^tBu amido bond found in **12**. It is interesting to note that the sum of all three S–N bonds in all known metal complexes (M=Li, Ba, Al, Zn) and in the triimidosulfonic acid **12** is constant at 470(2) pm. Although the SN₃ unit responds flexible to different electronic requirements induced by either different metal cations

(**13-15**) or conjugated S-substituents (**16**) the sulfur atom wouldn't allow to fall short of charge balance manifested in a fixed overall N^tBu environment. Among other, this experimentally emphasizes the predominantly ionic S–N bonding instead of valence expansion and d-orbital participation in bonding.^[99] Assuming a classical S=N double bond in polyimido sulfur species would not explain the facile NR transfer in transimidation reactions with this class of compounds.^[100] If there is much ionic contribution and negative hyperconjugation as anticipated from the computational chemistry^[99] it is obvious to employ polyimido sulfur compounds as NR transfer reagents. From this knowledge the differentiation of the mechanisms of reaction in nucleophilic addition of organometallics and insertion in the metal carbon bond seems arbitrary. In the course of the reaction most probably the metal center will be coordinated by the negatively charged imido nitrogen atom, followed by a 1,3 migration of the methanide anion to the electropositive sulfur atom.

3.3 Alkyltriimidosulfates

C_α-Deprotonation of the S-bounded substituent in diimidosulfates R₂(H)CS(NR)₂[−]^[101] yields the dianionic methylene diimidosulfites R₂CS(NR)₂^{2−}, the carba/imido analogues of SO₃^{2−}.^[102] In analogy to these reactions R₂CS(NR)₃^{2−}, the carba/imido analogues of SO₄^{2−} is prepared.

Syntheses and Structure of Methyltriimidosulfate 17

[(tmeda)₂Li₂{(CH₂)S(N^tBu)₃}] can be synthesised readily starting from lithium S-methyl-tri(*tert*butyl)triimidosulfonate H₃CS(N^tBu)₃[−] by deprotonation of the S-methyl group with methyllithium in high yields. The addition of two equivalents of MeLi to S-alkyl-tri(*tert*butyl)triimidosulfonic acid RS(N^tBu)₂NH^tBu (**12**) provides a second route to **17**. [(tmeda)₂Li₂{(CH₂)S(N^tBu)₃}], (**15**), crystallises in the presence of the donor base tmeda (tmeda=Me₂NCH₂CH₂NMe₂).



17 is, like $[(\text{thf})_2\text{Li}_2\{(\text{N}^t\text{Bu})_4\text{S}\}]^{[2k]}$ or $[\text{Li}_2\{(\text{N}^t\text{Bu})_3\text{S}\}]_2^{[2h]}$ air and moisture-sensitive. On exposure to air the color of a solution of **17** changes from colorless to red. The crystal structure of **17** consists of separated contact ion pairs. The sulfur atom is surrounded in a distorted tetrahedral fashion by three imido groups and one methylene moiety. The two lithium atoms bridge two opposite edges of the SN_3C tetrahedron, narrowing the related SN_2 angles ($\text{N}2\text{--S}1\text{--N}3$ $96.05(10)^\circ$) and SNC angle ($\text{C}1\text{--S}1\text{--N}1$ $97.66(12)^\circ$); (in contrast to av. $116.0(2)^\circ$ of the non-bridged angles). The av. S–N and Li–N bond lengths of 160.3 and 197.0 pm, respectively, are similar to those found in $[(\text{thf})_4\text{Li}_2(\text{N}^t\text{Bu})_4\text{S}]^{[2k]}$. The most remarkable structural feature involves the bonding and orientation of the CH_2 group.

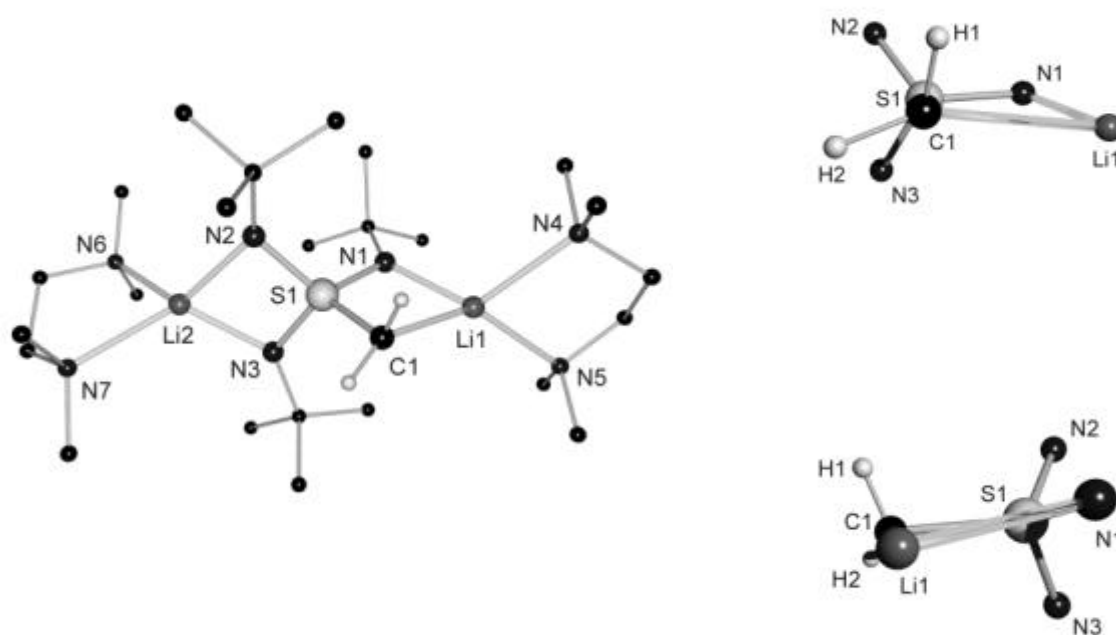


Figure 27: Solid-state structure of $[(\text{tmeda})_2\text{Li}_2\{(\text{CH}_2)\text{S}(\text{N}^t\text{Bu})_3\}]$ (**17**).

The $\text{S}1\text{--C}1$ bond length in **17** is only 172.5(3) pm and thus 6.7 pm shorter than the average value of 179.2 pm in the S-methyl tri(*tert*butyl)triimido sulfonate $\text{H}_3\text{CS}(\text{N}^t\text{Bu})_3^-$ anion.^[2k,22] However, this bond shortening upon deprotonation should not be attributed to $\text{S}=\text{C}$ bonding in the sulfur ylenic mesomeric form. Although this distance is considerably shorter than in most α -sulfonyl carbanions like $[(\text{tmeda})\text{Li}\{(\text{CH}_2)\text{SMe}\}]_2$ ($\text{S--C}(\text{M})$: 177.7(4) pm),^[103] $[(\text{tmeda})\text{Li}\{(\text{CH}_2)\text{SPh}\}]_2$ (175.9(2)

pm),^[103] [(thf)₃Li{PhCHSPh}] (176(1) pm),^[104] [(thf)₃Mg{(CH₂)SCH₃}₂] (av 176.4(3) pm)^[105] or [(thf)₃Mg{(CH₂)SPh}₂] (177.2(6) pm).^[105] In the 2,2-diphenyl-1-(phenylsulfonyl)cyclopropyllithium complex [(dme)Li{Ph₂C₃H₂SO₂(Ph)}]₂^[106] the corresponding distance is only 167.6(7) pm and the lithiated carbon atom clearly shows tetrahedral environment.

Table 11: Selected bond lengths [pm] and angles [°]:

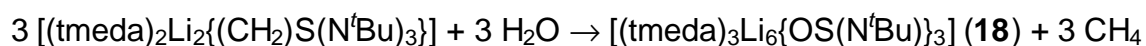
S1–N1:	160.50(19)	S1–N2:	159.0(2)	S1–N3:	161.4(2)
N1–Li1:	195.9(5)	N2–Li2:	199.8(4)	N3–Li2:	195.4(4)
S1–C1:	172.5(2)	C1–Li1:	213.2(5)		
C1–S1–N1:	97.66(12)	N2–S1–N3:	96.05(10)	N1–S1–N2:	117.32(11)
C1–S1–N3:	120.47(13)	C1–S1–N2:	111.64(14)	N1–S1–N3:	115.08(11)

The S–C bond length in **17** is similar to the observed S–C(sp) bond length of 171.8(3) pm in [(thf)₂Li{(N^tBu)₃S–C≡CPh}] (**16**). The metallated C1 in **17** is only 26 pm above the H1/H2/Li1- and H1/S1/Li1-plane suggesting a hybridisation state of C1 between sp³ and sp². Thus bond shortening has to be attributed to sp² vs sp³ C radius reduction, electrostatic S^{δ+}–C^{δ-} attraction and hyperconjugation^[107], rather than to d-orbital contribution. It is remarkable that the freely refined hydrogen atoms of the methylene group are not located along the bisector of the S1–C1–Li1 angle. H2 is tilted towards Li1 causing a relatively close Li1⋯H2 contact of 223(3) pm (Figure 27 bottom).

3.4 Triimidosulfate

Syntheses and Structure of [(tmeda)Li₂{(N^tBu)₃SO}]₃ (**18**)

Hydrolisation of [(tmeda)₂Li₂{(CH₂)S(N^tBu)₃}] (**17**), with one equivalent of water gives the trimeric triimidosulfate [(tmeda)Li₂{OS(N^tBu)₃}]₃ (**18**) and methane, and not, as one might expect, methylenediimidosulfate and the amine.



Isoelectronic replacement of the methylene group in $[(\text{tmeda})_2\text{Li}_2\{(\text{H}_2\text{C})\text{S}(\text{N}^t\text{Bu})_3\}]$, (**15**), by an oxygen atom leads to the trimer $[(\text{tmeda})\text{Li}_2\{\text{OS}(\text{N}^t\text{Bu})_3\}]_3$, (**18**). The triimido sulfate dianion is (N,N'),(N,O) chelated to two lithium cations on opposite edges of the OSN₃ tetrahedron (Figure 28, left). While the outer (N,N') chelated lithium cation is tetrahedrally coordinated by the additional chelating donor base tmeda, the (N,O) chelated lithium atom is trigonal planar coordinated providing the second intramolecular Li–O link around the threefold axis.

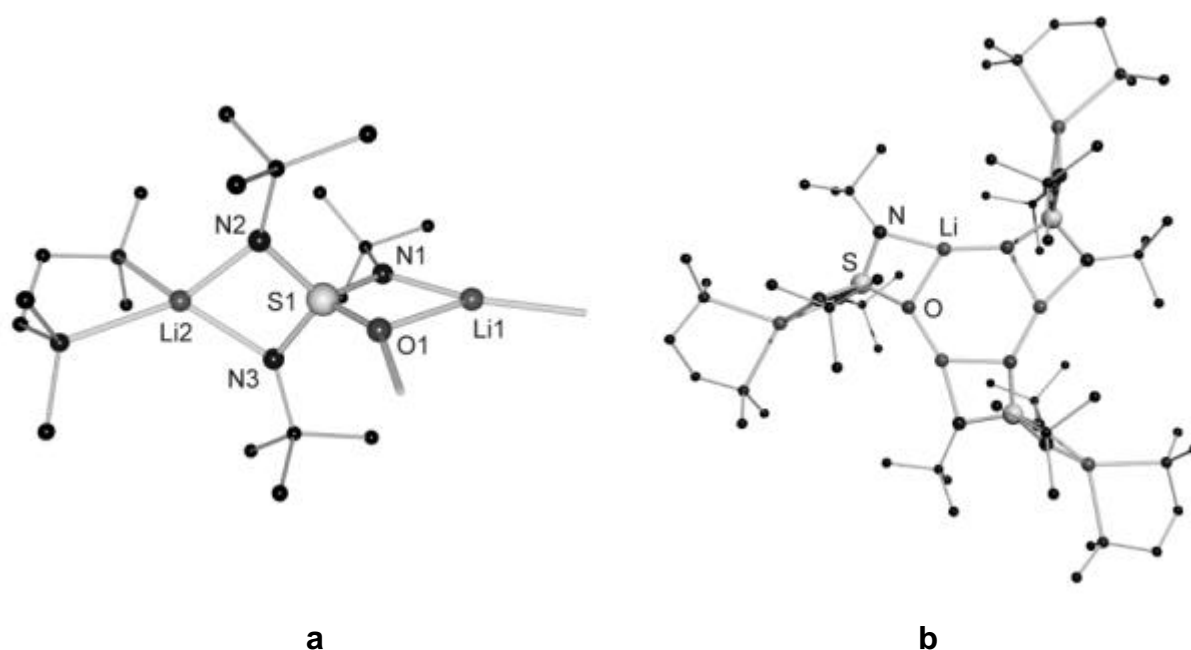


Figure 28: Solid-state structure of $[(\text{tmeda})\text{Li}_2\{(\text{N}^t\text{Bu})_3\text{SO}\}]_3$ (**18**); (a) shows a detailed structure, (b) shows the complete trimeric molecule.

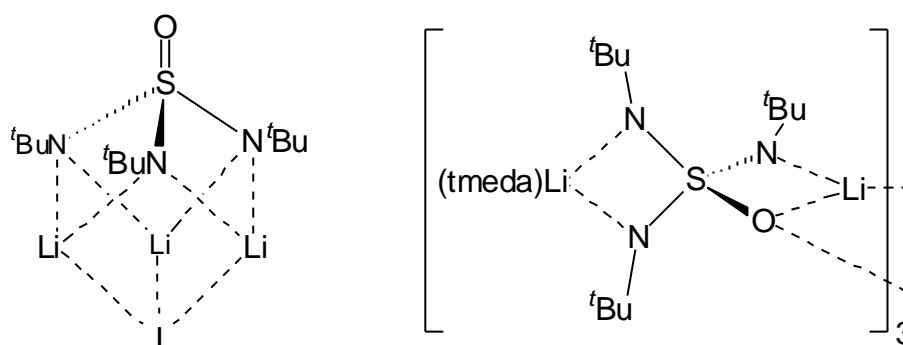
Table 12: Selected bond lengths [pm] and angles [°] of **18**:

S1–N1	157.5(3)	S1–N2	156.8(6)	S1–N3	153.8(6)
S1–O1	151.73(19)	O1–Li1	181.3(6)	O1–Li1A	196.5(6)
N1–Li1A	190.4(6)	N2–Li2	187.8(14)	N3–Li2	205.5(12)
O1–S1–N1	97.09(12)	N2–S1–N3	98.57(15)	N1–S1–N2	118.9(4)
O1–S1–N3	111.8(3)	O1–S1–N2	115.1(3)	N1–S1–N3	116.3(4)
Li1A–O1–Li1	117.2(3)	O1–Li1–O1A	122.8(3)		

Hence the trimer consists of a planar central Li₃O₃ six membered ring with three annelated planar LiOSN four membered rings. The three peripheral LiN₂S rings are

arranged orthogonal relative to these four fused rings (Figure 28, right). The lithium coordinated S1–O1 bond of 151.73(19) pm is considerably longer than the terminal S–O bond in the only other known example of a triimidosulfate dianion $\text{OS}(\text{N}^t\text{Bu})_3^{2-}$ (145.5(5) pm).^[34]

This difference is caused by the different coordination mode in the two compounds. In **18** the electron density has to be shared between the two lithium cations and the electropositive sulfur atom. In the earlier described structure the negative charges are delocalised over the S–N bonds and a formal S=O bond is formed.



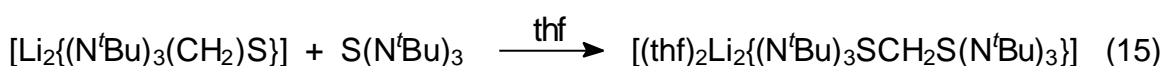
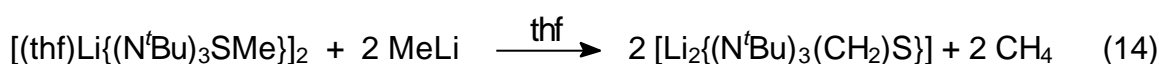
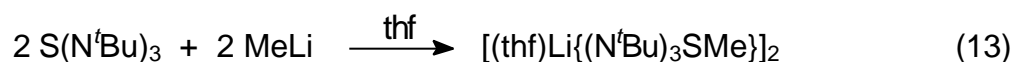
Scheme 15: Different coordination mode of triimidosulfate.

The 36 atom cluster compound of $[\text{Li}_2\{\text{OS}(\text{NR})(\text{NR}')\}]_6$, contains a pyramidal diimidosulfite dianion, with six oxygen atoms coordinated by three lithium atoms elongating the S–O bond to an average of 154.6(13) (R= $t\text{Bu}$, R'=SiMe₃) and also 158.7(7) pm (R=R'= $t\text{Bu}$), respectively.^[83] The metal diimidosulfates $\text{O}_2\text{S}(\text{N}^t\text{Bu})_2^{2-}$ tend to form clusters in the presence of two metal bridging oxygen atoms. The lithium diimidosulfate comprises an octamer^[84a] while the mixed Li/Mg metal cluster contains twelve dianions, eight lithium and two magnesium cations.^[108] The mixed Li/Al metal compounds form polymeric strands in the solid state.^[109] Compound **18** crystallised in the non centrosymmetric space group P6₃. An additional mirror plane in the O₃Li₃-ring plane to give the higher symmetric space group P6₃/m is precluded by the coordinated tmeda molecules and the N-bonded *tert*butyl groups. As the chirality is induced only in the periphery strictly spoken the molecule is not planar chiral.^[110]

3.5 Methane-di-triimidatosulfonates

3.5.1 Syntheses and Structure of $[(\text{thf})_2\text{Li}_2\{((\text{N}^t\text{Bu})_3\text{S})_2\text{CH}_2\}]$ (**19**)

To elucidate the reactivity of the carbanionic centre in $[(\text{tmeda})\text{Li}_2\{(\text{CH}_2)\text{S}(\text{N}^t\text{Bu})_3\}]$ (**17**), addition of **17** to the S=N double bond of sulfurtriiimide was carried out in analogy to the reaction of $[(\text{thf})\text{Li}\{(\text{CH}_2)\text{S}(\text{N}^t\text{Bu})_2\}]_2$ (**9**) with sulfurdiimide. This reaction leads to a methylene bridged methyl-di-tri(*tert*butyl)triimidatosulfonate (**19**). Compound **19** can also be synthesised directly by an one pot syntheses from sulfurtriiimide. In the first step, MeLi is added to sulfurtriiimide, leading to the known methyltriimidatosulfonate (eq. 13). In the second step, the methyl group, connected to sulfur is metallated with a second equivalent of methyllithium (eq. 14). *In situ* addition of one equivalent of sulfurtriiimide leads to **19** in good yields (Eq. 15). The direct route corresponding to the established Strecker synthesis^[111] to give alkane-disulfonates starting from dibromoalkanes and sodiumsulfite is precluded by complex redox processes of the required dilithium triimidatosulfite.



19

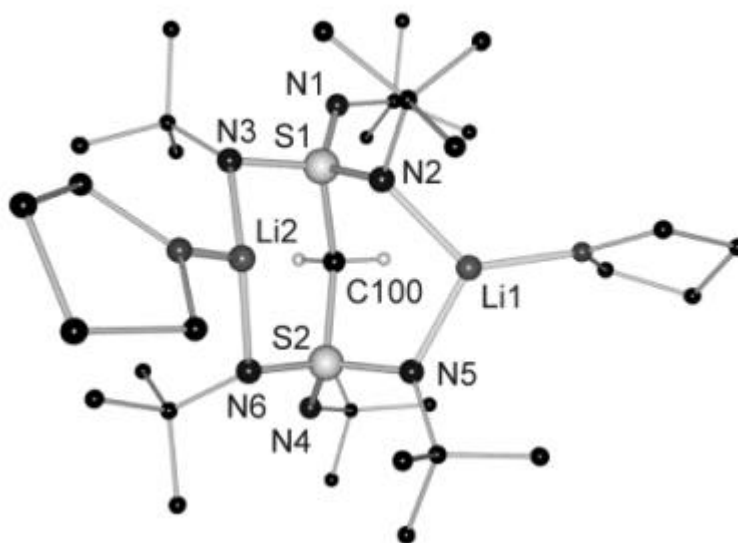


Figure 29: Solid-state structure of $[(\text{thf})_2\text{Li}_2\{(\text{N}^t\text{Bu})_3\text{SCH}_2\text{S}(\text{N}^t\text{Bu})_3\}]$ (**19**).

Different to the known salts of Ca^{2+} -, Cd^{2+} -, Ag^+ - or K^+ -methane-disulfonates,^[112] $[(\text{thf})_2\text{Li}_2\{(\text{N}^t\text{Bu})_3\text{SCH}_2\text{S}(\text{N}^t\text{Bu})_3\}]$, (**19**), forms donor base stabilised molecules (Figure 3-8). Both lithium cations are pincerred by two opposite nitrogen atoms of both staggered $\text{S}(\text{NR})_3$ -moieties, each. Additional complexation of a single thf-molecule leaves both metals threefold pyramidal coordinated.

The av. $\text{Li1-N}_{2,5}$ bonds are considerably longer than the $\text{Li2-N}_{3,6}$ bonds (203.3(11) vs. 193.9(11) pm). The longer Li-N bonds furnish the shorter av. $\text{S-N}(\text{Li})$ bonds and vice versa (156.4(5) vs. 157.6(5) pm). The nitrogen atoms of the pendant imido ligands ($\text{N}_{1,4}$) afford the shortest S-N bonds as there is no competition for the electron density from the metals (S1-N_1 , S2-N_4 : av. 152.3(5) pm). The av. $\text{S}_{1,2}\text{-C}_{100}$ bond length with 184.7(4) pm is 8 pm longer than the S-C bond in the methyl-triimidosulfonates (**12-15**). The unprecedented wide S-C-S angle of $126.7(2)^\circ$ reflects the considerable steric strain between the two triimidosulfonate groups reinforced by metal coordination.

Table 13: Selected bond lengths [pm] and angles [$^\circ$]:

S1-N_1	152.7(3)	S1-N_2	156.8(4)	S1-N_3	157.2(3)
S2-N_4	151.9(3)	S2-N_5	155.8(3)	S2-N_6	157.9(3)
S1-C_{100}	184.7(4)	$\text{C}_{100}\text{-S}_2$	184.5(4)	Li1-N_2	205.6(8)
Li1-N_5	204.9(8)	Li2-N_3	192.6(8)	Li2-N_6	195.1(8)
$\text{N}_1\text{-S}_1\text{-N}_2$	109.3(2)	$\text{N}_1\text{-S}_1\text{-N}_3$	120.51(19)	$\text{N}_2\text{-S}_1\text{-N}_3$	111.80(18)
$\text{N}_1\text{-S}_1\text{-C}_{100}$	107.40(18)	$\text{N}_2\text{-S}_1\text{-C}_{100}$	107.40(18)	$\text{N}_3\text{-S}_1\text{-C}_{100}$	98.61(18)
$\text{S1-C}_{100}\text{-S}_2$	126.7(2)	$\text{N}_4\text{-S}_2\text{-N}_5$	110.86(19)	$\text{N}_5\text{-S}_2\text{-N}_6$	107.40(18)
$\text{N}_4\text{-S}_2\text{-N}_6$	122.26(18)				

3.5.2 Syntheses and Structure of $\text{H}_2\text{C}\{\text{S}(\text{N}^t\text{Bu})_2(\text{NH}^t\text{Bu})\}_2$ (**20**)

Hydrolysis of **19** with two equivalents of *tert*butylammoniumchloride leads to the analogues imido compound of methane-disulfonic acid $\text{H}_2\text{C}\{\text{S}(\text{O})_2(\text{OH})\}_2$, synthesised for the first time more than 160 years ago.^[113] Since then, this very strong acid^[114] was structurally studied as the hydrates form stable dihydroxonium salts $[\text{H}_3\text{O}]_2[(\text{O}_3\text{S})_2\text{CH}_2]$ with strong hydrogen bonds.^[115] This feature was recently

employed in crystal engineering. It serve as a molecular pillar to separate two dimensional galleries in tuneable hydrogen bonded nanoporous materials.^[116]

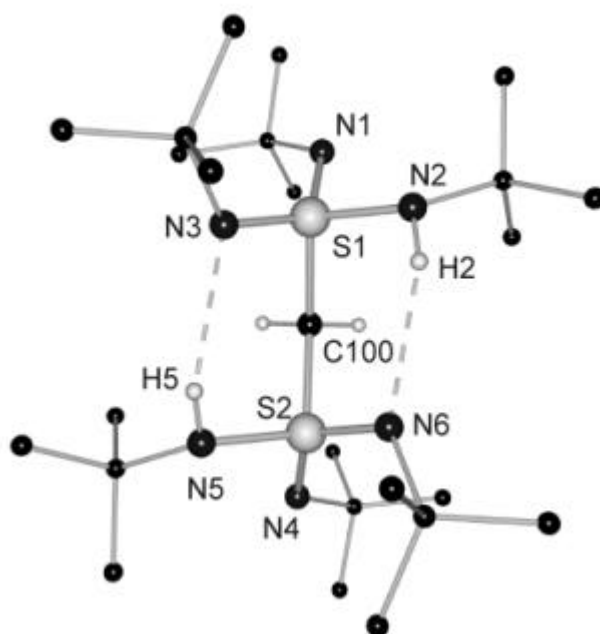
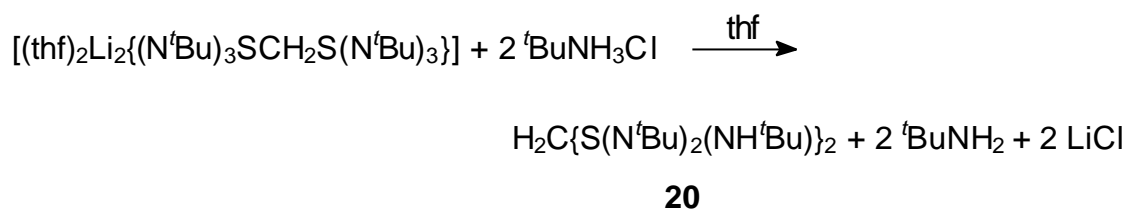


Figure 30: Solid-state structure of $\text{H}_2\text{C}\{\text{S}(\text{N}^t\text{Bu})_2(\text{NH}^t\text{Bu})\}_2$ (**20**).

Table 14: Selected bond lengths [pm] and angles [°]:

S1–N1	151.62(10)	S1–N2	164.94(11)	S1–N3	152.58(10)
S2–N4	151.74(17)	S2–N5	164.92(11)	S2–N6	152.63(19)
S1–C100	181.83(11)	C100–S2	181.83(11)	N2–H2	82.7(17)
N5–H5	85.6(19)	N6–H2	229.3	N3–H5	227.9
N1–S1–N2	102.11(6)	N1–S1–N3	126.88(6)	N2–S1–N3	110.45(6)
N1–S1–C100	110.61(5)	N2–S1–C100	105.82(5)	N3–S1–C100	99.60(6)
S1–C100–S2	122.10(6)	N4–S2–N5	102.34(6)	N5–S2–N6	110.00(6)
N4–S2–N6	126.94(6)				

The crystal structure of **20** shows individual molecules. Intramolecular bridging hydrogen bond between H2 to N6 and H5 to N3 is observed. Therefore three different types of S–N bonds are formed: two distinct formal S,N double bonds (S1-N1, S2-N4: av. 151.68(14) pm); two slightly elongated S,N double bonds (S1-N3, S2-N6: av. 152.60(15) pm) induced by the bridging hydrogens; and two single SN bonds (S1-N2, S2-N5: av. 164.93(11) pm). According to the Cahn-Ingold-Prelog rules, the illustrated structure in Figure 30 is S/S chiral. However, **20** crystallises in the centrosymmetric space group C2/c with both enantiomeric pairs, R/R and S/S present in the racemic lattice.

4 Conclusion

4.1 S(IV) and S(VI) Polyimido Compounds

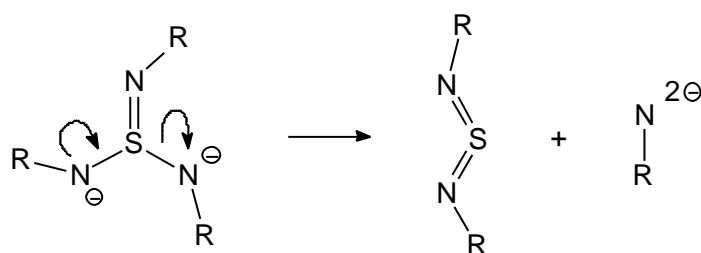
Established S(IV) and S(VI) polyimido compounds are the sulfurdiimides $S(NR)_2$, triimidosulfites $S(NR)_3^{2-}$, alkyldiimidosulfates $RS(NR)_2^-$, sulfurtriimides $S(NR)_3$, tetraimidosulfates $S(NR)_3^{2-}$, and S-methyltrimidosulfonates $RS(NR)_3^-$.

4.1.1 Triimidosulfites

Until now homoleptic stable complexes of the triimidosulfite dianion are only known from Li and Na. The direct syntheses of other homoleptic metal complexes of the triimidosulfite dianion via addition of metal amides to sulfurdiimide is precluded by the synthetic access of the corresponding soluble metal amides. Therefore, transmetalation reactions are the only preparative approach. In all transmetalation reactions with metal halides and metal amides, starting from the dilithium triimidosulfite compound, only parts of the present lithium cations are replaced by the corresponding metal derived from the amide. Yielded lithium halide or metal amide from the starting material is still co-coordinated to the triimidosulfite. The abstraction of the lithium halide is thermodynamically hindered, because, the equilibrium of the reaction between lithium triimidosulfite and solved lithium halides is considerable shifted towards formation of the known lithium halide triimidosulfite adducts (e.g 6).

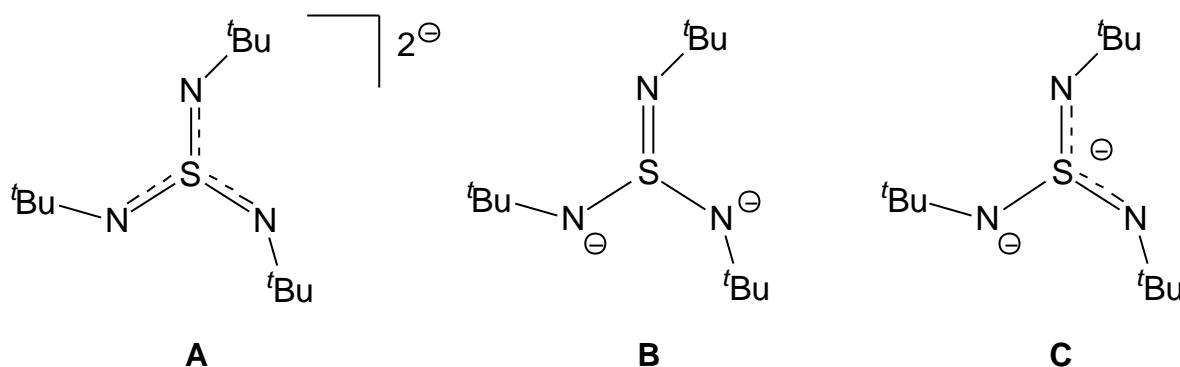
With strong Lewis acids like $GeCl_2$ and $SnCl_2$ complete disintegration of the triimidosulfite to metal *tert*.butylimide and sulfur was observed. With $Fe(AcAc)$ only one *tert*.butylimide is abstracted and sulfurdiimide is formed.

Thus, it might be possible to use the triimidosulfite as a transimidation reagent.



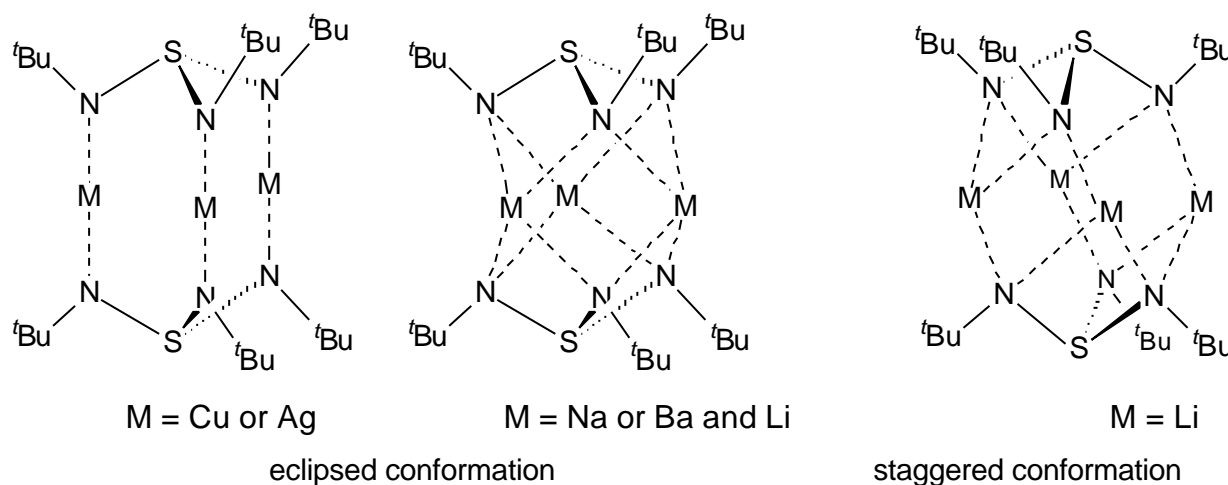
Scheme 16: Abstraction of a Imid and formation of sulfurdiimide.

The triimidosulfite dianion is electronically a very flexible ligand. It responds by shifting charge density in the SN_3 -backbone to the different requirements induced by hard or soft metals.^[117] **(A)**: The electron density is delocalized equally over all three SN-bonds in $[\text{Li}_2\{(\text{N}^t\text{Bu})_3\text{S}\}]_2$.^[2h] **(B)**: One formal double bond and two amidic nitrogen atoms could be found in **1-4**, $[(\text{thf})\text{LiSn}\{\text{N}(\text{SiMe}_3)_2\}\{(\text{N}^t\text{Bu})_3\text{S}\}]$ and $[(\text{thf})_2\text{CaLi}_2\{(\text{N}^t\text{Bu})_3\text{S}\}_2]$.^[34] **(C)**: Examples with one long and two short SN distances are $[(\text{thf})_2\text{Ba}_2\text{Li}\{\text{N}(\text{SiMe}_3)_2\}\{(\text{N}^t\text{Bu})_3\text{S}\}_2]$ ^[34] and $[(^t\text{BuN})(\text{Cl})_4\text{Sn}_2\{(\text{N}^t\text{Bu})_3\text{S}\}]$.^[118]



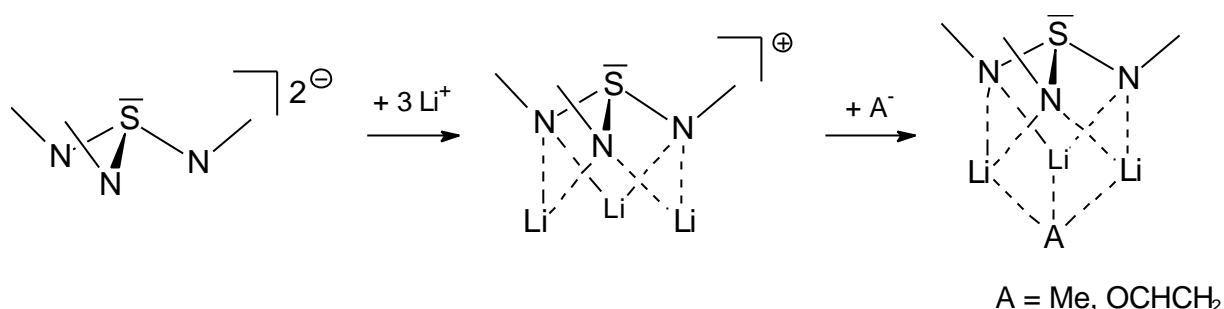
The coordination of the triimidosulfite ligand is mainly dominated by the metals. With main group metal cations, which might be described as point charges, the imido substituent tend to coordinate μ_2 . With coinage metal a linear orbital controlled coordination is observed.

In compounds with two triimidosulfite dianions the relative position to each other depends nearly on the amount of metals, coordinated between the two ligands. With three cations they are eclipsed and with four they are staggered to each other.



Scheme 17: Relative position of two triimidosulfite dianions depending onto the amount of coordinated metals between the two ligands.

A completely new chemical feature in the triimidosulfite dianion chemistry is the conversion of the tripodal coordinating dianion to a tripodal coordinating cation capable of anion solvation.



Scheme 18: Conversion of a tripodal coordinating dianion into a tripodal coordinating monocation.

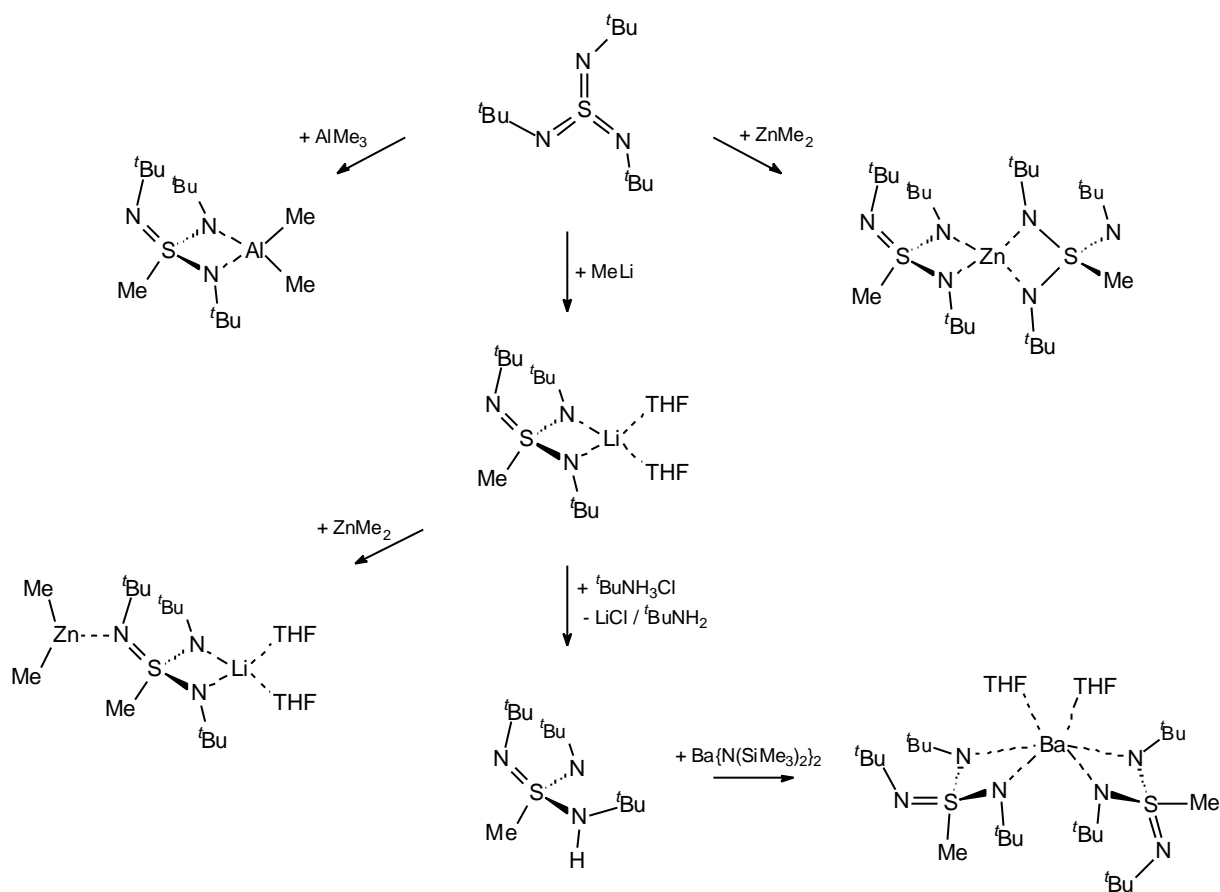
In this thesis I showed that it is not only possible to stabilise a carbanion like methanide, it is also possible to solvate reactive intermediates or products e.g. ethyleneoxide, formed by the decomposition reaction of thf with *tert*butyllithium. In all known complexes of this type the anion is η^3 coordinated by three lithium cations (Cl (**6**), Br,^[13] I,^[13] S²⁻,^[62] N₃⁻,^[60] Me⁻ (**7**), H₂CCHO⁻ (**8a,b**)). In the azid and the chloride adduct additional a dimerisation (Cl⁻) or polymerisation (N₃⁻) is observed. In the chloride adduct a Li₂Cl₂ square is formed. Obviously the [S(N^tBu)₃M₂] subunit functions as a terminator for lithium halide ladders.

The triimidosulfite dianion can be easily oxidised by several oxidants. In all cases the first step is a formation of a radical species. The nature of the reaction product depends on the oxidant: with halogens sulfurtriimide is formed; with oxygen triimidosulfate.

4.1.2 Alkyltriimidosulfonates

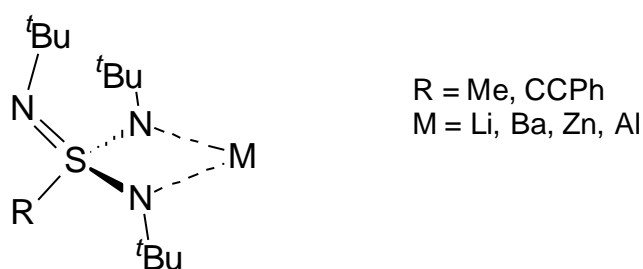
In the course of this thesis three different routes to S-alkyltriimidosulfonate metal complexes have been elaborated: The first involves deprotonation of the S-methyl-tri(*tert*butyl)triimidosulfonic acid MeS(N^tBu)₂NH^tBu (**10**). Alternatively, lithium-S-methyl-tri(*tert*butyl)triimidosulfonate [(thf)Li{(N^tBu)₃SMe}]₂ is a suitable starting material for transmetalation reactions with metal amides like [M{N(SiMe₃)₂}₂] (M = Ba,

Zn, Sn, Fe). Another route is the insertion reaction of sulfur triimide into the metal-carbon bond of a metalalkyl like dimethylzinc and trimethylaluminium.



Scheme 14: Syntheses of the known triimidosulfonates starting from sulfur triimide.

In all to date known complexes the triimidosulfonate monoanion exclusively chelates the metal fragments rather than coordinating in a tripodal fashion. The two adjacent $t\text{Bu}$ substituents are in plane with the SN_2M four membered ring while the third is twisted towards the open N_3 face.



However, the Lewis basicity of the lone pair at the pending imido nitrogen atom is high enough to be employed in $\text{N} \rightarrow \text{M}$ dative bonding in mixed metal complexes as shown in $[(\text{thf})_2\text{Li}\{\text{N}(t\text{Bu})_3\text{SMe}\} \cdot \text{ZnMe}_2]$ (**13**).

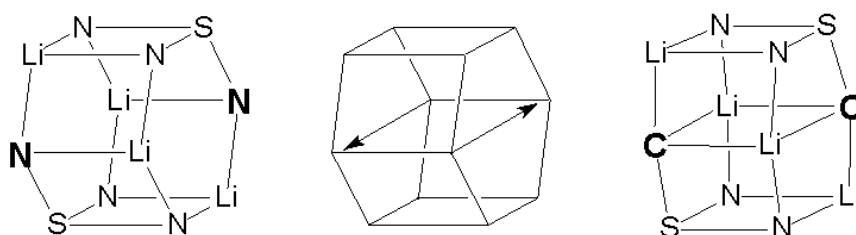
4.2 S(IV) and S(VI) carba/imido compounds

Two kinds of carba/imido compounds are described in this thesis. The alkylendiimidosulfites and the alkyltriimidosulfates, derived from the simple sulfur oxygen dianions SO_3^{2-} and SO_4^{2-} . A synthetic path has been opened to these compounds by the metalation of the sulfur bonded alkyl group in alkylendiimidosulfites or alkyltriimidosulfates.

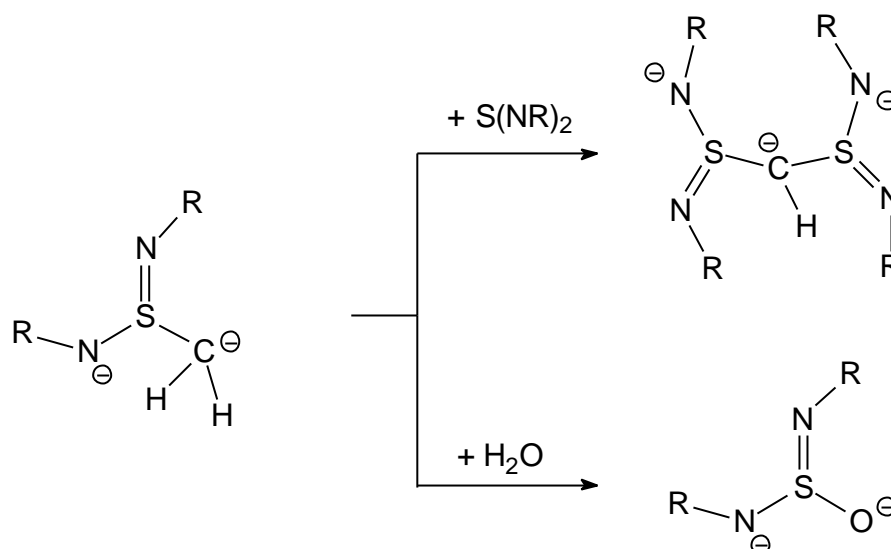
4.2.1 Alkylendiimidosulfites

$[\text{H}_2\text{CS}(\text{NR})_2]^{2-}$ (**7**) and $[(\text{Et})(\text{Me})\text{CS}(\text{NR})_2]^{2-}$ (**8**) can be synthesised via deprotonation of the related alkyl diimidosulfites. They can be rationalised as sulfite analogues, where two oxygen atoms are isoelectronically replaced by a NBu group and one oxygen is replaced by a CR_2 group. Like in sulfur ylides there is a positively charged sulfur atom next to a carbanionic centre. The ylidic or ionic form describes the S–C bonding best. The ylenic form seems to have no contribution.

The replacement of a single NR group in $\text{S}(\text{NR})_3^{2-}$ by a CR_2 group in $\text{S}(\text{NR})_2(\text{CR}_2)^{2-}$ has a dramatic effect on its coordination behaviour. It causes the hexagonal prismatic dimer to change into two face connected cubes. The anionic carbon centre prefers a μ_3 capping of a Li_3 triangle, a common structural feature of lithium organics like $[\text{MeLi}]_4$ or $[\text{BuLi}]_6$.

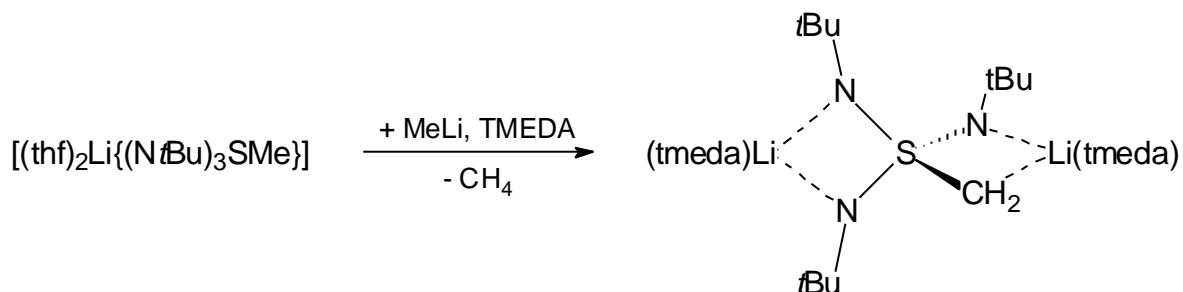


The reactivity is dominated by the hard carbanionic centre. Addition reactions are feasible e.g. the addition to the formal SN double bond of a sulfur diimide. Thus, the reaction leads to a new chemical class of alkan-di-diimidosulfites. Hydrolyses of the alkylendiimidosulfites yields diimidosulfite and methane.



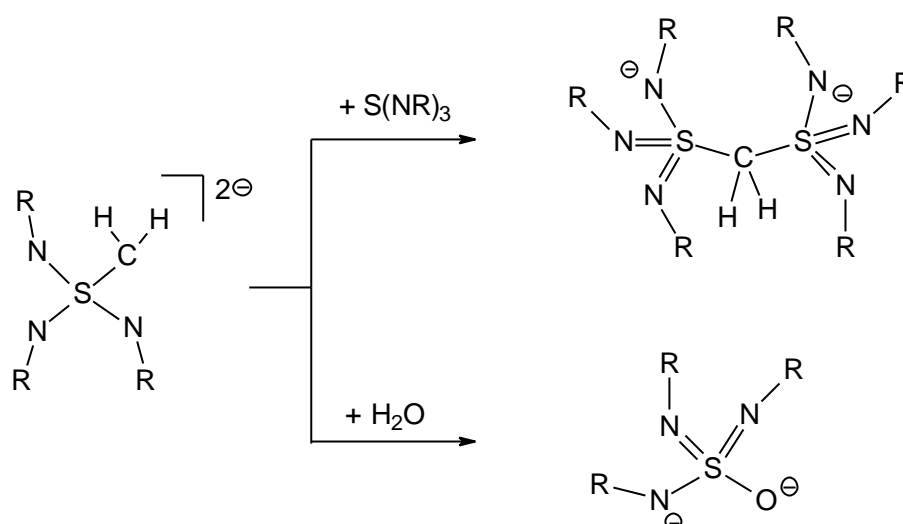
4.2.2 Methyltriimidosulfate

Starting from the methyl triimidosulfonate the alkylene triimidosulfate can readily be synthesized in reasonable yields by deprotonation of the α -carbon atom with one equivalent of methyl lithium.



In the solid state the methylenetriimidosulfate forms a monomeric contact ion pair with the α -carbon atom coordinated to only one lithium atom. The coordination geometry around the sulfur atom is distorted tetrahedral and the two negative charges are delocalised over all SN and SC bonds.

Hydrolysis of the methylene triimidosulfate yields triimidosulfate and methane. Also addition reactions are feasible e.g. the addition to the SN double bond of a sulfurtriimide. This reaction leads to the new chemical class of methyl-di-triimidosulfonates.



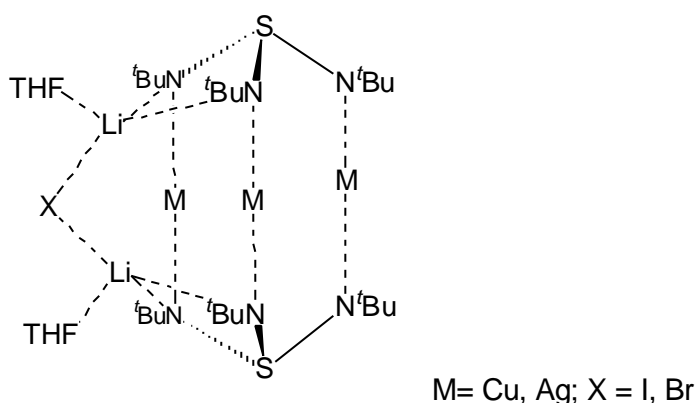
The alkyl diimidosulfonates and alkyl triimidosulfonates represent intriguing starting materials to synthesize an entire novel class of compounds: dianionic sulfur ylides. Due to the carbanionic character of the α -carbon atom addition reactions are feasible. We also expect Wittig type reactions, transfer of the CR_2 group to ketones or aldehydes and formation of diimidosulfite. The appealing advantage of these novel sulfur ylides is the chance to tune the reactivity of both the S–C and S–N bond via the organic substituents at the periphery.

5 Zusammenfassung

In unserer Arbeitsgruppe etablierte Verbindungen sind die Schwefeldiimide $S(NR)_2$, Triimidosulfite $S(NR)_3^{2-}$, Alkyldiimidosulfinate $RS(NR)_2^-$, Schwefeltriimide $S(NR)_3$, Tetraimidosulfate $S(NR)_4^{2-}$ und Alkyltriimidosulfonate $RS(NR)_3^-$. All diese Verbindungen leiten sich formal durch isoelektronischen Ersatz der Sauerstoffatome mit einer NR Gruppe von den allgemein bekannten Schwefelsauerstoffanionen ab.

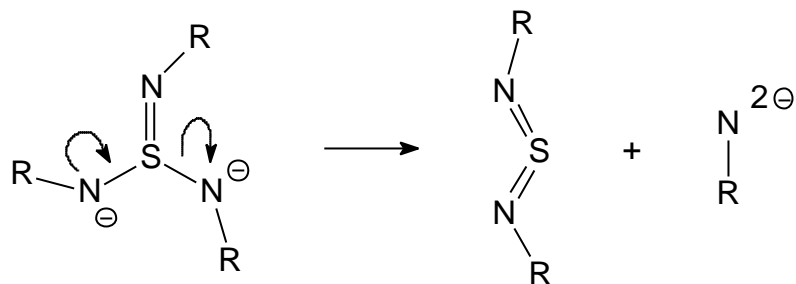
Bedingt durch die vielfältige Koordinations- und Redoxchemie, befaßte sich unser Arbeitskreis in den letzten 5 Jahren hauptsächlich mit der Chemie der Triimidosulfite und Tetraimidosulfate. Wenngleich bereits einige Transmetallierungen mit dem Di-Lithium-Triimidosulfit durchgeführt wurden (vorrangig $[(thf)_2M\{N(SiMe_3)_2\}_2]$, $M = Ca, Ba, Sn$), waren bisher noch keine Übergangsmetallverbindungen bekannt. Transmetallierungen mit CuI und $AgBr$ sind möglich.

Allerdings ist der Metallaustausch nicht vollständig. Ein Teil des gebildeten Lithiumhalogenids bleibt in der Peripherie der resultierenden Komplexe koordiniert. Da das chemische Gleichgewicht der Umsetzung von Lithiumtriimidosulfit mit gelöstem Lithiumchlorid deutlich auf die Seite des gebildeten Lithiumchloridaddukts verschoben ist (siehe Verb. **6**), ist es naheliegend, daß die Abstraktion des gebildeten Lithiumhalogenids thermodynamisch gehindert ist.

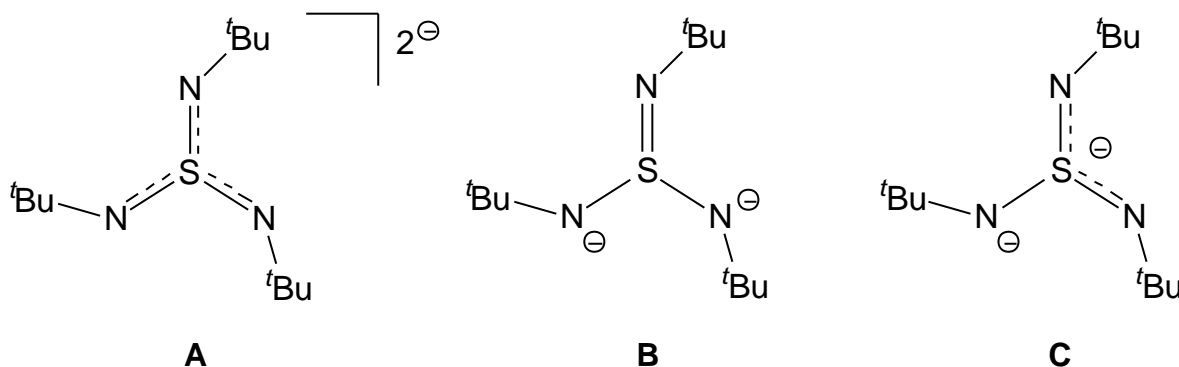


Mit starken Lewissäuren wie $GeCl_2$ und $SnCl_2$ findet eine komplette Zersetzung des Triimidosulfits zu Schwefel und Imid statt. Bei der Umsetzung mit $Fe(OAc)_2$ wird jedoch nur eine Imidgruppe heterolytisch vom Triimidosulfit abgespalten und Schwefeldiimid als Nebenprodukt gebildet. Dieses Produkt findet sich in $[Fe_2(\eta^2-$

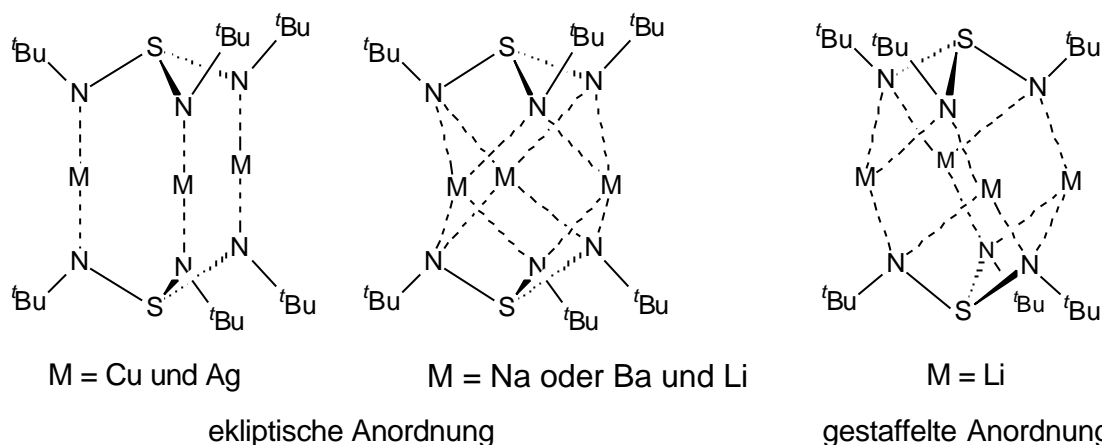
$\text{N}^t\text{Bu}_2\{(\text{N}^t\text{Bu})_2\text{S}\}_2$ (**5**) als chelatisierender Neutralligand wieder. Diese Abstraktion stellt formal den ersten Schritt einer Transimidierungsreaktion dar.



Das Triimidosulfit ist elektronisch ein äußerst flexibler Ligand. Abhängig von der Polarisierbarkeit des koordinierten Metalls tragen unterschiedliche Resonanzformeln zur bestmöglichen Beschreibung der Bindungsverhältnisse bei. Die Elektronendichte ist im $[\text{Li}_2\{(\text{N}^t\text{Bu})_3\text{S}\}_2]$.^[2h] gleichmäßig über alle drei SN-Bindungen delokalisiert (**A**). In **1-4**, $[(\text{thf})\text{LiSn}\{\text{N}(\text{SiMe}_3)_2\}\{(\text{N}^t\text{Bu})_3\text{S}\}]$ und $[(\text{thf})_2\text{CaLi}_2\{(\text{N}^t\text{Bu})_3\text{S}\}_2]$ ^[34] liegt eine kurze und zwei signifikant längere SN-Bindung vor (**B**). Beispiele mit einer langen und zwei kurzen SN-Bindungen sind $[(\text{thf})_2\text{Ba}_2\text{Li}\{\text{N}(\text{SiMe}_3)_2\}\{(\text{N}^t\text{Bu})_3\text{S}\}_2]$ ^[34] und $[(^t\text{BuN})(\text{Cl})_4\text{Sn}_2\{(\text{N}^t\text{Bu})_3\text{S}\}]$.^[118] Sie lassen sich am besten durch die Resonanzform (**C**) beschreiben.

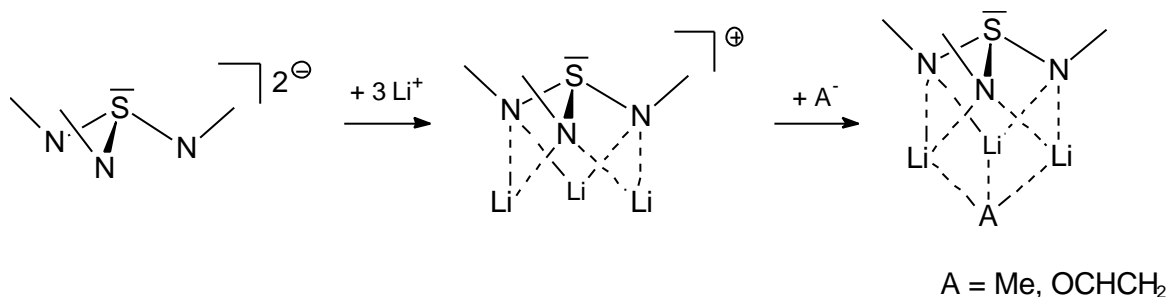


Auch das koordinative Verhalten des Triimidosulfits wird vom Metall dominiert. Mit Hauptgruppenmetallen, bei denen eher elektrostatische Wechselwirkungen eine Rolle spielen, koordiniert ein Imidosubstituent in der Regel μ_2 . Mit Münzmetallen, bei denen die Koordination orbitalkontrolliert ist, findet man eine lineare Anordnung. In Verbindungen mit zwei Triimidosulfit Dianionen ist die relative Lage der Kappen zueinander von der Anzahl der Metalle zwischen den beiden Liganden abhängig. Mit drei Kationen sind sie ekliptisch, mit vier Kationen gestaffelt angeordnet.



Scheme 15: Relative Anordnung zweier Triimidosulfitdianionen in Abhängigkeit der zwischen den beiden Liganden koordinierten Metallkationen.

Die Koordination von drei Lithiumkationen an das Triimidosulfit $\text{S}(\text{N}^t\text{Bu})_3^{2-}$ Dianion führt zu einem kationischen $\text{Li}_3(\text{N}^t\text{Bu})_3\text{S}^+$ Liganden. Dies beschreibt die Umwandlung eines tripodal koordinierenden Dianions in einen Inverspodanden, der leicht Anionen solvatisieren kann.

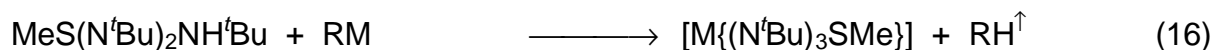


Das Li_3 -Dreieck als strukturelles Leitmotiv der lithiumorganischen Chemie ist nicht nur in der Lage, einzelne Carbanionen wie Methanid zu solvatisieren, es kann auch möglich reaktive Intermediate und Zwischenprodukte wie Ethylenoxid, gebildet aus der Zersetzungsreaktion von thf mit *Tert*butyllithium, stabilisieren. In allen Komplexen werden die Anionen η^3 von drei Lithiumkationen koordiniert (Cl^- (**6**), Br^- ,^[13] I^- ,^[13] S^{2-} ,^[62] N_3^- ,^[60] Me^- (**7**), H_2CCHO^- (**8a,b**)). Im Chlorid- und im Azidaddukt koordiniert das Anion an einen zweiten $\text{Li}_3(\text{N}^t\text{Bu})_3\text{S}^+$ -Liganden unter Ausbildung eines Dimers (Cl^-) bzw. Polymers (N_3^-).

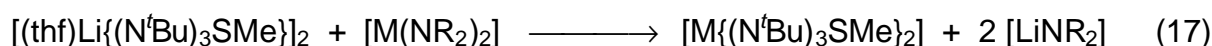
In dieser Arbeit wurden drei effiziente synthetische Routen zu Metallkomplexen des S-Alkyltriimidosulfonat erarbeitet. Die erste entspricht einer Deprotonierung der S-

Methyl-tri(*tert*butyl)triimididosulfonsäure (Gl. 16). Die zweite Möglichkeit ist die Transmetallierung des Lithium-S-methyl-tri(*tert*butyl)triimididosulfonats mit Metallamiden wie zum Beispiel $[M\{N(SiMe_3)_2\}_2]$ ($M = Ba, Zn, Sn, Fe$) (Gl. 17). Eine neue Methode ist die Insertion von Schwefeltriimid in die Metall-Kohlenstoffbindung von Metallalkylen wie zum Beispiel Trimethylaluminium oder Dimethylzink (Gl. 18).

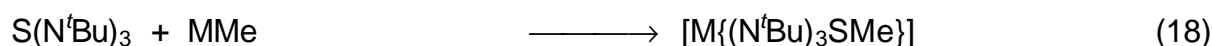
Deprotonierung:



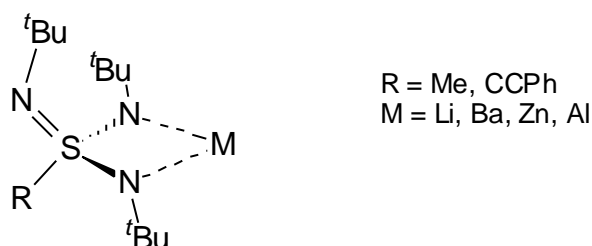
Transmetallierung:



Insertion:

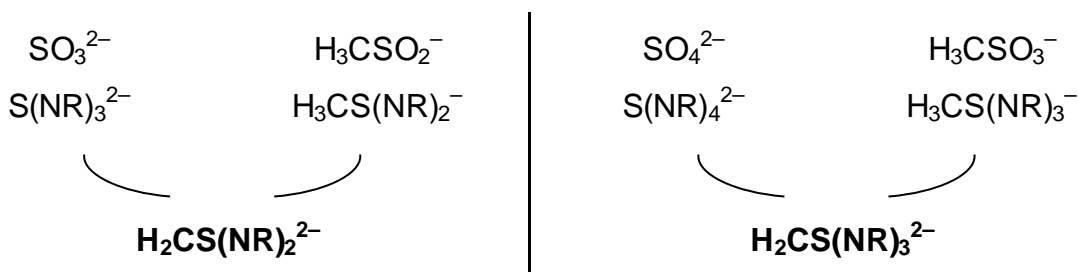


In allen Triimididosulfonat-Verbindungen wird das Metallkation η^2 -chelatisierend koordiniert. Die beiden tertiären Kohlenstoffatome der (M)N-gebundenen *tert*butylgruppen liegen in der SN_2M -Ebene. Die dritte *tert*butylgruppe ist zur offenen N_3 -Ebene gerichtet, was eine weitere Koordination des dritten Stickstoffatoms zum gleichen Metall verhindert.



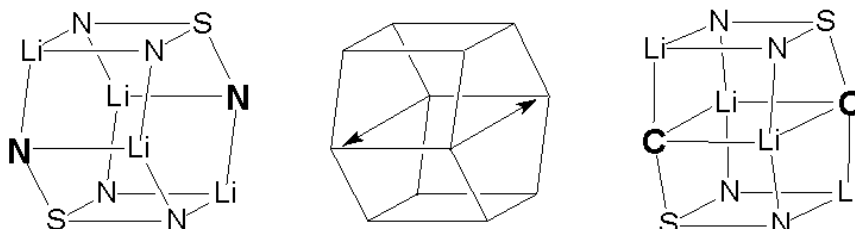
Anhand der Variation der Metallradien (Li, Ba, Zn, Al), sowie des sterischen Anspruchs des am schwefelgebundenen Substituenten (Me, CPh), kann ausgeschlossen werden, daß dies ein Effekt des sterischen Anspruchs der Metalle oder des am Schwefel gebundenen Substituenten ist. Vielmehr zeigt ein Vergleich mit dem Triimididosulfat, bei dem trotz eines an das Schwefelatom gebundenen Sauerstoffatoms eine tripodale Koordination stattfindet, daß für die Delokalisation der einfach negativen Ladung zwei Bindungen ausreichen. Die Addition eines Dimethylzink Fragments $[(thf)_2Li\{(N^tBu)_3SMe\}\cdot ZnMe_2]$ (**13**) belegt, daß eine weitere Koordination des dritten amidischen Stickstoffatoms an ein weiteres Metallzentrum möglich ist.

Einen völlig neuen Aspekt in die Chemie der Polyimidosphwefelanionen zeigt der isoelektronische Ersatz einer NR Gruppe durch einen CR_2 Substituenten auf. Eine in dieser Arbeit erarbeitete Synthesemöglichkeit ist die Metallierung der S-gebundenen Alkylgruppe in den Alkyldiimidosulfaten und Alkyltriimidosulfaten mit Methyllithium.



Der Austausch einer NR Gruppe im Triimidosulfit durch eine CR_2 Gruppe hat einen deutlichen Effekt auf dessen koordinatives Verhalten. Wie das Triimidosulfit bildet auch das Alkylendiimidosulfit einen dimeren Cluster.

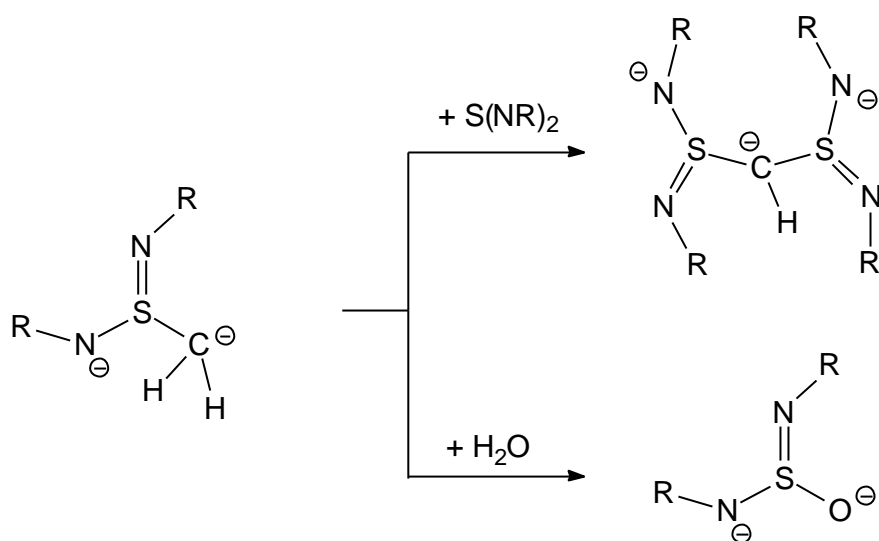
Da das carbanionische Kohlenstoffatom, analog der bekannten lithiumorganischen Verbindungen $[\text{MeLi}]_4$ und $[\text{BuLi}]_6$, bevorzugt μ_3 eine Li_3 Dreiecksfläche verbrückt, bewirkt dies eine Kontraktion des hexagonal prismatischen Dimers zu zwei seitenverknüpften Kuben.



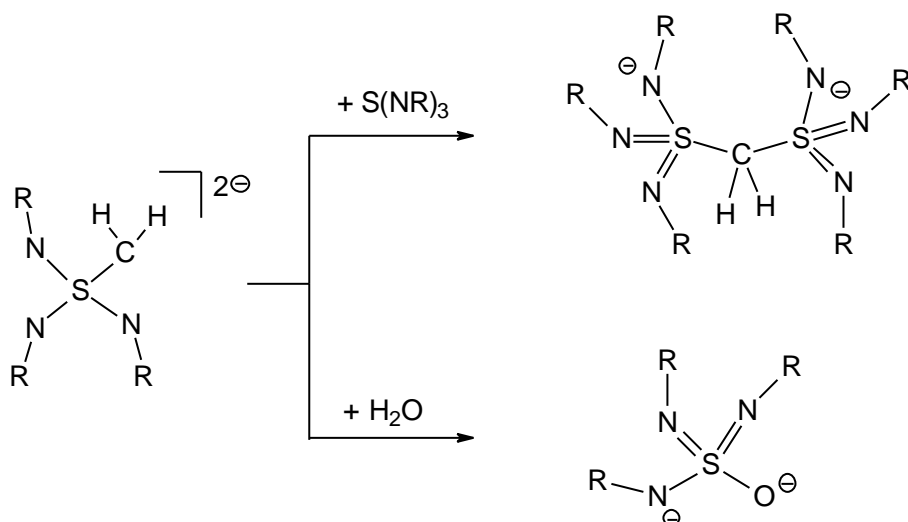
Das koordinative Verhalten des Methyltriimidosulfats entspricht dem des Tetraimidosulfats. Das Schwefelatom ist verzerrt tetraedrisch umgeben. Zwei NR Gruppen sowie eine NR und CR_2 Gruppe chelatisieren jeweils η^2 ein Lithiumatom. ist gleichfalls Das carbanionische Zentrum dominiert die Reaktivität des Methylendiimidosulfit und Methyltriimidosulfat in der Folgechemie.

Im Falle des Methylendiimidosulfit gelangt man durch Additionsreaktion des Methylkohlenstoffatoms an ein Schwefeldiimid zur neuen Substanzklasse der Alkylen-di-diimidosulfinate. Allerdings ist die Acidität der Wasserstoffatome der verbrückenden Methylengruppe so groß, daß nur die deprotonierte Form isoliert

werden konnte. Durch Hydrolyse von Alkylendiimidosulfit mit einem Äquivalent Wasser erhält man Diimidosulfit und Methan.



Das Methylentriimidosulfat zeigt eine analoge Reaktivität. Durch Addition an ein Schwefeltriimid gelangt man zur neuen Substanzklasse der Methan-di-triimidosulfonate, die imidoanalogen Verbindungen zu den seit über hundert Jahren bekannten Methan-di-sulfonaten. Die Hydrolyse des Methylentriimidosulfat mit einem Äquivalent Wasser ergibt Triimidosulfat und Methan.



Die Alkyldiimidosulfinate und Alkyltriimidosulfonate stellen faszinierende Ausgangsmaterialien zur Synthese einer komplett neuen Substanzklasse: den dianionischen Schwefelyliden Alkylendiimidosulfit und Alkylentriimidosulfat dar.

Bedingt durch den carbanionischen Charakter des α -Kohlenstoffatoms sind Additionsreaktionen möglich. Desweiteren erwarten wir analoge Reaktionen zu Wittig's Phosphoryliden; Übertragung der CR_2 Gruppe auf Ketone und Aldehyde unter Ausbildung von Diimidodisulfid oder Triimidodisulfat. Der reizvolle Vorteil dieser neuartigen Schwefelylide liegt in der Möglichkeit die Reaktivität der S–N sowie S–C Bindung mittels unterschiedlicher organischer Substituenten in der Peripherie zu steuern.

6 Experimental

All experiments were performed in a nitrogen atmosphere either by using modified Schlenk techniques or in a drybox. Solvents were freshly distilled from sodium-potassium alloy prior to use. ^1H -, ^7Li - and ^{13}C -NMR-spectra were recorded in C_6D_6 (^1H C_6HD_5 : $\delta = 7.15$; ^{13}C C_6D_6 : $\delta = 128.0$) using a JEOL Lambda 300 and a Bruker AMX 400 spectrometer. The solid-state ^6Li MAS and ^{13}C CP/MAS NMR experiments were performed using a Bruker DSX 400 spectrometer, while the 2D ^7Li MQMAS was recorded on a Bruker MSL 400 spectrometer. Several reaction controls were performed by GC on a Shimadzu GC-8A fitted with a Carbowax 20M on ChromosorbW-AW column and Helium 5.0 carrier gas. IR spectra were determined on a Bruker IFS 25 FT-IR spectrometer. Melting (decomposition) points were determined by using a MEL TEMP II, laboratory devices, melting point apparatus. Elemental analysis were performed at the analytical laboratory of the Institut für Anorganische Institut Würzburg.

[(thf) $_2$ Cu $_3$ Li $_2$ I{(N t Bu) $_3$ S} $_2$] (1): To a suspension of 1 g (5.25 mmol) CuI in 15 mL thf was dropped a solution of (1.31 mmol, 0.78 g) [(thf)Li $_2$ {(N t Bu) $_3$ S} $_2$] in 20 mL thf and stirred for 1 h. thf was removed in vacuum and the resulting white precipitate was solved in cold hexane. The remaining white precipitate (LiCl) was removed by filtration. Storage of the clear solution at -36 °C for 3 days affords colorless crystals of **1**, which were suitable for X-ray structure determination, (0.8 g, 63%). ^1H -NMR (300.4 MHz, C_6D_6): $\delta = 1.24$ (m, 8 H, thf), 1.43, 1.48 (2 s, 54 H, C(CH $_3$)), 3.70 (m, 8 H, thf); ^{13}C -NMR (100 MHz, C_6D_6): $\delta = 26.09$, 69.46 (thf), 35.30, 35.98 (C(CH $_3$) $_3$), 57.05, 57.74 (C(CH $_3$) $_3$). ^7Li -NMR (155.5 MHz, ext. sat. LiCl solution) $\delta = 1.16$.

[(thf) $_2$ Ag $_3$ Li $_2$ Br{(N t Bu) $_3$ S} $_2$] (2), [(thf)Ag $_3$ Li $_2$ Br{(N t Bu) $_3$ S} $_2$] $_2$ (3), [(thf) $_2$ Ag $_3$ Li $_6$ Br $_3$ {(N t Bu) $_3$ S} $_2$] (4): To a suspension of 1 g (5.33 mmol) AgBr in 15 mL thf was dropped a solution of (1.33 mmol, 0.78 g) [(thf)Li $_2$ {(N t Bu) $_3$ S} $_2$] in 20 mL thf and stirred for 1 h. thf was removed in vacuum and the white precipitate was resolved in cold hexane. The remaining white precipitate (LiCl) was removed by filtration. Storage of the solution at -36 °C for 3 days affords colorless crystals of **2-4**, which were suitable for X-ray structure determination. ^1H -NMR (300.4 MHz, C_6D_6): $\delta = 1.39$ (m, 8H, thf),

1.58, 1.60 (2 s, 54 H, C(CH₃)), 3.67 (m, 8 H, thf); ¹³C-NMR (100 MHz, C₆D₆): δ = 25.65, 68.25 (thf), 35.54, 35.61 (C(CH₃)₃), 55.96, 56.97 (C(CH₃)₃).

[Fe(N^tBu)((N^tBu)₂S)]₂ (5): To a suspension of 2 g (5.66 mmol) Fe(AcAc)₃ in 15 mL thf was dropped a solution of (11.32 mmol, 6.64 g) [(thf)Li₂{(N^tBu)₃S}]₂ in 20 mL thf and stirred for 1 h. The solution turns immediately black. Storage of the solution at –36 °C for several days affords black crystals which were suitable for X-ray structure determination (1.5 g, 44%). ¹H-NMR (300.4 MHz, C₆D₆): δ = 1.36, 1.40 (s, CH₃); ¹³C-NMR (100 MHz, C₆D₆): δ = 41.74, 41.82 (C(CH₃)₃), 58.3, 58.4 (C(CH₃)₃). Elemental analysis calcd (%): C 47.84, H 9.03, N 13.95, S 10.64; found C 47.67, H 9.39, N 13.04, S 10.08.

[(thf)₂Li₃Cl{(N^tBu)₃S}]₂ (6): To a solution of (17.20 mmol, 3.0 g) S(N^tBu)₂ and (17.20 mmol, 1.88 g) ^tBuNH₃Cl in 20 mL thf was dropped a solution of (34.40 mmol, 2.68 g) ^tBuNHLi in thf at –78 °C. Half of thf was removed in vacuum. Storage of the solution at –36 °C for several days affords colourless crystals which were suitable for X-ray structure determination (1.5 g, 44%). ¹H-NMR (300.4 MHz, C₆D₆): δ = 1.37 (m, 12H, thf), 1.57 (s, 54H, C(CH₃)), 3.72 (m, 12 H, thf); ¹³C-NMR (100 MHz, C₆D₆): δ = 25.47, 68.39 (thf), 34.45 (C(CH₃)₃), 53.24 (C(CH₃)₃); ⁷Li-NMR (155.5 MHz, ext. sat. LiCl solution) δ = 1.80. Elemental analysis calcd (%): C 53.87, H 9.72, N 9.43, S 7.19; found C 53.67, H 9.89, N 9.04, S 7.08.

[(thf)₃Li₃Me{(N^tBu)₃S}] (7): To a solution of (5.07 mmol, 3.0 g) [(thf)Li₂{(N^tBu)₃S}]₂ in 20 mL thf 3.4 mL of a 3 M solution of methyllithium (10.14 mmol) were slowly added at –78 °C and stirred for 1 h. The solution was stirred for two hours at room temperature. thf was removed in vacuum and the white precipitate was resolved in warm hexane. Storage of the solution at –36 °C for 3 days affords colourless crystals which were suitable for X-ray structure determination, (2.6 g, 78%). ¹H-NMR (300.4 MHz, C₆D₆): δ = –1.41 (s, 3H, CH₃), 1.34 (m, 12H, thf), 1.55 (s, 27H, C(CH₃)), 3.70 (m, 12 H, thf); ¹³C-NMR (100 MHz, C₆D₆): δ = 25.54, 68.46 (thf), 34.61 (C(CH₃)₃), 53.24 (C(CH₃)₃); ⁷Li-NMR (155.5 MHz, ext. sat. LiCl solution) δ = 2.16, (br s, 2Li), 2.67 (br s, 1Li). ⁶Li MAS NMR (58.9 MHz, ext. solid LiCl): δ = 2.1 (br s, 1Li), 2.8 (br s, 2Li); ¹³C CP/MAS NMR (100.6 MHz, ext. TMS): δ = –13.9 (Li₃CH₃), 25.8, 26.0, 26.2,

68.6, 69.0 (thf), 34.4, 34.8 (C(CH₃)₃), 52.5, 52.8, 53.0 (C(CH₃)₃); Elemental analysis calcd (%): C 60.34, H 10.94, N 8.45, S 6.44; found C 59.67, H 9.89, N 9.04, S 6.08.

[(thf)₃Li₃(OCHCH₂)(N^tBu)₃S]}₂ (8a,b): To a solution of (8.46 mmol, 5.0 g) [(thf)₂Li₂{(N^tBu)₃S}]₂ in 20 mL thf 4.97 mL of a 1.7 M solution of *tert*butyllithium (16.92 mmol) was slowly added at -78°C and stirred for 1 h. The solution was stirred for two hours at room temperature. Thf was reduced to half its volume in vacuum. Storage of the solution at -36 °C for several days affords colourless crystals, which were suitable for X-ray structure determination, (2.6 g, 78%). ¹H-NMR (300.4 MHz, C₆D₆): δ = 1.37 (12H, thf), 1.54 (s, 27H, C(CH₃)), 3.71 (12 H, thf), 4.03 (d, 2 H, OCHCH₂), 7.45 (t, 1 H, OCHCH₂); ¹³C-NMR (100 MHz, C₆D₆): δ = 25.52, 68.40 (thf), 33.89 (C(CH₃)₃), 52.99 (C(CH₃)₃) 82.15 (OCHCH₂), 159.68 (OCHCH₂); ⁷Li-NMR (155.5 MHz, ext. sat. LiCl solution) δ = 1.35, (br s, 3 Li).

[(thf)Li₂{(CH₂)(N^tBu)₂S}]₂ (9): To a solution of 3.0 g (8.82 mmol) [(thf)₂Li₂{(N^tBu)₂SMe}] in 20 mL thf 5.5 mL (8.82 mmol) of a 1.6M MeLi solution were added slowly at -78°C. Immediately evolution of methane gas was observed. The solution was stirred for another two hours at room temperature. The solvent was removed in vacuum and the white precipitate was dissolved in warm hexane. Storage of the solution for several days at -5°C affords colourless crystals suitable for X-ray crystallography, (2.1 g, 86%). Mp. 114°C (dec.). ¹H NMR (300 MHz, C₆D₆): δ = 0.97 (s, 4H; S-CH₂), 1.22 (m, 8 H; thf), 1.44 (s, 36 H; C(CH₃)₃), 3.48 (m, 8 H; thf); ¹³C NMR (100 MHz, C₆D₆): δ = 25.42, 68.70 (thf), 33.85 (C(CH₃)₃), 52.58 (C(CH₃)₃); ⁷Li NMR (116.7 MHz, ext. sat. LiCl solution) δ = 1.67, 2.73 (2 s, 4 Li); ⁶Li MAS NMR (58.9 MHz, ext. solid LiCl): δ = 1.9, 2.9 (2s, 1:1; 4Li); ¹³C CP/MAS NMR (100.6 MHz, ext. TMS): δ = -13.9 (S-CH₂), 25.8, 26.0, 26.2, 69.0 (thf), 34.2, 34.3, 34.8 (4 C(CH₃)₃), 52.8, 53.2 (C(CH₃)₃); elemental analysis calcd (%) for C₂₆H₅₆Li₄N₄O₂S₂ (548.63): C 56.92, H 10.29, N 10.21, S 11.69; found C 54.67, H 9.89, N 10.43, S 10.70.

[(thf)Li₂{(Et)(Me)CS(N^tBu)₂}]}₂ (10): To a solution of 22 g (57.37 mmol) [(thf)₂Li₂{(N^tBu)₂SCH(CH₃)(C₂H₅)}]} in 35 mL thf 35.5 mL (57.37 mmol) of a 1.6M MeLi solution were added slowly at -78°C. Immediately evolution of methane gas was observed. The solution was stirred for another two hours at room temperature. The

solvent was removed in vacuum and the white precipitate was dissolved in warm hexane. Storage of the solution for several days at -36°C affords colourless crystals suitable for X-ray crystallography, (12.7 g, 71%). Mp. 132°C (dec.). ^1H NMR (300 MHz, C_6D_6): $\delta = 1.43$ (4H; S-C $\underline{\text{C}}\text{H}_2\text{CH}_3$), 1.46 (6H; S-C $\underline{\text{C}}\text{H}_2\text{CH}_3$), 1.60 (s, 3H; S-C $\underline{\text{C}}\text{H}_3$), 1.33 (m, 8 H; thf), 1.48 (s, 36 H; C($\underline{\text{C}}\text{H}_3$) $_3$), 3.60 (m, 8 H; thf); ^{13}C NMR (100 MHz, C_6D_6): $\delta = 25.52$, 68.29 (thf), 33.11, 33.44, 34.27 (S-C $\underline{\text{C}}\text{H}_2\text{CH}_3$ or S-C $\underline{\text{C}}\text{H}_2\text{C}\underline{\text{H}}_3$ or S-C $\underline{\text{C}}\text{H}_3$), 34.51 (C($\underline{\text{C}}\text{H}_3$) $_3$), 53.56, 53.63 ($\underline{\text{C}}(\text{CH}_3)$ $_3$); ^7Li NMR (116.7 MHz, ext. sat. LiCl solution) $\delta = 1.92$ (s, 4 Li). elemental analysis calcd (%) for $\text{C}_{32}\text{H}_{68}\text{Li}_4\text{N}_4\text{O}_2\text{S}_2$ (632.78) C 56.92, H 10.29, N 10.21, S 11.69; found C 54.67, H 9.89, N 10.43, S 10.70.

[(thf)Li $_3$ {((N t Bu) $_2$ S) $_2$ CH}] $_2$ (11): To a solution of 1.05 g (2.2 mmol) **7** in 10 mL thf, 0.38 g (2.2 mmol) di-*tert*-butylsulfurdiimide was added slowly at room temperature. In the beginning the colour of the solution turns from yellow to red. At the end of the addition the colour turns back to yellow. After stirring the solution for two hours at room temperature the thf was removed in vacuum and the white precipitate was solved in warm hexane. Storage of the solution for several days at -36°C affords colourless crystals suitable for X-ray crystallography (0.9 g, 67%). Mp. 68°C (dec.). ^1H NMR (300 MHz, C_6D_6): $\delta = 1.33$ (m, 8 H; thf), 1.34 (s, 36 H; C($\underline{\text{C}}\text{H}_3$) $_3$), 3.57 (m, 8 H; thf), 1.54 (s, 2 H; S $\underline{\text{C}}\text{H}_2\text{S}$); ^{13}C NMR (100 MHz, C_6D_6): $\delta = 25.34$, 68.67 (thf), 34.22 (C($\underline{\text{C}}\text{H}_3$) $_3$), 52.63 ($\underline{\text{C}}(\text{CH}_3)$ $_3$) 64.00 (S-C $\underline{\text{H}}_2$ -S); ^7Li NMR (116.7 MHz, ext. sat. LiCl solution) $\delta = 1.58$, 2.06.

H(N t Bu) $_3$ SMe (12): A suspension of *tert*-butylammonium chloride (8 mmol, 0.88g) in thf (10 mL) was added at -5°C to a solution of [(thf) $_2$ Li $_2$ {(N t Bu) $_3$ SMe} $_2$] (4 mmol, 2.72 g) in thf (10 mL) and stirred for 1 h. All volatile material was removed under vacuum and pentane was added to the residue. After filtration from lithium chloride most of the pentane was removed in vacuum. After storage the oily solution at -36°C for 2 d colorless crystals were obtained and used for structure determination (0.8 g, 76 %). Mp. 18°C ; ^1H NMR (400 MHz, C_6D_6): δ 1.37 (s, 27 H, ^tBu), 2.79 (s, 3 H, CH_3), 2.80 (s, 1 H, NH); Elemental analysis calcd (%) for $\text{C}_{13}\text{H}_{31}\text{N}_3\text{S}$ (261.5): C 59.71, H 11.95, N 16.07, S 12.26; found: C 57.50, H 10.47, N 15.18, S 11.07; IR (Nujol) [cm^{-1}]: 3395.1 N(H), 3070-2860 (Nujol), 1465.6, 1408.8, 1379.3, 1356.6, 1300.3, 1247.5, 1129.4, 1024.0, 966.3, 941.9, 848.2, 829.8, 818.1, 745.5.

[Me₂Al{(N^tBu)₃SMe}] (13): To a solution of 0.98g (4.00 mmol) of tri(*tert*butyl)sulfur-triimide in 20 mL tetrahydrofuran 2 mL of a 2M Me₃Al solution in diethyl ether was added dropwise. The color of the solution changed instantaneously from yellow to colorless. After 3 h of stirring, 80 % of thf was removed in vacuum. After storage of the clear solution at -26 °C for 3 d colorless crystals were obtained and used for the structure determination (0.84 g, 66%). Mp. 133 °C; NMR: ¹H (400 MHz, C₆D₆) δ -0.921, -0.915 (s, 6 H, Al(CH₃)₂), 1.26 (s, 18 H, -NC(CH₃)₃), 1.27 (s, 9 H, =NC(CH₃)₃), 3.11 (s, 3H, SCH₃); ¹³C (C₆D₆): δ 30.07, 30.89 (-NC(CH₃)₃), 31.11 (=NC(CH₃)₃), 49.14, 50.24 (-NC(CH₃)₃), 51.51 (SCH₃), 53.39 (=NC(CH₃)₃). Elemental analysis calcd (%): C 56.74, H 11.43, N 13.24, S 10.10; found C 57.92, H 12.18, N 12.93; S 10.19.

[Zn{(N^tBu)₃SMe}₂] (14): To a solution of 2.50g (10.20 mmol) tri(*tert*butyl)sulfur-triimide in 20 mL tetrahydrofuran 2.55 mL of a 2M Me₂Zn solution in diethyl ether were added dropwise. After 3 h of stirring, the volume of the solution was reduced to the half and 10 mL hexane were added. Colorless crystals were grown by storage of the solution at -26 °C for 3 days and used for structure determination (1.93 g, 64%); Mp. 186 °C; NMR: ¹H (400 MHz, C₆D₆) δ 1.41 (s, 18 H, -NC(CH₃)₃), 1.50 (s, 18 H, -NC(CH₃)₃), 1.61 (s, 18 H, =NC(CH₃)₃), 2.96 (s, 3H, SCH₃); ¹³C (C₆D₆): δ 31.91, 32.05 (-NC(CH₃)₃), 32.31 (=NC(CH₃)₃), 50.65, 51.34 (-NC(CH₃)₃), 51.04 (SCH₃), 52.55 (=NC(CH₃)₃). Elemental analysis calcd (%): C 53.26, H 10.32, N 14.34, S 10.94; found C 52.24, H 10.16, N 13.25; S 11.13.

[(thf)₂Li{(N^tBu)₃SMe}·ZnMe₂] (15): To a solution of 2.00g (8.16 mmol) tri(*tert*butyl)sulfur-triimide in 20 mL tetrahydrofuran 5.10 mL of a 1.6M MeLi solution in diethyl ether was added dropwise. Subsequently, after stirring the solution for 1 h 4.08 mL of a 2M Me₂Zn solution in diethyl ether were added. After 3 hours of stirring, 50 % of thf was removed and 10 mL hexane were added. On storing the solution at -26 °C for 3 d colorless crystals were obtained and used for structure determination (3.2 g, 77%). Mp. 86 °C (dec.); NMR: ¹H (400 MHz, C₆D₆) δ -0.39 (s, 6 H, ZnMe₂), 1.39 (s, 27 H, NC(CH₃)₃), 1.34 (q, 8 H, thf), 3.53 (t, 8 H, thf), 3.16 (s, 3H, SCH₃); ¹³C (C₆D₆): δ -9.57 (ZnMe₂), 32.09 (NC(CH₃)₃), 51.75 (NC(CH₃)₃), 24.21 (thf), 66.64 (t, 8 H, thf), 47.23 (SCH₃); ⁷Li (155 MHz, C₆D₆): δ 0.56. Elemental analysis calcd (%): C 54.48, H 10.34, N 8.29, S 6.32; found C 52.12, H 9.22, N 9.07; S 6.89.

[(thf)₂Li{(N^tBu)₃SCCPh}] (16): To a solution of (22.76 mmol, 2.32 g) phenylacetylene in 20 mL thf 11.40 mL of 2 M solution of ⁿbutyllithium (22.76 mmol) were slowly added at –78°C and the reaction mixture was stirred for 1 h. To this solution tri-(*tert*butyl)sulfurtriimide (22.76 mmol, 5.8 g) was slowly added. The temperature has to be maintained below –20°C. At slightly higher temperatures the product decomposes indicated by a change of color from yellow through orange, brown to a finally green solution. 50% of thf was removed in vacuum. After storage of the concentrated solution at –36 °C for 3 days yellow crystals were obtained and used for structure determination. Because of the air sensitivity and thermolability at temperatures higher than –20°C no further analytical data could be obtained.

[(tmeda)₂Li₂{(CH₂S(N^tBu)₃}] (17): To a solution of (5.07 mmol, 3.0 g) [(thf)₂Li₂{(N^tBu)₃SMe₂}] in 20 mL thf 3.4 mL of a 3 M solution of methyllithium (10.14 mmol) were slowly added at –78°C and stirred for 1 h. rapid evolution of methane gas was observed. The solution was stirred for two hours at room temperature. thf was removed in vacuum and the white precipitate was resolved in warm hexane and tmeda. Storage of the solution at –36 °C for 3 days affords colourless crystals which were suitable for X-ray structure determination, (2.6 g, 78%). ¹H-NMR (300.4 MHz, C₆D₆): δ = 1.58 (2 H, SCH₂), 1.73 (s, 9 H, NC(CH₃)₃), 1.77 (s, 18 H, NC(CH₃)₃), 1.89 (s, 8 H, NCH₂CH₂N), 2.13 (s, 24 H, N(CH₃)₂); ¹³C-NMR (100 MHz, C₆D₆): δ = 34.61 (SCH₂), 34.85 (NC(CH₃)₃), 35.03 (NC(CH₃)₃), 46.55 (NCH₂CH₂N), 51.65 (NC(CH₃)₃), 52.17 (NC(CH₃)₃), 57.26 (s, 24 H, N(CH₃)₂); ⁷Li-NMR (155.5 MHz, ext. sat. LiCl solution) δ = 0.85, 1.24. Elemental analysis calcd (%): C 59.37, H 12.16, N 19.39, S 6.34; found: C 57.43, H 10.24, N 20.45, S 7.26.

[(tmeda)Li₂{OS(N^tBu)₃}]₃ (18): To a solution of (1.48 mmol, 0.75 g) **17** in 20 mL hexane 1.48 mmol of H₂O in 10 mL tmeda was slowly added at –10°C and stirred for 1 h. The solution was stirred for two hours at room temperature. Solvent was removed in vacuum and the white precipitate was resolved in warm hexane and tmeda. Storage of the solution at –36 °C for several days affords colourless crystals which were suitable for X-ray structure determination, (0.3 g, 51%). ¹H-NMR (400.13 MHz, C₆D₆): δ = 1.47 (s, 9 H, NC(CH₃)₃), 1.49 (s, 18 H, NC(CH₃)₃), 1.61 (s, 8 H, NCH₂CH₂N), 2.05 (s, 24 H, N(CH₃)₂); ¹³C-NMR (100 MHz, C₆D₆): δ = 33.39 (NC(CH₃)₃), 33.63 (NC(CH₃)₃), 34.62 (NCH₂CH₂N), 46.25 (NC(CH₃)₃), 51.70

($\text{NC}(\text{CH}_3)_3$); ^7Li -NMR (155.5 MHz, ext. sat. LiCl solution) $\delta = 0.55, 1.79$. Elemental analysis calcd (%): C 55.22, H 11.07, N 17.89, S 8.19; found: C 52.11, H 12.32, N 19.28, S 7.78.

[(thf) $_2$ Li $_2$ {(N^tBu) $_3$ S) $_2$ CH $_2$ }] (19): To a solution of 6.00 g (24.45 mmol) tri(*tert*butyl)sulfurtriimide in 20 mL tetrahydrofuran 15.3 mL of a 1.6M MeLi solution in diethyl ether were added dropwise. The color of the solution changed instantaneously from yellow to colorless. After 3 h of stirring another 15.3 mL of a 1.6M MeLi solution in diethyl ether was added. Immediate formation of methane gas was observed. After an hour 6.00 g (24.45 mmol) tri(*tert*butyl)sulfurtriimide in 20 mL tetrahydrofuran was added dropwise. 50 % of thf was removed in vacuum. After storage of the clear solution at $-26\text{ }^\circ\text{C}$ for 3 d colorless crystals were obtained, (15.9 g, 88%, Mp. $133\text{ }^\circ\text{C}$). ^1H -NMR (400 MHz, C_6D_6): $\delta = 1.28$ (8 H, thf), 1.62 (s, 54 H, NtBu), 3.52 (8 H, thf), 5.00 (s, 2 H, SCH $_2$ S); ^{13}C -NMR (100 MHz, C_6D_6): $\delta = 25.35, 68.40$ (thf), 33.54 (C($\underline{\text{C}}\text{H}_3$) $_3$), 53.89 ($\underline{\text{C}}(\text{CH}_3)_3$), 86.89 (S $\underline{\text{C}}\text{H}_2\text{S}$); ^7Li -NMR (155.5 MHz, ext. sat. LiCl solution) $\delta = 1.15$. Elemental analysis calcd (%): C 60.45, H 10.97, N 11.44, S 8.72; found C 59.95, H 10.65, N 12.01; S 9.01.

H $_2$ C{S(N^tBu) $_2$ (NH^tBu)} $_2$ (20): To a suspension of 2.60 g (23.85 mmol) ^tBuNH $_3$ Cl in 15 mL thf 15.9 g (23.85 mmol) of **19** in thf were added. The solution was stirred for 3 h. thf was removed under vacuum and 25 mL of hexane was added. The precipitated LiCl was filtered off. 50 % of the solvent was removed under vacuum. After storage of the clear solution at $-26\text{ }^\circ\text{C}$ for 3 d colorless crystals were obtained, (8.3 g, 69%, Mp. $128\text{ }^\circ\text{C}$). ^1H -NMR: (400 MHz, C_6D_6) δ 1.41 (s, 18 H, NHCC H_3), 1.49 (s, 36 H, =NC CH_3), 4.11 (s, 2 H, SCH $_2$ S), 6.85 (s, 2 H, NHC CH_3); ^{13}C -NMR (100 MHz, C_6D_6): δ 30.95 (NHC($\underline{\text{C}}\text{H}_3$) $_3$), 32.31 (=NC($\underline{\text{C}}\text{H}_3$) $_3$), 51.82 (NHC($\underline{\text{C}}\text{H}_3$) $_3$), 53.38 (=NC($\underline{\text{C}}\text{H}_3$) $_3$), 75.90 (S $\underline{\text{C}}\text{H}_2\text{S}$). Elemental analysis calcd (%): C 59.23, H 11.53, N 16.58, S 12.65; found C 59.95, H 11.65, N 16.01; S 13.01. IR (Nujol) [cm^{-1}]: 3146.7 m N(H), 3070-2860 s (Nujol), 1457.4 s, 1385.6 s, 1355.3 s, 1251.9 s, 1218.8 s, 1117.9 s.

7 Crystallographic Section

7.1 Crystal Application

A sample of the crystalline material was taken from the mother liquor, using standard Schlenk techniques and covered with an inert oil.^[119] The crystals were prepared in the inert oil (rewashing of satellites or checking for twinning under a microscope fitted with a polariser). A suitable crystal was mounted on the top of a glass fibre in a drop of inert oil and shock cooled on the diffractometer. All data were collected at low temperature.^[120]

7.2 Data collection

All data were measured using graphite monochromated MoK α radiation ($\lambda = 71.073$ pm). Data of compound **9a** and **17** were collected on an Enraf-Nonius CAD4 diffractometer; Data of compound **1**, **2b**, **3**, **5**, **6a**, **7**, **8**, **9b**, **9c**, **10-12** and **14** were collected on a STOE IPDS diffractometer and the data of compound **2a**, **2c**, **4**, **6b**, **13**, **15** and **16** were collected on a Bruker Smart Apex D8 diffractometer. Data of compound **18** was collected on a Bruker Smart 1000.

7.2.1 Procedure at the Enraf-Nonius CAD4 Diffractometer

After mounting and centering via a microscope, 25 reflections were searched in different Ewald sphere areas. After checking the profiles ($0.3^\circ - 0.45^\circ$ half width, shape, satellites) the reflections were indexed followed by a matrix refinement based on those 25 reflections. Furthermore, three dimensional ω - θ plots to optimize scan parameters were determined. Three intensive reflections for monitoring the intensity during the measurement and three reflections with a small deviation angle to check the matrix during the measurement, were selected. With the knowledge of the exact cell, data collection of the unique set together with a reasonable amount of equivalents to check the proposed symmetry restrictions, is started. The reflections

were collected in the $\omega/2\theta$ -scan mode with background-peak-background intensity measurement. Afterwards a psi-scan measurement is followed with 10 intensive reflections (χ angle $> 75^\circ$) for semiempirical absorption correction.^[121] Data reduction was performed with XCAD4B. With the obtained raw-file structure solution and refinement was processed.

7.2.2 Procedure at the STOE IPDS diffractometer

After mounting the crystal and centering with a microscope, some images were collected in a ϕ -range between $0^\circ - 360^\circ$ for screening the crystal quality and determining the unit cell. Several parameters are needed: The ϕ increment; The start and end position in phi depending on the symmetry restrictions and the desired redundancy; The detector distance and the irradiation time to get best intensities. The data collection is proceeded in a ϕ -scan mode with a stepsize usually between 0.4 and 1.0 degrees. Data integration is followed after determining a correct unit cell and a sensible mosaic spread. With the obtained raw-file structure solution and refinement was processed.

7.2.1 Procedure at the Bruker Smart Apex CCD D8 Diffractometer

After mounting the crystal and centering with a camera a rotation frame was taken to align the beam centre relative to the CCD camera. A single run (usually 50 frames in the ω -scan mode with a steps of 0.3°) is performed to check the crystals quality and the unit cell. Knowing the cell dimensions a useful strategy has to be planned by experience rather than application of push button systems like ASTRO or COSMO to get a complete dataset and a redundancy of at least 3 for a successful empirical absorption correction. Those programs failed totally and are not recommended to us at any straight. Data collection is performed depending on the strategy in the ω - and/or ϕ -scan mode with steps usually between $0.1^\circ - 0.3^\circ$. The program SAINT-NT^[122] was employed to integrate the frames. For every single run an exact orientation matrix has to be determined. The obtained data were empirical absorption corrected applying SADABS2.^[123] With the obtained hkl-file structure solution and refinement was processed.

7.3 Structure Solution and Refinement

General: All structures were solved by Patterson or direct methods with SHELXTL-NT V5.1.^[124] All structures were refined by full-matrix least-squares procedures on F^2 , using SHELXTL-NT V5.1.^[124] All non-hydrogen atoms were refined with anisotropic displacement parameters. Hydrogen atoms bonded to structure relevant atoms were located by difference Fourier syntheses and refined freely. All other hydrogen atoms of the molecule were refined using a riding model. The denoted R-values are defined as follows:

$$R1 = \frac{\sum ||F_o| - |F_c||}{\sum |F_o|}; \quad wR2 = \sqrt{\frac{\sum w(F_o^2 - F_c^2)^2}{\sum w(F_o^2)^2}}; \quad w = \frac{1}{s^2(F_o^2) + (g_1P)^2 + g_2P}; \quad P = \frac{(\max(F_o^2, 0) + 2F_c^2)}{3}.$$

Relevant data of the compounds **1-18** can be found in section 7.5.

Disorder: Several disorder problems occurred in the structures. A typical disorder phenomenon is the rotation around the N-C-bond of bonded *tert*butyl groups. Also twist disordering of coordinated thf molecules occurred. To refine disorder structures restraints are applied. The SAME instruction fits 1,2 and 1,3 distances of chemically equal groups with an effective standard deviation. The SADI instruction fits 1,2 distances with an effective standard deviation. The SIMU instruction fits U_{ij} of neighbored atoms to be the same with an effective standard deviation and the DELU instruction fits components of the anisotropic displacement parameters in the direction of the bond to be equal with an effective standard deviation.

7.3.1 Twin refinement

Prior to application of the crystal on the glass fibre the crystal was checked for twinning under a microscope fitted with a polariser. Usually two types of twinned crystals can be distinguished. Sometimes starting from one crystal nucleus two single crystals started to grown in different directions with an overlap (Figure 31, left). The symmetry element for this type of twinned crystal is a rotation axes. In other cases one plane is used as a base to grow another single crystal domain (Figure 31, right). The symmetry element for this type of twinned crystal is a mirror plane.

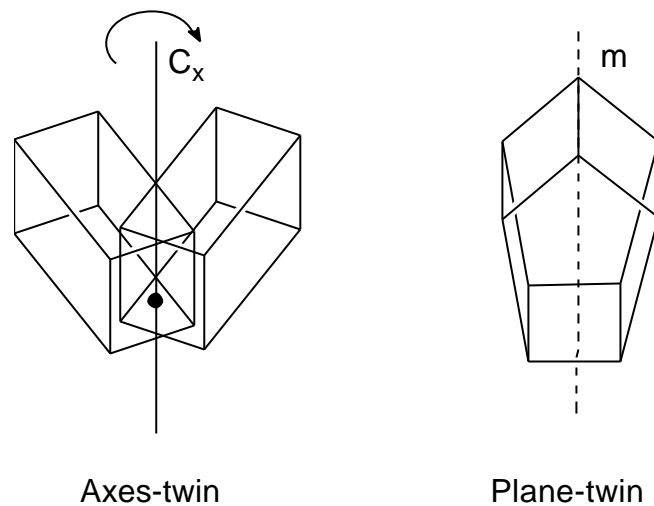


Fig. 31: Different kinds of macroscopic twinned crystals.

7.3.2 Twinning Types and its Effect on Reflections Overlap

Non-merohedral twins:

Generally each domain of a twinned crystal fulfill the Bragg conditions like a single crystal. Therefore some reflections of different domains can be overlapped. If there is only few coincidence of the reflections, the crystal is classified as a non-merohedral twin. Figure below shows a two dimensional projection of the reciprocal lattice of a non-merohedral twin. The two domains are visualised by different colours. White for the first domain and grey for the second.

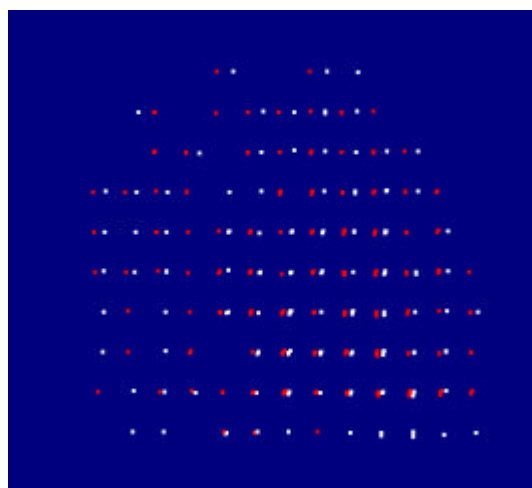


Fig. 32: Two dimensional projection of the reflections from a non-merohedral twin in the reciprocal space.

Partial-merohedral twins:

Reflections of a twinned crystal, in which every second or third (nth) layer in the reciprocal space is completely overlapped, are classified as partial merohedral twins of second or third (nth) order.

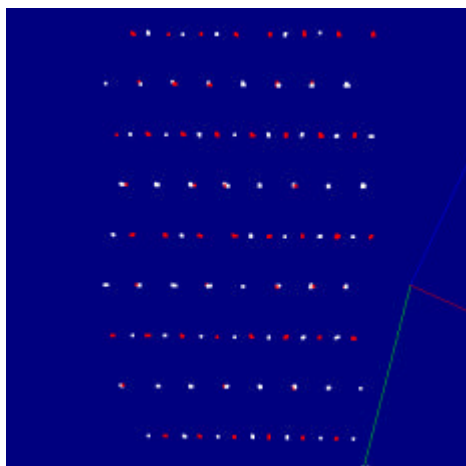


Fig. 33: Two dimensional projection of the reflections from a partial-merohedral twin in the reciprocal space.

Merohedral twins:

If the twin symmetry element belongs to the symmetry of the crystal system but not to the crystal class, all reflection of the two domains are overlapping, and the twin is classified as a merohedral twin.

7.3.3 Twin Solution Strategy

The important point in twin refinement is the separation of the overlapped reflections. Without separation, at the end of a normal refinement, the F_o^2 in comparison to its F_c^2 of many reflections are too large, and therefore the structure couldn't be refined well.

Non-merohedral twins:

The first step in twin solution is to determine the orientation matrices of every domain. This can be achieved in two different ways: first approach is the determination via the program GEMINI,^[125] which determines distances between the reflections in the reciprocal space and list possible cells and hits of how many reflections belong to this

cell. In a second step the orientation matrix of the second domain is determined in the same way by excluding the reflections belonging to the first domain.

The second approach is to separate the reflections of both domains with the program RLATT^[126] by a “pick and save routine”.

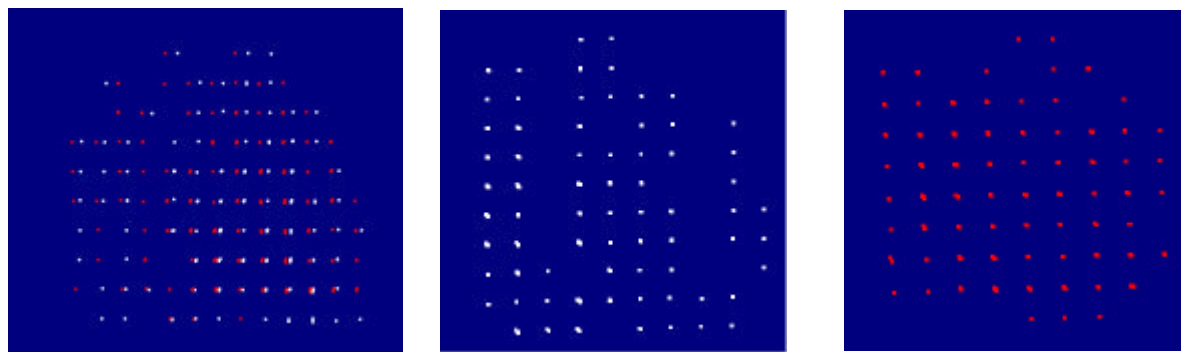


Fig. 34: Separation of the reflections via RLATT.^[126]

The matrices of the two domains were refined separately using the program SMART^[127]. Integration of the data in SAINT^[122] is performed with a fixed matrix and a fixed integration box for each domain. A suitable box size is determined in SMART^[127] with a scan over some reflections (Fig. 35 left).

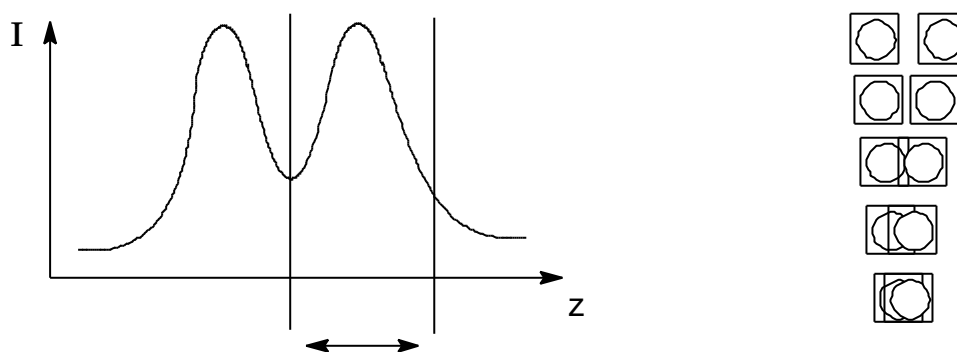


Fig. 35: Left side shows a scan along the z-axes of an overlapped reflection for determination of a suitable box size; right side shows the boxes during integration.

The resulting hkl- and p4p-files from integration serve as input for the program GEMINI.^[125] The program supplies a list of reflections sorted in separate ranges in reciprocal angstroms of each domain.

1. row: separation ranges in reciprocal angstroms
2. row: number of reflections in range of domain1
3. row: number of reflections in range of domain2

0.000	0.001	0.002	0.003	0.004	0.005	0.030	0.031	0.032	0.033	0.034
124	206	168	98	204	184	201	218	298	57	0
188	73	161	293	44	124	32	427	293	7	0

Usually the reflections are divided into five ranges. For every reflex a scaling factor is assigned depending on the degree of overlap and to which domain it belongs. Odd scaling factors for the first and even scaling factors for the second domain are assigned.

BASF numbers	Range (reciprocal angstroms)
1 2	0.0000 0.0070
3 4	0.0070 0.0140
5 6	0.0140 0.0210
7 8	0.0210 0.0280
9 10	0.0280 0.0350
1 2 >	0.0350 non-overlap

For structure solution, a HKLF 4 file is written which contains exclusively non-overlapped reflections of the main domain.

For structure refinement a HKLF 5 file is generated with all reflections of both domains. In the instruction file starting values for the scaling factors have to be given. In the upper example 9 values for 10 scaling factors. The tenth value is calculated via 1 minus the sum of all other values.

Partial merohedral twin:

The solution strategy of a partial merohedral twin is almost the same as for non-merohedral twins. First the orientation matrices have to be determined for both domains with the program RLATT^[126] and subsequently refined in SMART.

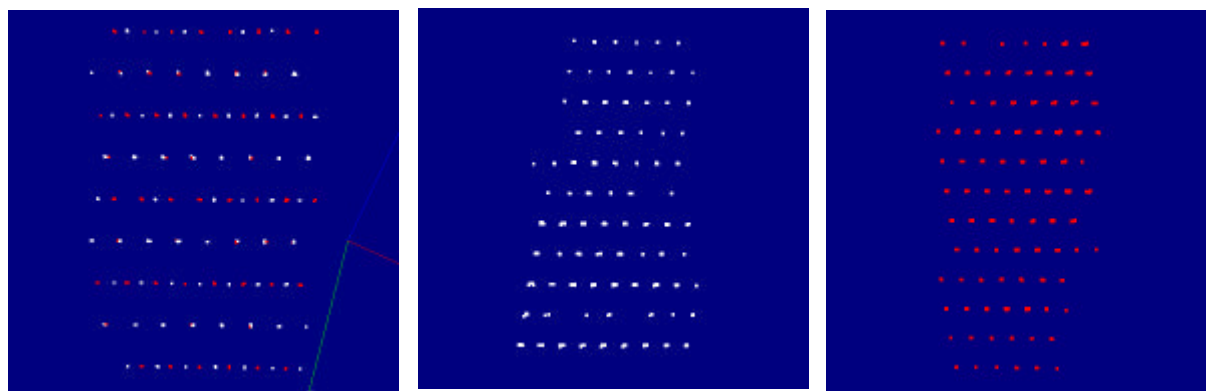


Fig. 36: Separation of the reflections with the program RLATT.

Integration of the data in SAINT^[126] is followed with a fixed matrix and a fixed box size for each domain.

The obtained raw- and p4p-files serve as input for the program GEMINI.^[125]

1. row: separation ranges in reciprocal angstroms
2. row: number of reflections in range of domain1
3. row: number of reflections in range of domain2

0.000	0.001	0.002	0.003	0.004	0.023	0.024	0.025	0.026	0.027	0.028
1607	3853	641	0	0	0	54	2120	3837	0	0
1584	3352	939	7	0	0	230	2197	3679	0	0

In the resulting list of reflections one can clearly distinguish the two overlapping ranges of the reflections (0.000 to 0.004 and 0.023 to 0.027). Therefore the hole range from 0.000 to 0.028 is divided into two ranges. (0.000 to 0.015, and 0.015 to 0.035).

BASF numbers Range (reciprocal angstroms)

1	2	0.0000	0.0150
3	4	0.0150	0.0350
1	2	> 0.0350	non-overlap

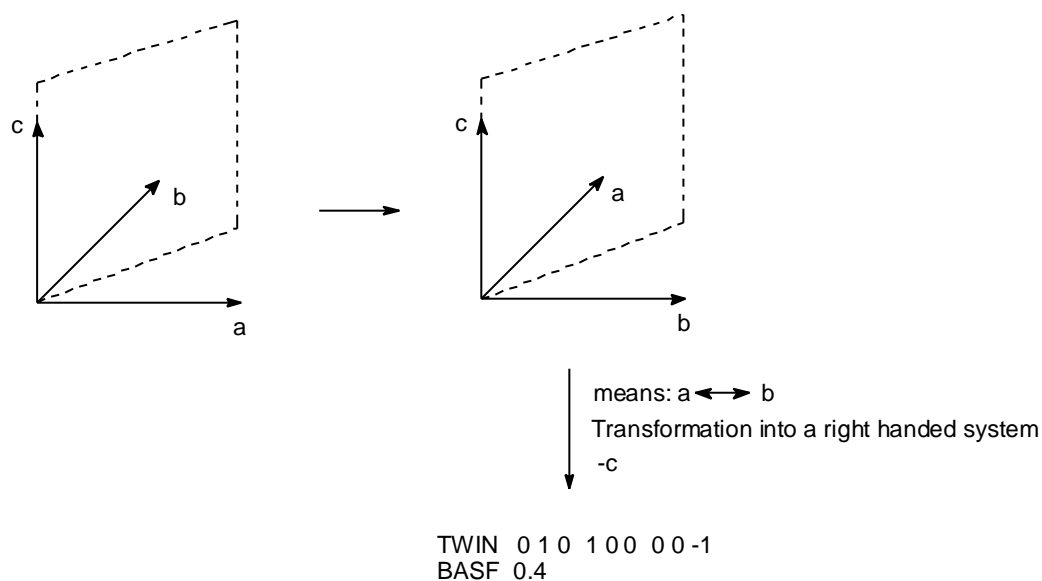
For structure solution, a HKLF 4 file is written which contains exclusively non overlapped reflections of the main domain.

For structure refinement a HKLF 5 file is generated with all reflections of both domains. In the instruction file starting values for the scaling factors have to be given. For the partiell merohedral case 3 values for 4 scaling factors. The fourth value is calculated via 1 minus the sum of all other values.

Merohedral twin:

In the case of merodric twins no separation of reflections is possible. Therefore it is important to determine the twin law (rotation axes or mirror plane) and the transformation matrix.

For example in the tetragonal crystal systems it is possible, that for the space group P4/m a diagonal mirror plane orthogonal to a and b pretends the higher symmetric space group P4/mmm. For determination of the transformation matrix see Scheme 21.



Scheme 21 Determination of the transformation matrix.

7.4 Structural Details

7.4.1 [(thf)₂Cu₃Li₂I{(N^tBu)₃S}₂] (1):

Compound **1** crystallises in the centrosymmetric, orthorhombic space group Pbcn. The asymmetric unit contains the complete molecule. The disordered thf molecules coordinated to Li1 and Li2 were refined using distance and adp restraints (SAME, SIMU, DELU) to split occupancies of 0.34/0.66 and 0.69/0.31. The disordered iodine atom was refined with distance restraints (SADI) to a split occupancy of 0.60/0.40.

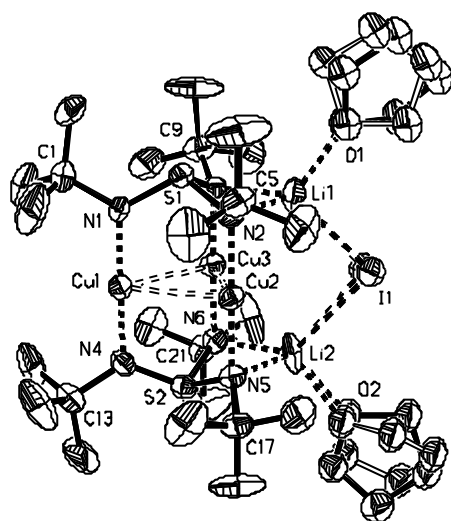


Figure 37: Asymmetric unit of **1** in the solid state; anisotropic displacement parameters are depicted at the 50% probability level.

7.4.2 [(thf)₂Ag₃Li₂Br{(N^tBu)₃S}₂] (2), [(thf)Ag₃Li₂Br{(N^tBu)₃S}₂]₂ (3), [(thf)₂Ag₃Li₃Br₂{(N^tBu)₃S}₂]₂ (4):

Compound **2** crystallised as a second order partial merohedral twin in the centrosymmetric monoclinic space group P2₁/c. The following matrices of the two domains have been determined:

$$\text{Orientation matrix 1} = \begin{pmatrix} 0.04909793 & 0.00239869 & 0.04372003 \\ -0.00443887 & -0.05067220 & 0.02172061 \\ 0.02149297 & -0.01594466 & -0.06245106 \end{pmatrix}$$

with the unit cell parameters,

$a = 18.8562$, $b = 18.8056$, $c = 12.7931$, $\alpha = 90.000$, $\beta = 99.558$, $\gamma = 90.000$, and

$$\text{orientation matrix } 2 = \begin{pmatrix} 0.04902566 & -0.00240312 & -0.01934586 \\ -0.00441433 & 0.05064767 & -0.02383247 \\ 0.02149436 & 0.01588277 & 0.07307091 \end{pmatrix}$$

with the unit cell parameters:

$a = 18.8956$, $b = 18.8203$, $c = 12.8056$, $\alpha = 90.000$, $\beta = 99.838$, $\gamma = 90.000$.

BASF numbers		Range (reciprocal angstroms)	
1	2	0.0000	0.0150
3	4	0.0150	0.0350
1	2	> 0.0350 non-overlap	

The scale factors refined to 0.5363, 0.1263, 0.2699 and 0.0675. The disordered thf molecules coordinated to Li1 and Li2 were refined using distance and adp restraints (SAME, SIMU, DELU) to split occupancies of 0.68/0.32 and 0.51/0.49, respectively.

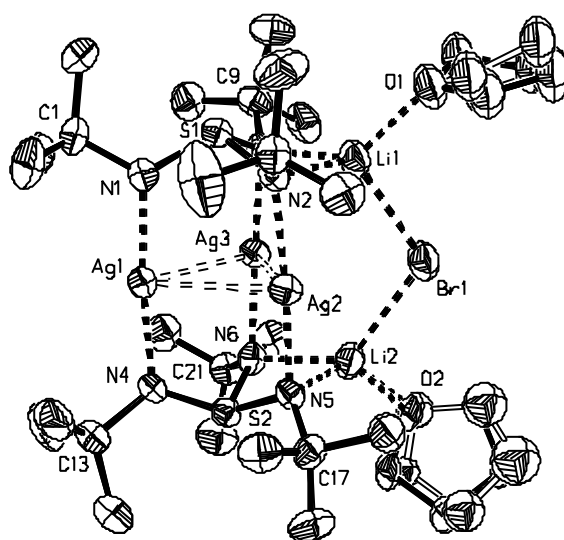


Figure 38: Asymmetric unit of 2 in the solid state; anisotropic displacement parameters are depicted at the 50% probability level.

Compound **3** crystallises in the non centrosymmetric, orthorhombic space group $Pca2_1$. As the Flack x-parameter^[128] refined to 0.37(4) the absolute structure could not be determined reliably. The asymmetric unit contains the complete molecule. The disordered thf molecules coordinated to Li2 and Li4 were refined using distance and adp restraints (SAME, SIMU, DELU) to split occupancies of 0.71/0.29 and 0.75/0.25, respectively.

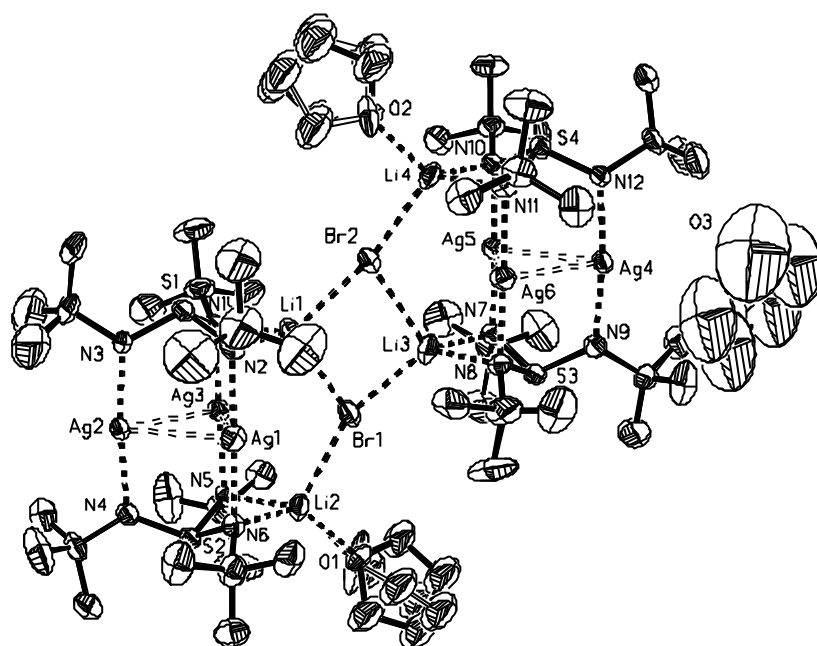


Figure 39: Asymmetric unit of **3** in the solid state; anisotropic displacement parameters are depicted at the 50% probability level.

Compound **4** crystallises in the centrosymmetric, monoclinic space group $P2_1/c$. The asymmetric unit contains half of the molecule. The complete molecule is generated by inversion at the origin followed by (2,1,1) translation. The disordered thf molecule coordinated to Li3 was refined with distance and adp restraints (SAME, SIMU, DELU) to split occupancies of 0.26/0.47/0.27.

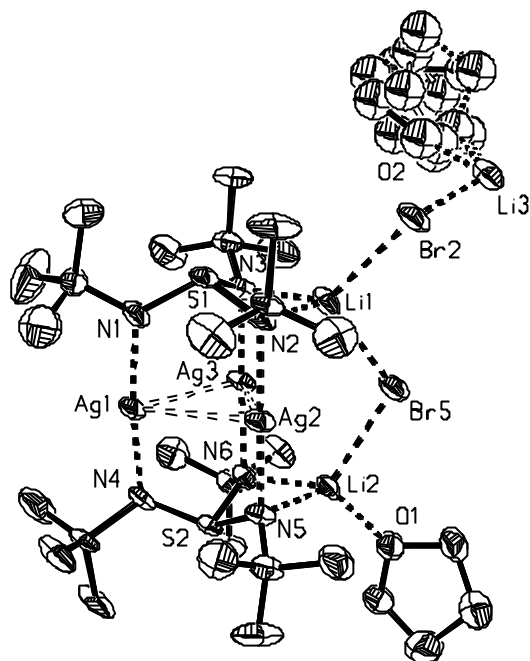


Figure 40: Asymmetric unit of **4** in the solid state; anisotropic displacement parameters are depicted at the 50% probability level.

7.4.3 [Fe(N^tBu)((N^tBu)₂S)]₂ (**5**):

Compound **5** crystallises in the centrosymmetric, monoclinic space group $P2_1/c$. The asymmetric unit contains half of the molecule. The complete molecule is generated by inversion at the origin followed by (1,0,2) translation. The *tert*butyl groups were restrained with SAME.

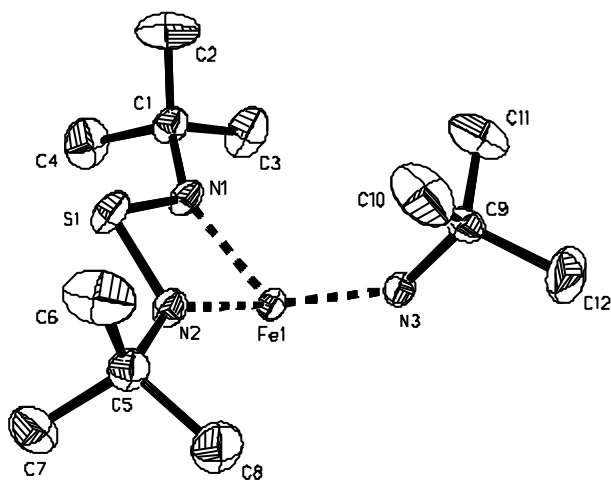


Figure 41: Asymmetric unit of **5** in the solid state; anisotropic displacement parameters are depicted at the 50% probability level.

7.4.4 [(thf)₂Li₃Cl{(N^tBu)₃S}]₂ (6):

Compound **6** crystallises in the centrosymmetric, monoclinic space group P2₁/n. The asymmetric unit shows half of the molecule and half of a lattice hexane molecule. The second part of the dimer is generated via inversion at the origin followed by (0,1,1) translation. The second half of the hexane molecule is generated via inversion at the origin followed by (0,2,1) translation. The disordered thf molecules coordinated to Li1 and Li2 were refined using distance and adp restraints (SAME, SIMU, DELU) to split occupancies of 0.75/0.25 and 0.43/0.57, respectively.

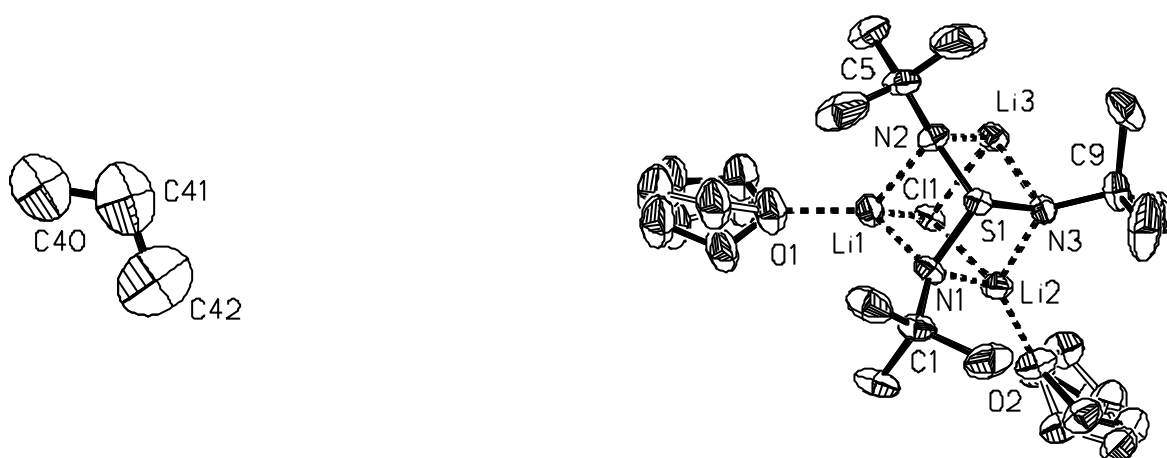


Figure 42: Asymmetric unit of **6** in the solid state; anisotropic displacement parameters are depicted at the 50% probability level.

7.4.5 [(thf)₃Li₃Me{(N^tBu)₃S}] (7):

Compound **7** crystallises as a non-merohedral twin in the centrosymmetric, monoclinic space group P2₁/c. For data processing only the reflections of one domain are selected. Reflections which are overlapped with reflections of the second domain are rejected. The asymmetric unit contains the complete molecule. The disordered thf molecule coordinated to Li3 was refined using distance and adp restraints (SAME, SIMU, DELU) to a split occupancy of 0.48/0.52. The hydrogen atoms at the coordinated methanide anion were refined with a distance constraint (DFIX) to a bond length of 0.98(3) pm.

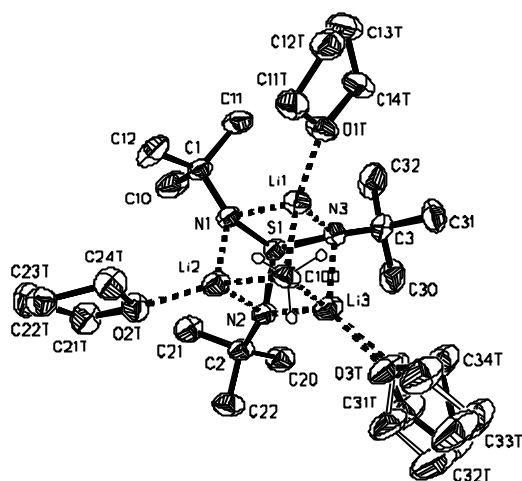


Figure 43: Asymmetric unit of **7** in the solid state; anisotropic displacement parameters are depicted at the 50% probability level.

7.4.6 $[(\text{thf})_3\text{Li}_3(\text{OCHCH}_2)\{(\text{N}^t\text{Bu})_3\text{S}\}]$ (**8a,b**):

Compound **8a** crystallises in the centrosymmetric, monoclinic space group $P2_1/n$. The asymmetric unit contains the complete molecule. The disordered ethyleneoxide molecule was refined using distance and adp restraints (SAME, SIMU, DELU) to a split occupancies of 0.79/0.10/0.11. All thf molecules show disordering and were refined using distance and adp restraints (SAME, SIMU, DELU) to split occupancies of 0.45/0.55, 0.78/0.22 and 0.58/0.42, respectively.

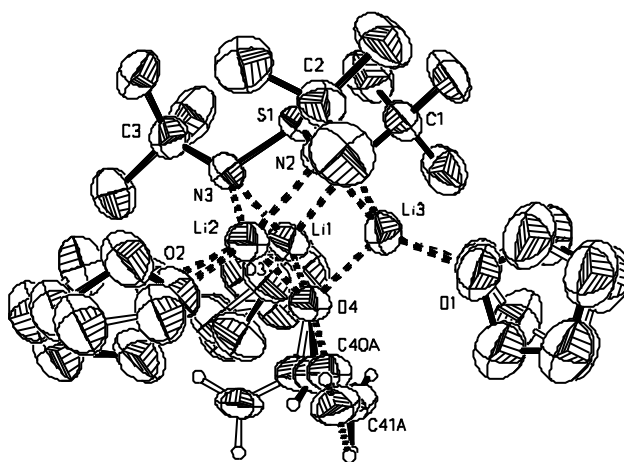


Figure 44: Asymmetric unit of **8a** in the solid state; anisotropic displacement parameters are depicted at the 50% probability level.

Compound **8b** crystallises in the centrosymmetric, monoclinic space group $P2_1/c$. It crystallises as a non-merohedral twin. Following matrices of the two domains have been determined:

$$\text{Orientation matrix 1} = \begin{pmatrix} -0.01313640 & 0.00251542 & -0.06563157 \\ 0.05078330 & -0.04093599 & -0.01144438 \\ -0.03501859 & -0.06031185 & 0.00499226 \end{pmatrix}$$

with unit cell parameters of

$a = 15.8605$, $b = 13.7107$, $c = 14.9729$, $\alpha = 90.027$, $\beta = 91.444$, $\gamma = 90.001$, and

$$\text{orientation matrix 2} = \begin{pmatrix} 0.00998795 & -0.00250503 & -0.06555843 \\ -0.05128947 & 0.04092534 & -0.01144766 \\ 0.03522075 & 0.06026635 & 0.00500707 \end{pmatrix}$$

with unit cell parameters of

$a = 15.8746$, $b = 13.7190$, $c = 14.9889$, $\alpha = 89.971$, $\beta = 91.481$, $\gamma = 89.983$.

BASF numbers		Range (reciprocal angstroms)	
1	2	0.0000	0.0040
3	4	0.0040	0.0120
5	6	0.0120	0.0240
7	8	0.0240	0.0310
9	10	0.0310	0.0350
1	2	> 0.0350 non-overlap	

The scale factors refined to 0.16093, 0.14268, 0.10801, 0.09990, 0.09074, 0.08261, 0.08360, 0.07604, 0.08009 and 0.07540. The disordered ethyleneoxid molecule was refined using distance and adp restraints (SAME, SIMU, DELU) to a split occupancy of 0.79/0.21. The disordered thf molecule coordinated at Li1 was refined using distance and adp restraints (SAME, SIMU, DELU) to a split occupancy of 0.48/0.51.

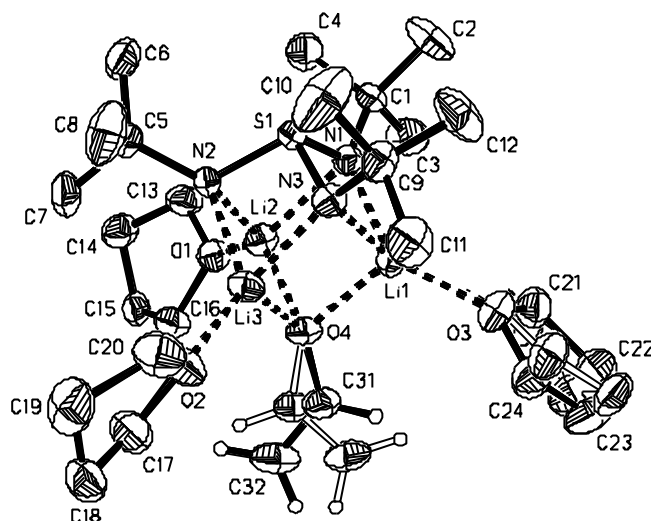


Figure 45: Asymmetric unit of **8b** in the solid state; anisotropic displacement parameters are depicted at the 50% probability level.

7.4.7 [(thf)Li₂{(CH₂)(N^tBu)₂S}]₂ (**9**):

Compound **9** crystallises in the centrosymmetric, monoclinic space group P2₁/c. The H-atoms at C3 were located by difference Fourier syntheses and refined freely. The asymmetric unit contains half of the molecule. The complete molecule is generated by inversion at the origin followed by (1,2,2) translation.

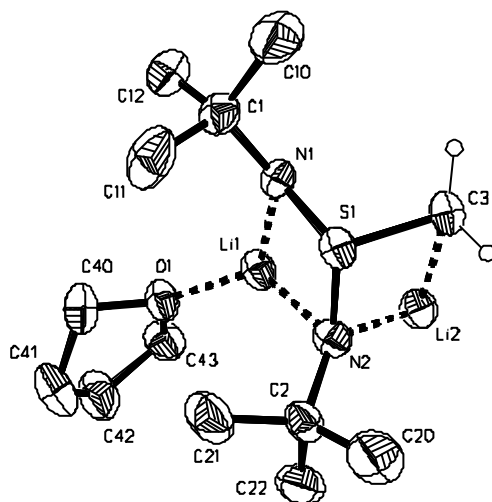


Figure 46: Asymmetric unit of **9** in the solid state; anisotropic displacement parameters are depicted at the 50% probability level.

7.4.8 [(thf)Li₂{(Et)(Me)CS(N^tBu)₂}]₂ (10):

Compound **10** crystallises in the centrosymmetric, triclinic space group $P\bar{1}$. The asymmetric unit contains half of two symmetry independent molecules. The complete molecules are generated by inversion at the origin followed by (2,2,1) translation for the left molecule in fig. 5-16 and (1,1,2) for the other. The disordered thf molecule coordinating at Li2 was refined using distance restraints (SAME) to a split occupancy of 0.58/0.42.

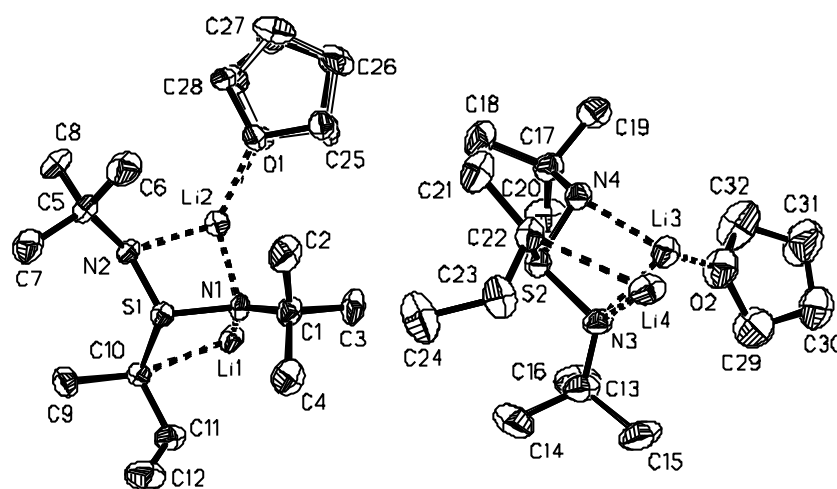


Figure 47: Asymmetric unit of **10** in the solid state; anisotropic displacement parameters are depicted at the 50% probability level.

7.4.9 [(thf)Li₃{((N^tBu)₂S)₂CH}]₂ (11a-c):

Compound **11a** crystallises in the centrosymmetric, triclinic space group $P\bar{1}$. The asymmetric unit contains three lattice thf molecules. The disordered thf molecules were refined using distance restraints (SAME, SIMU, DELU) to split occupancies of 0.48/0.52 (O1t-C14t), 0.39/0.61 (O2t-C24t), 0.65/0.35 (O3t-C34t), 0.31/0.69 (O4t-C44t), 0.6/0.4 (O5t-C54t), 0.53/0.47 (O6t-C64t), 0.5/0.5 (O7t-C74t) and 0.64/0.36 (O8t-C84t), respectively. The disordered *tert*butyl group at N7 was refined using distance and adp restraints (SAME, SIMU, DELU) to a split occupancy of 0.48/0.52.

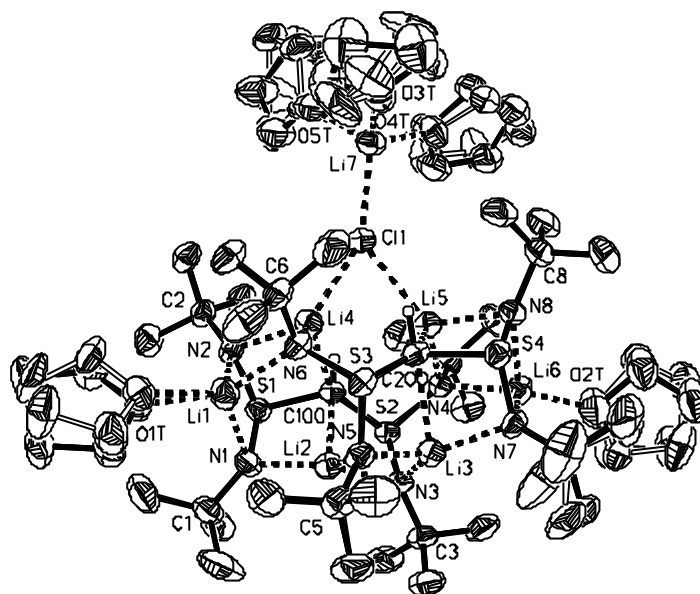


Figure 48: Asymmetric unit of **11a** in the solid state; anisotropic displacement parameters are depicted at the 50% probability level. Uncoordinated solvent molecules are omitted for clarity. Ground structure for **11b** and **11c** is the same.

Compound **11b** crystallises in the centrosymmetric, triclinic space group $P\bar{1}$. The asymmetric unit contains an uncoordinated diethoxymethane molecule. The disordered thf molecules were refined using distance restraints (SAME, SIMU, DELU) to split occupancies of 0.61/0.39 (O3t-C34t), 0.15/0.85 (O4t-C44t) and 0.74/0.26 (O5t-C54t), respectively.

Compound **11c** crystallises in the centrosymmetric, monoclinic space group $P2_1/n$. The asymmetric unit contains a pentan molecule which is refined isotropically.

7.4.10 $H(N^tBu)_3SMe$ (**12**):

Compound **12** crystallises in the polar non-centrosymmetric monoclinic space group Cc . The Flack x -parameter^[128] refined to 0.00(2) and confirms the correct assignment of the absolute structure. Therefore the absolute structure is described correctly. The H-atoms at N1 were located by difference Fourier syntheses and refined independently. The *tert*butyl groups were restrained with SAME.

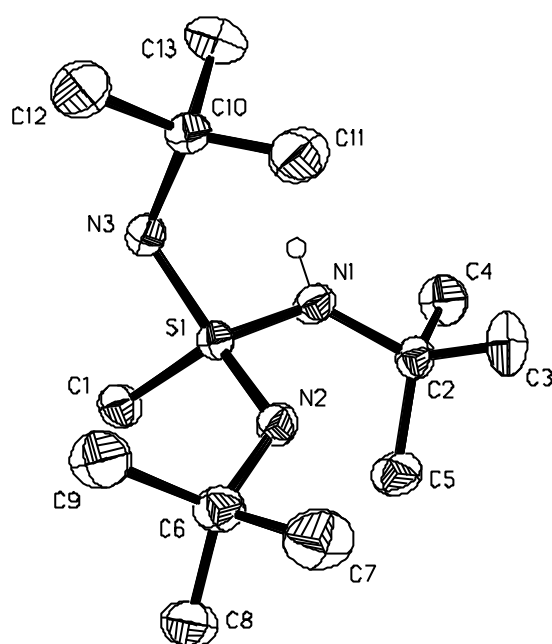


Figure 49: Asymmetric unit of **12** in the solid state; anisotropic displacement parameters are depicted at the 50% probability level.

7.4.11 $[\text{Me}_2\text{Al}\{(\text{N}^t\text{Bu})_3\text{SMe}\}]$ (**13**):

Compound **13** crystallises in the centrosymmetric, monoclinic space group $P2_1/c$. The asymmetric unit contains two symmetry independent molecules. The disordered *tert*butyl group at N5 was refined using distance and adp restraints (SAME, SIMU, DELU) to a split occupancy of 0.64/0.36.

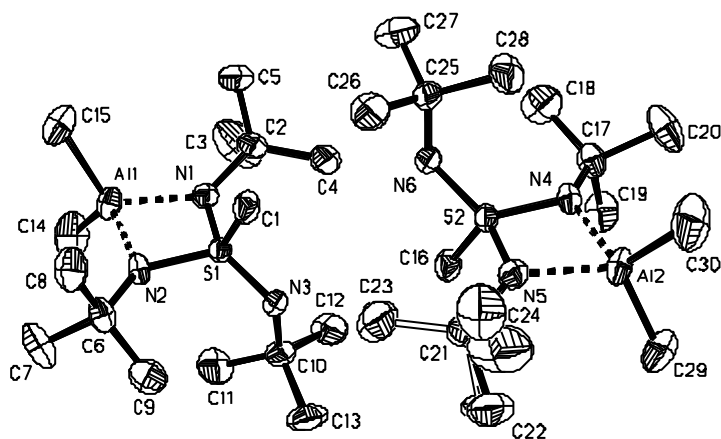


Figure 50: Asymmetric unit of **13** in the solid state; anisotropic displacement parameters are depicted at the 50% probability level.

7.4.12 [Zn{(N^tBu)₃SMe}₂] (14):

Compound **14** crystallises in the centrosymmetric, monoclinic space group I2/a. The asymmetric unit contains half of the molecule. The complete molecule is generated by a C₂ axes at (1/4,y,0) followed by (0,0,1) translation. The disordered *tert*butyl group at N1 was refined using distance and adp restraints (SAME, SIMU, DELU) to a split occupancy of 0.83/0.17.

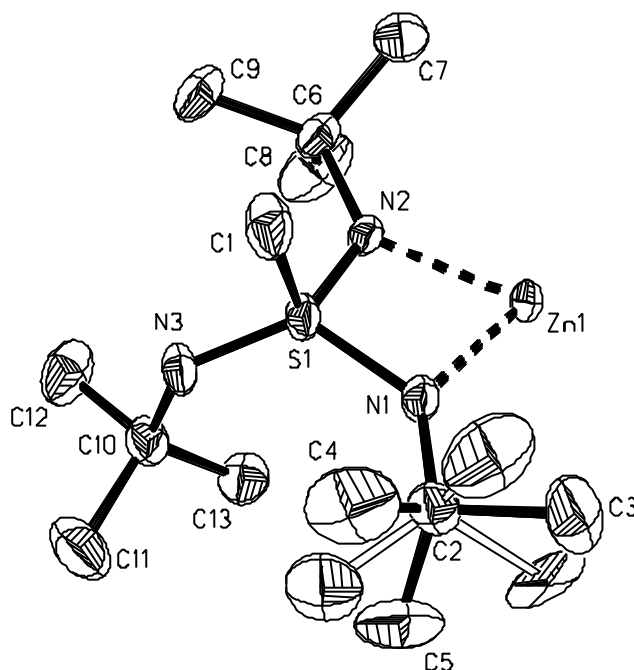


Figure 51: Asymmetric unit of **14** in the solid state; anisotropic displacement parameters are depicted at the 50% probability level.

7.4.13 [(thf)₂Li{(N^tBu)₃SMe}·ZnMe₂] (15):

Compound **15** crystallises in the centrosymmetric, monoclinic space group P2₁/c. The disordered thf molecules were refined using distance and adp restraints (SAME, SIMU, DELU) to split occupancies of 0.46/0.54 and 0.30/0.70, respectively.

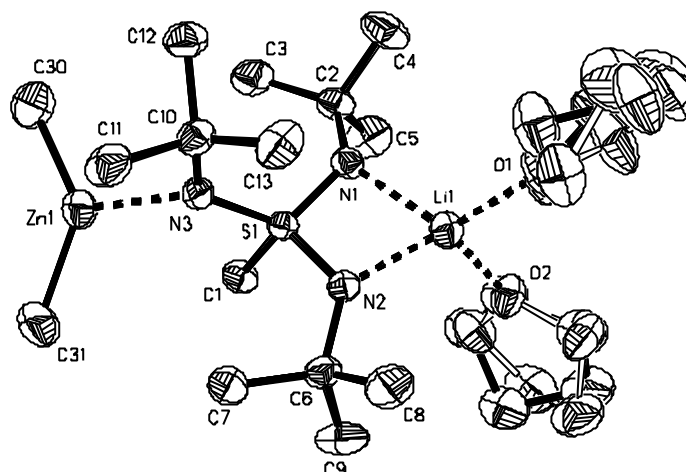


Figure 52: Asymmetric unit of **15** in the solid state; anisotropic displacement parameters are depicted at the 50% probability level.

7.4.14 [(thf)₂Li{(N^tBu)₃SCCPh}] (**16**):

Compound **16** crystallises in the centrosymmetric, monoclinic space group $P2_1/n$. The disordered thf molecules were refined using distance and adp restraints (SAME, SIMU, DELU) to split occupancies of 0.51/0.49 and 0.57/0.43, respectively. The disordered *tert*butyl group at N3 was refined using distance and adp restraints (SAME, SIMU, DELU) to a split occupancy of 0.57/0.43.

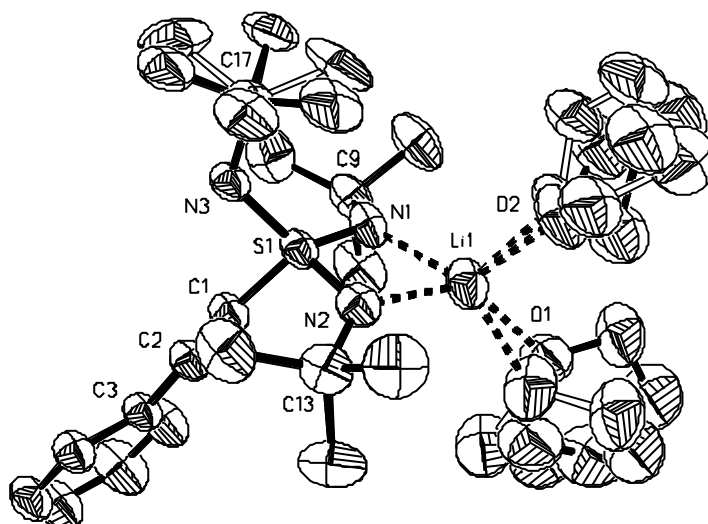


Figure 53: Asymmetric unit of **16** in the solid state; anisotropic displacement parameters are depicted at the 50% probability level.

7.4.15 [(tmeda)₂Li₂{(CH₂)S(N^tBu)₃}] (17):

Compound **17** crystallises in the centrosymmetric, orthorhombic space group *Pbca*. The hydrogen atoms at C1 were located in the difference Fourier syntheses and refined freely.

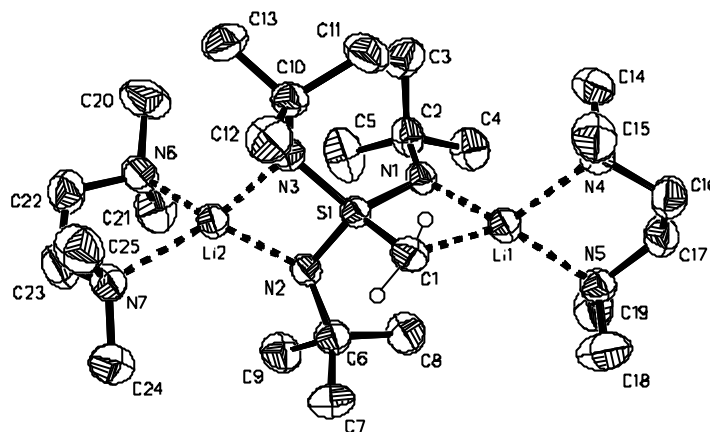


Figure 54: Asymmetric unit of **17** in the solid state; anisotropic displacement parameters are depicted at the 50% probability level.

7.4.16 [(tmeda)Li₂{(O)S(N^tBu)₃}]₃ (18):

Compound **18** crystallises in the polar non centrosymmetric hexagonal space group *P6₃*. The Flack *x*-parameter^[128] refined to 0.2(3). Therefore the absolute structure could be determined unequivocally. The disordered *tert*butyl group at N2 was refined using distance and adp restraints (SAME, SIMU, DELU) to a split occupancy of 0.51/0.49. The disordered tmeda molecule was refined using distance and adp restraints (SAME, SIMU, DELU) to a split occupancy of 0.54/0.46. The *tert*butyl group at N1 was refined using the ISOR restrain (*U*_{ij} values are restrained to be approximately isotropic thermal motion of the atoms). The asymmetric unit contains one third of the complete molecule. Second third is generated by a *C*₃ axes clockwise at (0,0,*z*) followed by (1,0,0) translation. Third part is generated by a *C*₃ axes anticlockwise at (0,0,*z*) followed by (1,1,0) translation.

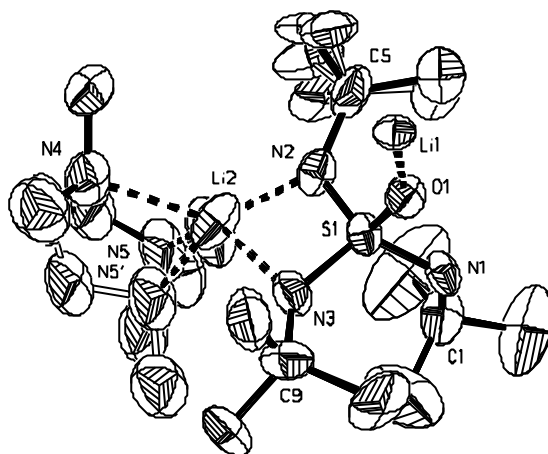


Figure 55: Asymmetric unit of **18** in the solid state; anisotropic displacement parameters are depicted at the 50% probability level.

7.4.17 $[(\text{thf})_2\text{Li}_2\{((\text{N}^t\text{Bu})_3\text{S})_2\text{CH}_2\}]$ (**19**):

Compound **19** crystallises in the centrosymmetric, monoclinic space group $P2_1/c$. The disordered thf molecule coordinated to Li1 was refined using distance and adp restraints (SAME, SIMU, DELU) to a split occupancy of 0.45/0.55. The uncoordinated thf molecule was refined using distance and adp restraints (SAME, SIMU, DELU) to split occupancies of 0.49/0.35/0.16. The hydrogen atoms at C100 were located in the difference Fourier syntheses and refined freely.

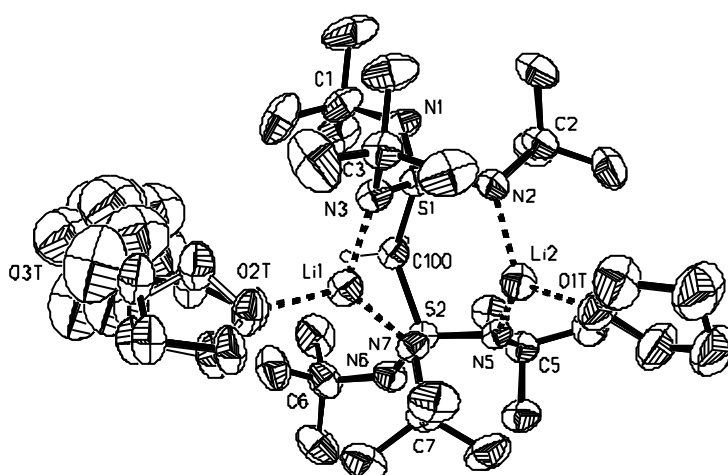
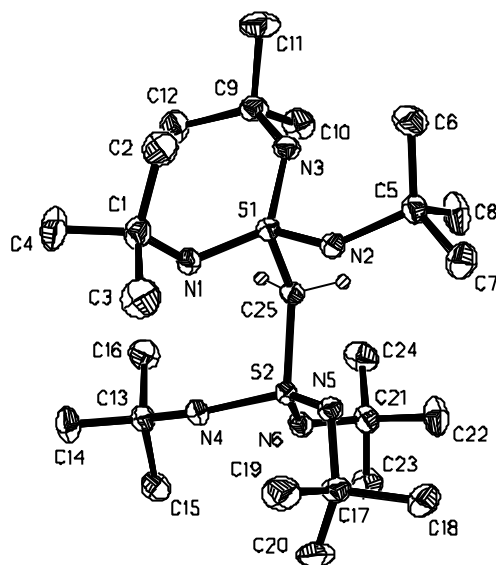


Figure 56: Asymmetric unit of **19** in the solid state; anisotropic displacement parameters are depicted at the 50% probability level.

7.4.18 $\text{H}_2\text{C}\{\text{S}(\text{N}^t\text{Bu})_2(\text{NH}^t\text{Bu})\}_2$ (20**):**

Compound **20** crystallises in the centrosymmetric, monoclinic space group $P2_1/n$. The H-atoms at N2 and N4 were located in the difference Fourier syntheses and refined freely.



*Figure 57: Asymmetric unit of **20** in the solid state; anisotropic displacement parameters are depicted at the 50% probability level.*

7.5 Crystallographic Data

Table 15: Crystal data and structure refinement for **1**, **2** and **3**

	1	2	3
formula	C ₃₂ H ₇₀ Cu ₃ Li ₂ N ₆ O ₂	C ₃₂ H ₇₀ Ag ₃ BrLi ₂ N ₆	C ₆₀ H ₁₃₂ Ag ₆ Br ₂ Li ₄ N ₁₂
	S ₂	O ₂ S ₂	O ₃ S ₄
diffractometer	Stoe IPDS	Bruker Smart Apex	Stoe IPDS
M_r	966.46	1052.46	2032.82
crystal size [mm]	0.4 x 0.3 x 0.2	0.4 x 0.3 x 0.3	0.4 x 0.4 x 0.3
space group	Pbcn	P2 ₁ /c	Pca2 ₁
a [pm]	4030.5(8)	1885.62(18)	2232.2(5)
b [pm]	1241.4(3)	1880.56(17)	1954.7(4)
c [pm]	1777.2(4)	1279.31(12)	1963.4(4)
b [°]	90	99.559(2)	90
V [nm ³]	8892(3)	4473.5(7)	8567(3)
Z	8	4	4
r_{calc} [Mgm ⁻³]	1.444	1.565	1.576
m [mm ⁻¹]	2.243	2.320	2.419
$F(000)$	3984	2136	4112
Q -range [°]	2.23 – 24.12	1.54 – 26.58	2.10 – 24.74
no. of refln. measd.	37894	11563	56554
no. of unique refln.	7074	11563	7539
$R(\text{int})$	0.0983	0.0362	0.1166
data/restraints/param	7074 / 370 / 553	11595 / 252 / 521	7539 / 608 / 951
goodness-of-fit on F^2	0.808	0.941	1.032
$R1$ [$ I > 2s(I)$]	0.0478	0.0438	0.0416
$wR2$ (all data)	0.1183	0.1183	0.1063
$g1/g2$	0.0671/0.0000	0.0629/0.0000	0.0840/0.0000
largest diff.	608 / -896	994 / -710	1139 / -1278
peak/hole [e nm ⁻³]			

Table 16: Crystal data and structure refinement for **4**, **5** and **6**

	4	5	6
formula	C ₃₂ H ₇₀ Ag ₃ Br ₂ Li ₂ N ₆ O ₂ S ₂	C ₂₄ H ₅₄ Fe ₂ N ₆ S ₂	C ₂₃ H ₅₀ ClLi ₃ N ₃ O ₂ S
diffractometer	Bruker Smart Apex	STOE IPDS	Bruker Smart Apex
M_r	1139.31	301.28	488.99
crystal size [mm]	0.4 x 0.4 x 0.3	0.6 x 0.5 x 0.4	0.4 x 0.4 x 0.3
space group	P2 ₁ /c	P2 ₁ /c	P2 ₁ /n
a [pm]	1226.60(9)	1011.2(2)	1037.54(10)
b [pm]	1073.36(8)	1011.5(2)	17.3973(16)
c [pm]	3652.9(3)	1687.8(3)	17.1851(16)
β [°]	94.352(3)	106.83(3)	91.152(2)
V [nm ³]	4795(6)	1652.5(6)	3101.4(5)
Z	4	4	4
r_{calc} [Mgm ⁻³]	1.578	1.211	1.074
μ [mm ⁻¹]	2.998	1.025	0.211
$F(000)$	2288	648	1068
Q range [°]	1.12 – 24.71	2.91 – 27.97	1.67 – 26.48
no. of refln. measd.	11253	12652	33463
no. of unique refln.	7338	3918	6359
$R(\text{int})$	0.0966	0.0641	0.0587
data/restraints/param.	7338 / 115 / 473	3918 / 18 / 163	5310 / 382 / 400
goodness-of-fit on F^2	1.047	1.200	1.150
$R1$ [$I > 2s(I)$]	0.0721	0.0747	0.0764
$wR2$ (all data)	0.2047	0.1957	0.1875
$g1/g2$	0.1312 / 8.4046	0.0465 / 10.036	0.1000
largest diff. peak/hole [e nm ⁻³]	2003 / 1252	1753 / -601	587 / -27

Table 17: Crystal data and structure refinement for **7**, **8a** and **8b**

	7	8a	8b
formula	C ₂₅ H ₅₄ Li ₃ N ₃ O ₃ S	C ₂₆ H ₅₄ Li ₃ N ₃ O ₄ S	C ₂₆ H ₅₄ Li ₃ N ₃ O ₄ S
diffractometer	STOE IPDS	STOE IPDS	Bruker Smart Apex
CCDC no.	153453	165029	165030
<i>M_r</i>	497.58	525.60	525.60
crystal size [mm]	0.2 x 0.2 x 0.1	0.4 x 0.3 x 0.3	0.3 x 0.25 x 0.2
space group	P2 ₁ /c	P2 ₁ /n	P2 ₁ /c
<i>a</i> [pm]	1574.7(3)	1003.5(2)	1586.05(11)
<i>b</i> [pm]	1376.1(3)	2331.1(5)	1371.07(10)
<i>c</i> [pm]	1449.9(3)	1469.6(3)	1497.29(11)
<i>b</i> [°]	92.40(3)	101.55(3)	91.444(2)
<i>V</i> [nm ³]	3191.1(11)	3368.3(12)	3255.0(4)
<i>Z</i>	4	4	4
<i>r</i> _{calcd} [Mgm ⁻³]	1.053	1.036	1.073
<i>m</i> [mm ⁻¹]	0.130	0.126	0.130
<i>F</i> (000)	1096	1152	1152
<i>Q</i> range [°]	2.39 – 26.46	2.43 – 24.71	1.28 – 26.50
no. of refln. measd.	4520	22142	13380
no. of unique refln.	4520	5718	13380
<i>R</i> (int)	0.0000	0.0558	0.0000
data/restraints/param.	4520 / 369 / 384	5718 / 718 / 520	13380 / 305 / 426
goodness-of-fit on <i>F</i> ²	1.079	1.203	1.041
<i>R</i> 1 [<i>I</i> > 2 <i>s</i> (<i>I</i>)]	0.0621	0.0747	0.0775
<i>wR</i> 2 (all data)	0.1888	0.1949	0.2113
<i>g</i> 1/ <i>g</i> 2	0.1051 / 0.4226	0.1100 / 0.0000	0.1489 / 0.0000
largest diff. peak/hole [e nm ⁻³]	315 / -272	406 / -274	539 / -445

Table 18: Crystal data and structure refinement for **9**, **10** and **11a**

	9	10	11a
formula	C ₂₆ H ₅₆ Li ₄ N ₄ O ₂ S ₂	C ₃₂ H ₆₈ Li ₄ N ₄ O ₂ S ₂	C ₆₆ H ₁₃₈ ClLi ₇ N ₈ O ₈ S ₄
diffractometer	STOE IPDS	STOE IPDS	Enraf-Nonius CAD4
CCDC no.	151664	151663	151662
M_r	548.63	632.78	1384.11
crystal size [mm]	0.2 x 0.2 x 0.1	0.4 x 0.3 x 0.2	0.3 x 0.3 x 0.2
space group	P2 ₁ /c	P $\bar{1}$	P $\bar{1}$
a [pm]	960.89(19)	1057.3(2)	1521.27(10)
b [pm]	1884.0(4)	1216.0(2)	1537.61(10)
c [pm]	1008.0(2)	1612.7(3)	1934.79(10)
α [°]	90	97.99(3)	83.588(10)
β [°]	111.06(3)	91.47(3)	79.912(10)
γ [°]	90	106.92(3)	68.434(10)
V [nm ³]	1702.9(6)	1959.7(7)	4.1383(4)
Z	2	2	2
ρ_{calcd} [Mgm ⁻³]	1.070	1.072	1.111
μ [mm ⁻¹]	0.182	0.166	0.197
$F(000)$	600	696	1512
Q range [°]	2.42 – 24.75	2.34 – 24.71	3.04 - 22.48
no. of refln. measd.	11032	12756	11685
no. of unique refln.	2909	6274	10751
$R(\text{int})$	0.0994	0.0675	0.0258
data/restraints/param.	2909 / 77 / 186	6274 / 30 / 459	10751 / 1690 / 1278
goodness-of-fit on F^2	0.879	0.933	1.020
$R1$ [$I > 2s(I)$]	0.0442	0.0567	0.0480
$wR2$ (all data)	0.0971	0.1582	0.1226
$g1/g2$	0.0376 / 0.0000	0.1004 / 0.0000	0.0541 / 2.2189
largest diff. peak/hole [e nm ⁻³]	198 / -254	1182 / -434	254 / -213

Table 19: Crystal data and structure refinement for **11b**, **11c** and **12**

	11b	11c	12
formula	C ₅₀ H ₁₂₆ ClLi ₇ N ₈ O ₅ S ₄	C ₅₀ H ₁₂₆ ClLi ₇ N ₈ O ₇ S ₄	C ₁₃ H ₃₁ N ₃ S
diffractometer	STOE IPDS	STOE IPDS	STOE IPDS
CCDC no.	-----	-----	163257
<i>M_r</i>	1239.94	1271.94	261.47
crystal size [mm]	0.3 x 0.2 x 0.2	0.4 x 0.4 x 0.3	0.5 x 0.5 x 0.4
space group	P $\bar{1}$	P2 ₁ /n	Cc
<i>a</i> [pm]	1392.6(3)	1400.8(3)	914.20(18)
<i>b</i> [pm]	1573.2(3)	1571.8(3)	2236.7(5)
<i>c</i> [pm]	1808.4(4)	3495.3(7)	904.06(18)
<i>a</i> [°]	80.89(3)	90	90
<i>b</i> [°]	75.09(3)	95.99(3)	117.08(3)
<i>g</i> [°]	86.63(3)	90	90
<i>V</i> [nm ³]	3779.5(13)	7654(3)	1.6459(6)
<i>Z</i>	4	8	4
<i>r</i> _{calcd} [Mgm ⁻³]	1.090	1.104	1.055
<i>m</i> [mm ⁻¹]	0.206	0.207	0.185
<i>F</i> (000)	1356	2776	584
<i>Q</i> range [°]	2.24 – 24.71	2.20 – 24.71	2.66 to 28.08
no. of refln. measd.	34405	35303	7546
no. of unique refln.	12110	12785	3789
<i>R</i> (int)	0.0622	0.0830	0.0211
data/restraints/param.	12110 / 468 / 766	12785 / 760 / 947	3789 / 92 / 169
goodness-of-fit on <i>F</i> ²	1.060	0.885	1.093
<i>R</i> 1 ^a) [<i>I</i> > 2 <i>s</i> (<i>I</i>)]	0.0810	0.0611	0.0260
<i>wR</i> 2 ^b) (all data)	0.2263	0.1596	0.0687
Flack <i>x</i> ^[128]			0.00(1)
<i>g</i> 1/ <i>g</i> 2 ^c)	0.0844 / 0.0000	0.0864 / 11.5683	0.0442 / 0.2389
largest diff. peak/hole [e nm ⁻³]	839 / -509	835 / -291	173 / -206

Table 20: Crystal data and structure refinement for **13**, **14** and **15**

	13	14	15
formula	C ₁₅ H ₃₆ AlN ₃ S	C ₂₆ H ₆₀ N ₆ S ₂ Zn	C ₂₃ H ₅₂ LiN ₃ O ₂ SZn
diffractometer	STOE IPDS	STOE IPDS	Bruker Smart Apex
CCDC no.	163258	163259	163260
<i>M_r</i>	317.51	586.29	507.05
crystal size [mm]	0.4 x 0.3 x 0.2	0.3 x 0.2 x 0.2	0.5 x 0.3 x 0.2
space group	P2 ₁ /c	I2/a	P2 ₁ /c
<i>a</i> [pm]	1064.2(2)	1790.4(4)	1076.50(7)
<i>b</i> [pm]	1644.7(3)	878.48(18)	1763.96(12)
<i>c</i> [pm]	2344.1(5)	2120.4(4)	1534.56(11)
<i>a</i> [°]	90	90	90
<i>b</i> [°]	92.39(3)	98.40(3)	93.3720(10)
<i>g</i> [°]	90	90	90
<i>V</i> [nm ³]	4.099.1(14)	3.2993(12)	2908.9(3)
<i>Z</i>	8	4	4
<i>r</i> _{calcd} [Mgm ⁻³]	1.029	1.180	1.158
<i>m</i> [mm ⁻¹]	0.198	0.894	0.937
<i>F</i> (000)	1408	1280	1104
<i>Q</i> range [°]	2.41 to 24.73	2.51 to 26.38	1.76 - 26.42
no. of refln. measd.	26478	12277	14853
no. of unique refln.	7001	3347	5891
<i>R</i> (int)	0.0494	0.0549	0.0240
data/restraints/param.	7001 / 30 / 416	3347 / 150 / 200	5891 / 140 / 384
goodness-of-fit on <i>F</i> ²	0.847	0.839	1.043
<i>R</i> 1 ^a) [<i>I</i> > 2 <i>s</i> (<i>I</i>)]	0.0357	0.0322	0.0410
<i>wR</i> 2 ^b) (all data)	0.0910	0.0711	0.1074
<i>g</i> 1/ <i>g</i> 2 ^c)	0.0542 / 0.0000	0.0233 / 0.0000	0.0574 / 1.0629
largest diff. peak/hole [e nm ⁻³]	199 / -263	319 / -415	425 / -194

Table 21: Crystal data and structure refinement for **16**, **17** and **18**

	16	17	18
formula	C ₅₆ H ₉₆ Li ₂ N ₆ O ₄ S ₂	C ₂₅ H ₆₁ Li ₂ N ₇ S	C ₁₈ H ₄₃ Li ₂ N ₅ OS
diffractometer	STOE IPDS	Bruker Smart Apex	Bruker Smart Apex
CCDC no.	163261	164904	164905
M_r	995.39	505.75	391.51
crystal size [mm]	0.2 x 0.2 x 0.1	0.4 x 0.3 x 0.2	0.3 x 0.2 x 0.2
space group	P2 ₁ /n	Pbca	P63
a [pm]	1002.4(2)	1996.67(13)	1768.91(8)
b [pm]	1808.5(4)	1649.92(10)	1768.91(8)
c [pm]	1694.6(3)	2027.39(14)	1506.06(10)
a [°]	90	90	90
b [°]	94.53(3)	90	90
g [°]	90	90	120
V [nm ³]	3062.4(11)	6678.9(8)	4081.2(4)
Z	2	8	6
r_{calcd} [Mgm ⁻³]	1.079	1.006	0.956
m [mm ⁻¹]	0.132	0.120	0.132
$F(000)$	1088	2256	1296
Q range [°]	2.33 - 24.72	1.89 – 23.20	1.90 – 23.24
no. of refln. measd.	14126	26858	16134
no. of unique refln.	5192	4730	3887
$R(\text{int})$	0.0445	0.0931	0.0647
data/restraints/param.	5192 / 384 / 443	4730 / 0 341	3887 / 289 / 337
goodness-of-fit on F^2	0.929	1.029	1.046
$R1^{\text{a}}$ [$ >2s(I) $]	0.0587	0.0657	0.0627
$wR2^{\text{b}}$ (all data)	0.1674	0.1880	0.1679
Flack x^{128}			0.20(30)
$g1/g2^{\text{c}}$	0.1130 / 0.0000	0.1225 / 1.6000	0.0974 / 0.0000
largest diff. peak/hole [e nm ⁻³]	429, -444	629 / -488	303 / -170

Table 22: Crystal data and structure refinement for **19** and **20**

	19	20
formula	C ₃₇ H ₈₀ Li ₂ N ₆ O ₃ S ₂	C ₂₅ H ₅₈ N ₆ S ₂
Diffractionmeter	Enraf Nonius CAD4	Bruker Smart 1000
CCDC no.	171900	171901
M_r	735.07	506.89
crystal size [mm]	0.5 x 0.4 x 0.4	0.4 x 0.3 x 0.2
space group	P2 ₁ /c	P2 ₁ /c
a [pm]	1614.3(8)	1736.4(4)
b [pm]	1453.40(18)	1143.1(2)
c [pm]	1942.9(8)	1764.7(4)
a [°]	90	90.000(3)
b [°]	92.779(18)	117.28(3)
g [°]	90	90.000(3)
V [nm ³]	4553(3)	3113.1(11)
Z	4	4
r_{calcd} [Mgm ⁻³]	1.072	1.082
m [mm ⁻¹]	0.155	0.193
$F(000)$	1624	1128
Q range [°]	3.03 – 21.96	2.60 – 28.28
no. of refln. measd.	10144	36881
no. of unique refln.	5527	7720
$R(\text{int})$	0.0660	0.0492
data/restraints/param.	5527 / 566 / 602	7720 / 0 / 324
goodness-of-fit on F^2	1.044	1.011
$R1^{\text{a}}$ [$I > 2s(I)$]	0.0639	0.0340
$wR2^{\text{b}}$ (all data)	0.1767	0.0988
$g1/g2^{\text{c}}$	0.0695 / 9.0558	0.0600 / 0.5469
largest diff. peak/hole [e nm ⁻³]	337 / -404	458 / -259

8 Literature

- (1) I. Langmuir, *J. Am. Chem. Soc.* **1919**, *41*, 868 and 1543.
- (2) Rev.: T. Chivers, J. K. Brask, *Angew. Chem.* **2001**, *113*, 4082; *Angew. Chem. Int. Ed. Engl.* **2001**, *40*, 3988.
 - (a) $\text{Si}(\text{NR})_3^{2-}$: M. Veith, R. Lisowsky, *Angew. Chem.* **1988**, *102*, 1124; *Angew. Chem. Int. Ed. Engl.* **1988**, *27*, 1087. (b) $\text{Si}(\text{NR})_4^{4-}$: J. K. Brask, T. Chivers, M. Parvez, *Inorg. Chem.* **2000**, *39*, 2505. (c) $\text{P}(\text{NR})_3^-$: E. Niecke, M. Frost, M. Nieger, V. v. d. Gönna, A. Ruban, W.W. Schoeller, *Angew. Chem.* **1994**, *106*, 2170; *Angew. Chem. Int. Ed. Engl.* **1994**, *33*, 2111. (d) $\text{As}(\text{NR})_3^{3-}$: M. A. Beswick, S. J. Kidd, M. A. Paver, P. R. Raithby, A. Steiner, D. S. Wright, *Inorg. Chem. Comm.* **1999**, *2*, 612. and (e) L. T. Burke, J. C. Jeffery, A. P. Leedham, C. A. Russell, *J. Chem. Soc. Dalton Trans.* **2001**, 423. (f) $\text{Sb}(\text{NR})_3^{3-}$: A. J. Edwards, M. A. Paver, P. R. Raithby, M.-A. Rennie, C. A. Russell, D. S. Wright, *Angew. Chem.* **1994**, *106*, 1334; *Angew. Chem. Int. Ed. Engl.* **1994**, *33*, 1277. (g) $\text{P}(\text{NR})_4^{3-}$: P. R. Raithby, C. A. Russell, A. Steiner, D. S. Wright, *Angew. Chem.* **1997**, *109*, 676; *Angew. Chem. Int. Ed. Engl.* **1997**, *36*, 649. (h) $\text{S}(\text{NR})_3^{2-}$: R. Fleischer, S. Freitag, F. Pauer, D. Stalke, *Angew. Chem.* **1996**, *108*, 208; *Angew. Chem. Int. Ed. Engl.* **1996**, *35*, 204. (i) $\text{Se}(\text{NR})_3^{2-}$: T. Chivers, M. Parvez, G. Schatte, *Inorg. Chem.* **1996**, *35*, 4094. (j) $\text{Te}(\text{NR})_3^{2-}$: T. Chivers, X. Gao, M. Parvez, *Angew. Chem.* **1995**, *107*, 2756; *Angew. Chem. Int. Ed. Engl.* **1995**, *34*, 2549. (k) $\text{S}(\text{NR})_4^{2-}$: R. Fleischer, A. Rothenberger, D. Stalke, *Angew. Chem.* **1997**, *109*, 1140; *Angew. Chem. Int. Ed. Engl.* **1997**, *36*, 1105.
- (3) P. J. Bradley, A. J. Blake, M. Kryszczuk, S. Parsons, D. Reed, *J. Chem. Soc., Chem. Commun.* **1995**, 1647.
- (4) M. Veith, R. Lisowsky, *Angew. Chem.*, **1988**, *100*, 1124; *Angew. Chem. Int. Ed. Engl.* **1988**, *27*, 1087.
- (5) (a) R. A. Alton, D. Barr, A. J. Edwards, M. A. Paver, P. R. Raithby, M.-A. Rennie, C. A. Russel, D. S. Wright, *J. Chem. Soc., Chem. Commun.* **1994**, 1481 (b) A. J. Edwards, M. A. Beswick, J. R. Galsworthy, M. A. Paver, P. R. Raithby, M.-A. Rennie, C. A. Russel, K. L. Verhorevoort, D. S. Wright, *Inorg. Chim. Acta.* **1996**, *248*, 9. (c) A. Bashall, M. A. Beswick, C. N. Harmer, A. D.

- Hopkins, M. McPartlin, M. A. Paver, P. R. Raithby, D. S. Wright, *J. Chem. Soc., Dalton Trans.* **1998**, 1389. (d) M. A. Beswick, N. Choi, C. N. Harmer, A. D. Hopkins, M. McPartlin, M. A. Paver, P. R. Raithby, A. Steiner, M. Tombul, D. S. Wright, *Inorg. Chem.* **1998**, 37, 2177. (e) M. A. Beswick, E. A. Harron, A. D. Hopkins, P. R. Raithby, D. S. Wright, *J. Chem. Soc., Dalton Trans.* **1999**, 107. (f) A. Bashall, M. A. Beswick, E. A. Harron, A. D. Hopkins, S. J. Kidd, M. McPartlin, P. R. Raithby, A. Steiner, D. S. Wright, *Chem. Commun.* **1999**, 1145.
- (6) (a) T. Chivers, X. Gao, M. Parvez, *Inorg. Chem.* **1996**, 35, 4336. (b) T. Chivers, *J. Chem. Soc. Dalton Trans.* **1996**, 1185 (c) T. Chivers, M. Parvez, G. Schatte, *J. Organomet. Chem.* **1998**, 550, 213.
- (7) (a) F. P. Burt, *J. Chem. Soc.* **1910**, 1171. (b) M. M. Labes, P. Love, L. F. Nichols, *Chem. Rev.* **1979**, 79, 1.
- (8) M. Goehring, G. Weis, *Angew. Chem.* **1956**, 68, 678.
- (9) (a) K. B. Sharpless, T. Hori, L. K. Truesdale, C. O. Dietrich, *J. Am. Chem. Soc.* **1976**, 98, 269. (b) I. Dyong, H. Friege, T. zu Höhne, *Chem. Ber.* **1982**, 115, 256. (c) R. Bussas, G. Kresze, H. Münsterer, A. Schwöbel, *Sulfur Rep.* **1983**, 2, 215. (d) G. Kresze, H. Münsterer, *J. Org. Chem.* **1983**, 48, 3561.
- (10) K. B. Sharpless, T. Hori, *J. Org. Chem.* **1976**, 41, 176.
- (11) (a) G. Kresze, *Angew. Chem.* **1972**, 84, 1154; *Angew. Chem. Int. Ed. Engl.* **1972**, 11, 1106. (b) N. Schönberger, G. Kresze, *Liebigs Ann. Chem.* **1975**, 1725. (c) R. Bussas, G. Kresze, *Liebigs Ann. Chem.* **1980**, 629.
- (12) (a) F. Pauer, D. Stalke, *J. Organomet. Chem.* **1991**, 416, 127. (b) F. Pauer, J. Rocha, D. Stalke, *J. Chem. Soc. Chem. Commun.* **1991**, 1477. (c) F. T. Edelman, F. Knösel, F. Pauer, D. Stalke, W. Bauer, *J. Organomet. Chem.* **1992**, 438, 1. (d) S. Freitag, W. Kolodziejcki, F. Pauer, D. Stalke, *J. Chem. Soc. Dalton Trans.* **1993**, 3779.
- (13) R. Fleischer, S. Freitag, D. Stalke, *J. Chem. Soc. Dalton Trans.* **1998**, 193.
- (14) J. K. Brask, T. Chivers, B. McGarvey, G. Schatte, R. Sung, R. T. Boere, *Inorg. Chem.* **1998**, 37, 4633.
- (15) (a) H. Lecher, K. Köcherle, P. Stöcklin, *Chem. Ber.* **1925**, 58, 423. (b) Y. Miura, V. Makita, M. Kinoshita, *Tetrahedron Lett.* **1975**, 2, 127.
- (16) Y. Miura, H. Asada, M. Kinoshita, *J. Phys. Chem.* **1983**, 87, 3450.
- (17) G. Brunton, J. F. Taylor, K. U. Ingold, *J. Am. Chem. Soc.* **1976**, 98, 4879.

- (18) A. J. Banister, N. Bricklebank, I. Lavender, J. M. Rawson, C. I. Gregory, B. K. Tanner, W. Clegg, M. R. J. Elsegood, F. Palacio, *Angew. Chem.* **1996**, *108*, 2648; *Angew. Chem. Int. Ed. Engl.* **1996**, *35*, 2621.
- (19) R. T. Oakley, *Prog. Inorg. Chem.* **1988**, *36*, 299.
- (20) (a) O. Glemser, J. Wegener, *Angew. Chem.* **1970**, *82*, 324; *Angew. Chem. Int. Ed. Engl.* **1970**, *9*, 309. (b) O. Glemser, S. Pohl, F. M. Tesky, R. Mews, *Angew. Chem.* **1977**, *89*, 324; *Angew. Chem. Int. Ed. Engl.* **1977**, *16*, 789.
- (21) W. Lidy, W. Sundermeyer, W. Z. Verbeek, *Z. Anorg. Allg. Chem.* **1974**, *406*, 228.
- (22) R. Fleischer, B. Walfort, A. Gburek, P. Scholz, W. Kiefer, D. Stalke, *Chem. Eur. J.* **1998**, *4*, 2266.
- (23) R. Appel, J. Kohnke, *Chem. Ber.* **1971**, *104*, 3875.
- (24) (a) R. Appel, J. Kohnke, *Chem. Ber.* **1970**, *103*, 2125. (b) R. Appel, J. Kohnke, *Chem. Ber.* **1971**, *104*, 2648.
- (25) N. Y. Derkach, G. G. Barashenkov, *Zh. Org. Khim.* **1976**, *12*, 2484.
- (26) M. Herberhold, W. Jellen, *Z. Naturforsch.* **1986**, *B 41*, 144.
- (27) T. Chivers, X. Gao, M. Parvez, *J. Chem. Soc. Chem. Commun.* **1994**, 2149.
- (28) (a) W. A. Nugent, R. L. Harlow, *Inorg. Chem.* **1980**, *19*, 777. (b) W. A. Nugent, *Inorg. Chem.* **1983**, *22*, 965
- (29) (a) A. A. Danopoulos, G. Wilkinson, B. Hussain-Bates, M. B. Hursthouse, *J. Chem. Soc., Chem. Commun.* **1989**, 896. (b) A. A. Danopoulos, G. Wilkinson, B. Hussain-Bates, M. B. Hursthouse, *Polyhedron* **1989**, *8*, 2947 (c) A. A. Danopoulos, G. Wilkinson, B. Hussain-Bates, M. B. Hursthouse, *J. Chem. Soc., Dalton Trans.* **1990**, 2753.
- (30) A. Gieren, P. Narayanan, *Acta Crystallogr.* **1975**, *A 31*, 120.
- (31) H. W. Roesky, W. Schmieder, W. Isenberg, W. S. Sheldrick, G. M. Sheldrick, *Chem. Ber.* **1982**, *115*, 2714.
- (32) (a) S. Trofimenko, *Prog. Inorg. Chem.* **1986**, *34*, 115. (b) S. Trofimenko, *Chem. Rev.* **1993**, *93*, 943.
- (33) (a) J. D. Brauer, H. Bürger, G. R. Liewald, J. Wilke, *J. Organomet. Chem.* **1986**, *305*, 119. (b) S. Friedrich, L. Gade, A. Edwards, M. McPartlin, *Chem. Ber.* **1993**, *126*, 1797. (c) L. H. Gade, N. Mahr, *J. Chem. Soc. Dalton Trans.* **1993**, 489. (d) L. H. Gade, C. Becker, W. J. Lauher, *Inorg. Chem.* **1993**, *32*, 2308. (e) P. Kosse, E. Popowski, M. Veith, V. Huch, *Chem. Ber.* **1994**, *127*,

2103. (f) I. Hemme, U. Klingebiel, S. Freitag, D. Stalke, *Z. Anorg. Allg. Chem.* **1995**, 621, 2093. (g) H. Bürger, R. Mellies, K. Wiegel, *J. Organomet. Chem.* **1997**, 142, 55.
- (34) R. Fleischer, D. Stalke, *Organometallics* **1998**, 17, 832.
- (35) (a) S. R. Hall, C. L. Raston, B. W. Skelton, A. H. White, *Inorg. Chem.* **1983**, 22, 4070. (b) C. L. Raston, B. W. Skelton, C. R. Whitaker, A. H. White, *Aust. J. Chem.* **1988**, 41, 1925. (c) C. L. Raston, C. R. Whitaker, A. H. White, *Inorg. Chem.* **1989**, 28, 163. (d) A. J. Edwards, M. A. Paver, P. R. Raithby, C. A. Russell, D. S. Wright, *J. Chem. Soc., Dalton Trans.* **1993**, 3265. (e) F. Neumann, F. Hampel, P. v. R. Schleyer, *Inorg. Chem.* **1995**, 34, 6553.
- (36) (a) J. Beck, J. Strähle, *Angew. Chem.* **1985**, 97, 419; *Angew. Chem. Int. Ed. Engl.* **1985**, 24, 409. (b) S. Wingerter, H. Gornitzka, G. Bertrand, D. Stalke, *Eur. J. Inorg. Chem.* **1999**, 173.
- (37) (a) A. Heine, D. Stalke, *Angew. Chem.* **1993**, 105, 90; *Angew. Chem. Int. Ed. Engl.* **1993**, 32, 121. (b) A. Heine, R. Herbst-Irmer, D. Stalke, *J. Chem. Soc. Chem. Commun.* **1993**, 1729.
- (38) (a) P. K. Mehrotra, R. Hoffmann, *Inorg. Chem.* **1978**, 17, 2187. (b) P. Pyykkö, *Chem. Rev.* **1997**, 97, 597. (c) P. Pyykkö, N. Runeberg, F. Mendizabal, *Chem. Eur. J.* **1997**, 3, 1451. (d) P. Pyykkö, F. Mendizabal, *ibid.* **1997**, 3, 1458.
- (39) (a) R. I. Papasergio, C. L. Raston, A. H. White, *J. Chem. Soc. Chem. Commun.* **1983**, 1419. (b) R. I. Papasergio, C. L. Raston, A. H. White, *J. Chem. Soc. Dalton Trans.* **1987**, 3085.
- (40) Cambridge Structural Database, October 2001, Release; F. H. Allen, O. Kennard, *Chem. Des. Automation News* **1993**, 8, 131.
- (41) R. I. Papasergio, C. L. Raston, A. H. White, *Chem. Commun.* **1984**, 612.
- (42) D. Fenske, G. Baum, A. Zinn, K. Dehnicke, *Z. Naturforsch.* **1990**, B 45, 1273.
- (43) J. Beck, J. Strähle, *Z. Naturforsch.* **1986**, B 41, 4.
- (44) E. R. Humphrey, Z. Reeves, J. C. Jeffrey, J. A. McCleverty, M. D. Ward, *Polyhedron* **1999**, 18, 1335.
- (45) B. T. Usubaliev, E. M. Movsumov, I. R. Amiraslanov, A. I. Akhmedov, A. A. Musaev, Kh. S. Mamedov, *Zh. Strukt. Khim.* **1981**, 22, 98.
- (46) *LiCl*: (a) C. L. Raston, B. W. Skelton, C. R. Whitaker, A. H. White, *J. Chem. Soc., Dalton Trans.* **1988**, 897. (b) C. L. Raston, C. R. Whitaker, A. H. White,

- J. Chem. Soc., Dalton Trans.* **1988**, 991. (c) F. E. Hahn, S. Rupprecht, *Z. Naturforsch.* **1991**, B 46, 143. *Lil*: (a) C. L. Raston, B. W. Skelton, C. R. Whitaker, A. H. White, *Aust. J. Chem.* **1988**, 41, 1925. (b) C. L. Raston, W. T. Robinson, B. W. Skelton, C. R. Whitaker, A. H. White, *Aust. J. Chem.* **1990**, 43, 1163. (c) M. R. Kopp, B. Neumüller, *Z. Naturforsch.* **1999**, B 54, 818. (d) C. Doriat, R. Koppe, E. Baum, G. Stosser, H. Kohnlein, H. Schnöckel, *Inorg. Chem.* **2000**, 39, 1534.
- (47) (a) R. E. Mulvey, *Chem. Soc. Rev.* **1991**, 20, 167. (b) R. E. Mulvey, *Chem. Soc. Rev.* **1998**, 27, 339.
- (48) D. Hoffmann, A. Dorigo, P. v. R. Schleyer, H. Reif, D. Stalke, G. M. Sheldrick, E. Weiss, M. Geissler, *Inorg. Chem.* **1995**, 34, 262.
- (49) (a) J. Erfkamp, A. Müller, *ChiuZ.* **1990**, 6, 267. (b) J. Kim, D. C. Rees, *Nature*, **1992**, 360, 553. (c) M. M. Georgiadis, H. Komiya, P. Chakrabarti, D. Woo, J. J. Kornuc, D. C. Rees, *Science* **1992**, 257, 1653. (d) J. Kim, D. C. Rees, *Biochemistry* **1994**, 33, 389.
- (50) (a) E. Hurt, G. Hanska, R. Malkin, *FEBS Lett.* **1981**, 134, 1. (b) J. R. Mason, R. Cammack, *Annu. Rev. Microbiol.* **1992**, 46, 277. (c) M. G. Golinelli, J. Gagnon, J. Meyer, *Biochemistry*, **1997**, 36, 11797.
- (51) R. Fleischer, D. Stalke, *Organometallics* **1998**, 17, 832.
- (52) M. Herberhold, S. Gerstmann, W. Milius, B. Wrackmeyer, H. Borrmann, *Phosphorus, Sulfur and Silicon, Relat. Elem.* **1996**, 112, 261.
- (53) C. T.-W. Chu, R. S. Gall, L. F. Dahl, *J. Am. Chem. Soc.* **1982**, 104, 737.
- (54) E. J. Wucherer, M. Tasi, B. Hansert, A. K. Powel, M.-T. Garland, J.-F. Halet, J.-Y. Saillard, H. Vahrenkamp, *Inorg. Chem.* **1989**, 28, 3564.
- (55) R. J. Doedens, *Inorg. Chem.* **1969**, 8, 570.
- (56) R. Meij, K. Olie, *Cryst. Struct. Commun.* **1975**, 4, 515.
- (57) C. Mahabiersing, W. G. J. de Lange, K. Goubitz, D. J. Stufkens, *J. Organomet. Chem.* **1993**, 461, 127.
- (58) R. T. Kops, E. van Aken, H. Schenk, *Acta Crystallogr., Sect B* **1973**, 29, 913.
- (59) N. W. Alcock, A. F. Hill, M. S. Roe, *J. Chem. Soc., Dalton Trans.* **1990**, 1737.
- (60) R. Fleischer, D. Stalke, *J. Chem. Soc. Chem. Commun.* **1998**, 343.
- (61) D. Ilge, D. S. Wright, D. Stalke, *Chem. Eur. J.* **1998**, 4, 2275.
- (62) R. Fleischer "Synthetic Routes to Sulfur Nitrogen Analogues of some simple Sulfur Oxygen Compounds", Göttingen: Cuvillier, **1998**, ISBN 3-89712-069-0.

- (63) T. Chivers, M. Parvez, G. Schatte, *Inorg. Chem.* **2001**, *40*, 540.
- (64) T. Kottke, D. Stalke, *Angew. Chem.* **1993**, *105*, 619; *Angew. Chem., Int. Ed. Engl.* **1993**, *32*, 580.
- (65) (a) H. Dietrich, *Acta Crystallogr.* **1963**, *16*, 681. (b) H. J. Dietrich, *J. Organomet. Chem.* **1981**, *205*, 291.
- (66) (a) E. A. C. Lucken, E. Weiss, *J. Organomet. Chem.* **1964**, *2*, 197. (b) E. Weiss, G. Henken, *J. Organomet. Chem.* **1970**, *21*, 265. (c) E. Weiss, T. Lambertsen, B. Schubert, J. K. Cockcroft, A. Wiedemann, *Chem. Ber.* **1990**, *123*, 79.
- (67) U. Siemeling, T. Redecker, B. Neumann, H.-G. Stammer, *J. Am. Chem. Soc.* **1994**, *116*, 5507.
- (68) monomeric MeLi has been trapped in the coordination sphere of d- and f-block organometallic moieties, e. g. (a) K.-R. Pörschke, K. Jonas, G. Wilke, R. Benn, R. Mynott, R. Goddard, C. Krüger, *Chem. Ber.* **1985**, *118*, 275; (b) P. B. Hitchcock, M. F. Lappert, R. G. Smith, *J. Chem. Soc. Chem. Commun.* **1989**, 369; monomeric alkyllithium other than MeLi has been trapped in lithium amide moieties, e. g. (c) J. Jubb, P. Berno, S. Hao, S. Gambarotta, *Inorg. Chem.* **1995**, *43*, 3563; (d) P. G. Williard, C. Sun, *J. Am. Chem. Soc.*, **1997**, *119*, 11693.
- (69) Review: A. Maercker, *Angew. Chem.* **1987**, *99*, 1002; *Angew. Chem., Int. Ed. Engl.* **1987**, *26*, 972.
- (70) (a) J. Jubb, S. Gambarotta, R. Duchateau and J. H. Teuben, *J. Chem. Soc., Chem. Commun.* **1994**, 2641. (b) S. De Angelis, E. Solari, C. Floriani, A. Chiesi-Villa and C. Rizzoli, *J. Chem. Soc., Dalton Trans. Commun.* **1994**, 2467. (c) H. C. Aspinall and M. R. Tillotson, *Inorg. Chem. Commun.* **1996**, *35*, 2163 (d) C. Hilf, F. Bosold, K. Harms, M. Marsch and G. Boche, *Chem. Ber./Recl.* **1997**, *130*, 1213.
- (71) D. Seebach, *Angew. Chem.* **1988**, *100*, 1685; *Angew. Chem., Int. Ed. Engl.* **1988**, *27*, 1624.
- (72) T. Kottke, R. J. Lagow, D. Hoffmann and R. D. Thomas, *Organometallics* **1997**, *16*, 789.
- (73) C. Sun and P. G. Williard, *J. Am. Chem. Soc. Commun.* **2000**, *122*, 7829.
- (74) K. Sorger, P. v. R. Schleyer, R. Fleischer and D. Stalke, *J. Am. Chem. Soc.* **1996**, *118*, 6924.

- (75) A. Steiner and D. S. Wright, *J. Chem. Soc., Chem. Commun.* **1997**, 283.
- (76) A. Abbotto, A. Streitwieser and P. v. R. Schleyer, *J. Am. Chem. Soc.* **1997**, *119*, 11255.
- (77) R. E. Mulvey, *J. Chem. Soc., Chem. Commun.* **2001**, 1049.
- (78) B. Walfort, L. Lameyer, W. Weiss, R. Herbst-Irmer, R. Bertermann, J. Rocha and D. Stalke, *Chem. Eur. J.* **2001**, *7*, 1417.
- (79) (a) G. R. Desiraju, *Crystal Engineering-The Design of Organic Solids*, Elsevier, Amsterdam, **1989**; (b) J. Starbuck, R. Docherty, M. H. Charlton and D. Buttar, *J. Chem. Soc., Perkin Trans. 2*, **1999**, 677. (c) J. Wouters and F. Ooms, *Curr. Pharm. Des.* **2001**, *7*, 529.
- (80) Reviews: (a) H. König, *Fortschr. Chem. Forsch.* **1968**, *9*, 487; (b) L. Weber, *Angew. Chem.* **1983**, *24*, 568; *Angew. Chem. Int. Ed. Engl.* **1983**, *95*, 539.
- (81) see for example: (a) G. Opitz, *Angew. Chem.* **1967**, *4*, 161; *Angew. Chem. Int. Ed. Engl.* **1967**, 107; (b) J. F. King, R. Rathore, *The Chemistry of Sulphonic Acids, Esters and their Derivatives (Hrsg.: S. Patai, Z. Rappoport)*, Wiley, Chichester, **1991**, 697.
- (82) (a) G. Boche, K. Marsch, K. Harms, G. M. Sheldrick, *Angew. Chem.* **1985**, *97*, 577; *Ang. Chem. Int. Ed.* **1985**, *24*, 573; (b) H. J. Gais, U. Dingerdissen, C. Krüger, K. Angermund, *J. Am. Chem. Soc.* **1987**, *109*, 3775; (c) M. Zehnder, J. F. Müller, M. Neuburger, *Acta Cryst. Sec. C* **1997**, *53*, 419; (d) J. F. K. Müller, M. Neuburger, M. Zehnder, *Helv. Chim. Acta* **1997**, *80*, 2182.
- (83) J. K. Brask, T. Chivers, M. Parvez, G. Schatte, *Angew. Chem.* **1997**, *109*, 2075; *Angew. Chem. Int. Ed. Engl.* **1997**, *36*, 1986.
- (84) Recent examples: (a) J. K. Brask, T. Chivers, G. P. A. Yap, *Inorg. Chem.* **1999**, *38*, 5588; (b) J. Storre, C. Schnitter, H. W. Roesky, H.-G. Schmidt, M. Noltemeyer, R. Fleischer, D. Stalke *J. Am. Chem. Soc.*, **1997**, *119*, 7505.
- (85) J. K. Brask, T. Chivers, M. Parvez, *Angew. Chem.* **2000**, *112*, 988; *Angew. Chem. Int. Ed. Engl.* **2000**, *39*, 958.
- (86) (a) S. Pohl, B. Krebs, U. Seyer, G. Henkel, *Chem. Ber.* **1979**, *112*, 1751. (b) M. Herberhold, S. Gerstmann, B. Wrackmeyer, H. Borrmann, *J. Chem. Soc. Dalton Trans.* **1994**, 633. (c) M. Herberhold, S. Gerstmann, W. Milius, B. Wrackmeyer, H. Borrmann, *Phosphorus, Sulfur and Silicon, Relat. Elem.* **1996**, *112*, 261.
- (87) G. M. Sheldrick, W. S. Sheldrick, *J. Chem. Soc. A.* **1969**, 2279.

- (88) A. Heine, D. Stalke, *Angew. Chem. Int. Ed. Engl.* **1992**, *31*, 854.
- (89) Me_2Al^+ with Py_2CH^- : (a) H. Gornitzka, D. Stalke, *Angew. Chem.* **1994**, *106*, 695; *Angew. Chem. Int. Ed. Engl.* **1994**, *33*, 693. Py_2N^- : (b) H. Gornitzka, D. Stalke, *Eur. J. Inorg. Chem.* **1998**, 311. Py_2P^- : (c) A. Steiner, D. Stalke, *Organometallics* **1995**, *14*, 2422. (d) M. Pfeiffer, F. Baier, T. Stey, D. Leusser, D. Stalke, B. Engels, D. Moigno, W. Kiefer, *J. Mol. Model.* **2000**, *6*, 299.
- (90) U. Dembowski, M. Noltemeyer, J. W. Gilje, H. W. Roesky, *Chem. Ber.* **1991**, *124*, 1917.
- (91) A. Haaland, K. Hedberg, P. P. Power, *Inorg. Chem.* **1984**, *23*, 1972.
- (92) (a) A. Haaland, *Angew. Chem. Int. Ed. Engl.* **1989**, *28*, 992. (b) S. Wingerter, H. Gornitzka, G. Bertrand, D. Stalke, *Eur. J. Inorg. Chem.* **1999**, 173. (c) M. Westerhausen, T. Bollwein, K. Z. Polborn, *Naturforsch.* **2000**, *55b*, 51.
- (93) H. Gornitzka, C. Hemmert, G. Bertrand, M. Pfeiffer, D. Stalke, *Organometallics*, **2000**, *19*, 112.
- (94) C. Bolm, J. F. K. Müller, G. Schlingloff, M. Zehnder, M. Neuburger, *J. Chem. Soc. Chem. Commun.* **1993**, 182.
- (95) M. Kaupp, H. Stoll, H. Preuss, W. Kaim, T. Stahl, G. van Koten, E. Wissing, W. J. J. Smeets, A. L. Spek, *J. Am. Chem. Soc.* **1991**, *113*, 5606.
- (96) (a) P. O'Brien, M. B. Hursthouse, M. Motevalli, J. R. Walsh, A. C. Jones, *J. Organomet. Chem.* **1993**, *449*, 1. (b) E. Wissing, M. Kaupp, J. Boersma, A. L. Spek, G. van Koten, *Organometallics* **1994**, *13*, 2349.
- (97) M. Westerhausen, M. Wieneke, W. Ponikwar, H. Nöth, W. Schwarz, *Organometallics* **1998**, *17*, 1438.
- (98) Reviews: (a) R. Fleischer, D. Stalke, *Coord. Chem. Rev.* **1998**, *176*, 431. (b) D. Stalke, *Proc. Indian Acad. Sci.* **2000**, *112*, 155.
- (99) (a) W. Kutzelnigg, *Angew. Chem.* **1984**, *96*, 262; *Angew. Chem. Int. Ed. Engl.* **1984**, *23*, 272. (b) A. E. Reed, P. v. R. Schleyer, *J. Am. Chem. Soc.* **1990**, *112*, 1434. (c) R. Steudel, *Chemie der Nichtmetalle*, de Gruyter, Berlin, 1998.
- (100) (a) D. Hänssgen, H. Salz, S. Rheindorf, C. J. Schrage, *Organomet. Chem.* **1993**, *443*, 61. (b) T. J. Katz, S. Shi, *J. Org. Chem.* **1994**, *59*, 8297. (c) B. Walfort, R. Bertermann, D. Stalke, *Chem. Eur. J.*, **2001**, *7*, 1424.
- (101) (a) D. Hänssgen, R. Steffens, *J. Organomet. Chem.* **1982**, *236*, 53; (b) D. Hänssgen, R. Steffens, *Z. Naturforsch.* **1985**, *40b*, 919. (c) D. Hänssgen, R. Plum, *Chem. Ber.* **1987**, *120*, 1063.

- (102) (a) D. Hänssgen, H. Hupfer, M. Nieger, M. Pfendtner, R. Steffens, *Z. Anorg. Allg. Chem.* **2001**, 627, 17; (b) B. Walfort, R. Bertermann, D. Stalke, *Chem. Eur. J.*, **2001**, 7, 1424.
- (103) R. Armstutz, T. Laube, W. B. Schweizer, D. Seebach, J. D. Dunitz, *Helv. Chim. Acta* **1984**, 67, 224.
- (104) W. Zarges, M. Marsch, K. Harms, W. Koch, G. Frenking, G. Boche, *Chem. Ber.* **1991**, 124, 543.
- (105) D. Steinborn, T. Ruffer, C. Bruhn, F. W. Heinemann, *Polyhedron* **1998**, 17, 3275.
- (106) W. Hollstein, K. Harms, M. Marsch, G. Boche, *Angew. Chem.* **1988**, 100, 868; *Angew. Chem. Int. Ed. Engl.* **1988**, 28, 852.
- (107) (a) A. E. Reed, F. Weinhold, *J. Am. Chem. Soc.* **1986**, 108, 3586; (b) D. A. Bors, A. Streitwieser, *J. Am. Chem. Soc.* **1986**, 108, 1397; (c) U. Salzner, P. v. R. Schleyer, *J. Am. Chem. Soc.* **1993**, 115, 10231; (d) T. Stefan, R. Janoschek, *J. Mol. Model.* **2000**, 6, 282.
- (108) J. K. Brask, T. Chivers, M. Parvez, G. P. A. Yap, *Inorg. Chem.* **1999**, 38, 3594.
- (109) P. Blais, J. K. Brask, T. Chivers, G. Schatte, *Inorg. Chem.* **2001**, 40, 384.
- (110) R. S. Cahn, C. Ingold, V. Prelog, *Angew. Chem.* **1966**, 78, 413; *Angew. Chem. Int. Ed. Engl.* **1966**, 5, 385.
- (111) A. Strecker, *Liebigs Ann. Chem.* **1868**, 148, 90.
- (112) (a) M. R. Truter, *J. Chem. Soc.* **1962**, 3393. (b) F. Chabonnier, R. Faure, H. Loiseleur, *Rev. Chim. Miner.* **1979**, 16, 555. (c) F. Chabonnier, R. Faure, H. Loiseleur, *Acta Crystallogr., Sect. E* **1979**, 35, 1773. (d) A. Karipides, *Acta Crystallogr., Sect. B* **1981**, 37, 2232. (e) R. E. Marsh, *Acta Crystallogr., Sect. B (Str. Sci.)* **1995**, 51, 897.
- (113) (a) K. Magnus, *Liebigs Ann. Chem.* **1833**, 6, 152. (b) J. v. Liebig, *Liebigs Ann. Chem.* **1835**, 13, 35. (c) H. J. Backer, *Rec. Trav. Chim.* **1929**, 48, 949.
- (114) T. L. Smith, J. H. Elliott, *J. Am. Chem. Soc.* **1953**, 75, 3566.
- (115) (a) D. Mootz, H. Wunderlich, *Acta Crystallogr. Sect. B*, **1970**, 26, 1820. (b) P. Sartori, R. Juschke, R. Boese, D. Bläser, *Z. Naturforsch. Teil E*, **1994**, 49, 1467.
- (116) V. A. Russell, C. C. Evans, W. Li, M. D. Ward, *Science* **1997**, 276, 575.
- (117) H. Werner, *Chem. Unserer Zeit* **1967**, 1, 135.

-
- (118) B. Walfort, unpublished result.
- (119) D. Stalke, *Chem. Soc. Rev.* **1998**, 27, 171.
- (120) (a) H. Hope, *Acta Crystallogr.* **1988**, B 44, 22. (b) T. Kottke, D. Stalke, *J. Appl. Crystallogr.* **1993**, 26, 615. (c) T. Kottke, R. J. Lagow, D. Stalke, *J. Appl. Crystallogr.* **1996**, 29, 465.
- (121) A. C. T. North, D. Phillips, F. S. Mathews, *Acta Crystallogr.* **1968**, A 24, 351.
- (122) Bruker AXS, Inc. Madison WI **2000**, *Program for data processing*.
- (123) G. M. Sheldrick, *Program for empirical absorption correction*, Universität Göttingen **2000**.
- (124) G. M. Sheldrick, Universität Göttingen **2000**, *Program for the refinement of crystal structures*.
- (125) Bruker AXS, Inc. Madison WI **2000**, *Program for twinning solution*.
- (126) Bruker AXS, Inc. Madison WI **2000**, *Program for data processing*.
- (127) Bruker AXS, Inc. Madison WI **2000**, *Program for data collection and processing*.
- (128) (a) H. D. Flack, *Acta Crystallogr., Sect. A* **1983**, 39, 876. (b) G. Bernadinelli, H. D. Flack, *Acta Crystallogr., Sect A* **1985**, 41, 500.

Lebenslauf

Persönliche Daten

Name: Bernhard Walfort
Geburtstag: 29. Januar 1971
Geburtsort: Marbach am Neckar
Staatsangehörigkeit: deutsch

Schule

09/77 – 08/81 Grundschule Affalterbach
09/81 – 05/90 Friedrich-Schiller-Gymnasium Marbach
Abschluß: Abitur

Wehrdienst

06/90 – 05/91 Grundwehrdienst / Marine (Decksdienst)

Studium

09/91 – 09/92 Studium der Mathematik (Diplom), Universität Stuttgart
10/92 – 05/99 Studium der Chemie (Diplom), Universität Würzburg
08/98 – 05/99 Diplomarbeit im Arbeitskreis von Prof. Dr. D. Stalke mit dem Thema „Polyimidoschwefelanionen in der Metallkoordination“, Anorganische Chemie, Universität Würzburg
seit 05/99 Arbeiten an der Dissertation im Arbeitskreis von Prof. Dr. D. Stalke am Institut für Anorganische Chemie der Universität Würzburg mit dem Thema: “Novel Dianionic Sulfur Ylides and Related Compounds”
seit 05/99 Wissenschaftlicher Angestellter am Institut für Anorganische Chemie der Universität Würzburg

Würzburg, 13.12.2001

Bernhard Walfort

Publikationen

1. Fleischer, Roland; Walfort, Bernhard; Gbureck, Axel; Scholz, Peter; Kiefer, Wolfgang; Stalke, Dietmar; „Raman spectroscopic investigation and coordination behavior of the polyimido S(VI) anions $[\text{RS}(\text{NR})_3]^-$ and $[\text{S}(\text{NR})_4]^{2-}$ “ *Chemistry, Eur. J.* **1998**, *4*, 2266.
2. Steiner, Alexander; Lawson, Gavin; Walfort, Bernhard; Leusser, Dirk; Stalke, Dietmar; „ $[(\text{THF})_6\text{Ba}_6(\text{dmpz})_8\{(\text{OSiMe}_2)_2\text{O}\}_2]$ (dmpz = 3,5-dimethylpyrazolate): a molecule with six barium cations in a plane capped by two siloxane dianions and framed by eight dmpz anions“ *J. Chem. Soc., Dalton Trans.* **2001**, *3*, 219.
3. Walfort, Bernhard; Bertermann, Rüdiger; Stalke, Dietmar; „A new class of dianionic sulfur-ylides: alkylendiazasulfites“ *Chemistry, Eur. J.* **2001**, *7*, 1424.
4. Walfort, Bernhard; Lameyer, Lutz; Weiss, Wilfried; Herbst-Irmer, Regine; Bertermann, Rüdiger; Rocha, Joao; Stalke, Dietmar; „ $[\{(\text{MeLi})_4(\text{dem})_{1.5}\}_\infty]$ and $[(\text{thf})_3\text{Li}_3\text{Me}\{(\text{NtBu})_3\text{S}\}]$ – how to reduce aggregation of parent methyllithium“ *Chemistry, Eur. J.* **2001**, *7*, 1417.
5. Walfort, Bernhard; Leedham, Angela P.; Russel, Christopher A.; Stalke, Dietmar; „Triimidosulfonic Acid and Organometallic Triimidosulfonates – S^+-N^- versus $\text{S}=\text{N}$ Bonding“ *Inorg. Chem.* **2001**, *40*, 5668.
6. Walfort, Bernhard; Stalke, Dietmar; „Methylene triimidosulfate $\text{H}_2\text{CS}(\text{NtBu})_3^{2-}$ – The First Dianionic Sulfur(VI)-Ylide“ *Angew. Chem.* **2001**, *113*, 3965.
7. Walfort, Bernhard; Stalke, Dietmar; „The inverse podant $[\text{Li}_3(\text{NBu}^t)_3\text{S}]^+$ stabilises a single lithium enolate $\text{LiOCH}=\text{CH}_2$ in a high and low temperature solid state phase of $[(\text{thf})_3\text{Li}_3(\text{OCH}=\text{CH}_2)\{(\text{NBu}^t)_3\text{S}\}]$ “ *Chem. Comm.* **2001**, *17*, 1640.

Erklärung

Hiermit erkläre ich an Eides statt, daß ich die Dissertation "Novel Dianionic Sulfur Ylides and Related Compounds" selbständig angefertigt und keine anderen als die von mir angegebenen Quellen oder Hilfsmittel benutzt habe.

Ich erkläre außerdem, das diese Dissertation weder in gleicher noch in anderer Form bereits in einem anderen Prüfungsverfahren vorgelegen hat.

Ich habe außer den mit dem Zulassungsgesuch urkundlich vorgelegten Graden keine weiteren akademischen Grade erworben oder zu erwerben versucht.

Würzburg, den 13.12.2001

(Bernhard Walfort)